Assessment of Sequentially- Versus Fully-Coupled Dynamic Analysis of Offshore Wind Turbines

Executive Summary

A loads analysis on fixed-bottom offshore wind turbines (OWT) was conducted focusing on the differences in Ultimate Limit State load predictions between the so-called fully coupled (FC) and the sequentially coupled (SC) modelling approaches. The FC approach is deemed more accurate and rigorous, as it simultaneously accounts for aerodynamics, structural dynamics, control dynamics, and hydrodynamics. In the SC method widely used by the offshore wind industry, the turbine OEM and the substructure designers work independently on their respective subsystems exchanging only loads and stiffness properties at the interface between substructure and tower. As such, this method does not require sharing design specifics and thus protects proprietary information and clearly defines liability bounds for all parties involved in the OWT design.

The analysis was conducted through aero-hydro-servo-elastic simulations of 5-MW OWTs on a monopile and on a jacket substructure; these two are the most common substructures and are expected to be sited in different water depths and to have significantly different dynamic behaviors. Two sites along the Eastern U.S. seaboard were selected corresponding to two offshore energy lease areas that could host a monopile-based and a jacket-based OWT, respectively, and for which we could gather metocean data. We simulated power production (operational) and parked (extreme event) load cases on publically available models of turbine and substructures, and extracted loads on several subcomponents.

When considering the maximum load values across all operational cases (A001-A008), the RNA and tower loads were found to be within 3% and 6% for the jacket and the monopile configuration, respectively. When considering the maximum load values across all parked cases (B001-B008), the RNA and tower loads were within 13% and 7% for the jacket and the monopile configuration, respectively, and with the SC results being less conservative than the FC results. For the substructure loads across all power-production cases, results showed differences up to 60% for the jacket members, and with the SC approach overestimating the loads; the monopile maximum loads were in close agreement (6-11%) and with no clear over/underestimation by any particular method. Across all the parked cases (B001—B008), one jacket member load channel was overestimated by ~50% under SC, whereas several other member loads were underestimated up to 39% when compared to FC; the monopile loads were underestimated by up to 11% by the SC method.

Our findings yielded some significant differences that require further investigation in order to address any remaining concern regarding the practicability of the sequentially coupled analysis method for the design of offshore wind systems. Some of these differences can have important consequences on the design of the support structures, with potentially either overdesigned or underdesigned components, and should be further investigated.

Table of Contents

Executive Summary 1
1 Nomenclature 3
2 Background 5
3 Definition of the Analysis Methods 8
3.1 Sequentially Coupled Analysis 9
3.2 Fully Coupled Analysis 11
4 Select Environmental and Turbine Parameters 12
4.1 Environmental Conditions 12
4.1.1 Frying Pan Shoals (NOAA Buoy 41013): 12
4.1.2 Long Island Site (NOAA Buoy 44025): 13
4.1.3 Overview of Metocean Conditions: 14
4.1.4 Characterization of Soil Conditions: 15
4.2 Wind Turbine Configuration 15
5 Support Structure Definition 16
5.1 Overview of the Monopile Configuration 16
5.2 Overview of the Jacket Configuration 18
6 Modeling Assumptions and Design Load Cases 19
6.1 Hydrodynamics 19
6.2 Coordinate Systems, Load Channels and Substructure Nodes of Interest 20
6.2.1 Load Channels 21
6.3 Exchange Data Format 23
6.4 Design Load Cases 23
7 Model to Model Verification 26
8 Maximum Loads Comparison for ULS Load Cases 29
8.1 Monopile – Power Production – Comparison of overall Maximum Loads 29
8.1.1 Blade Loads (as shown in Appendix A) 30
8.1.2 Shaft Loads (as shown in Appendix A) 31
8.1.3 Tower-Top (Yaw-Bearing) Loads (as shown in Appendix A) 31
8.1.4 Tower-Base Loads (as shown in Appendix A) 32
8.1.5 Substructure Loads (as shown in Appendix A) 32
8.2 Monopile – Extreme Conditions – Comparison of overall Maximum Loads 32

8.2.1 Blade Loads (as shown in Appendix A) 33
8.2.2 Shaft Loads (as shown in Appendix A) 33
8.2.3 Tower-Top (Yaw-Bearing) Loads (as shown in Appendix A) 34
8.2.4 Tower-Base Loads (as shown in Appendix A) 34
8.2.5 Substructure Loads (as shown in Appendix A) 34
8.3 Jacket – Power Production – Comparison of overall Maximum Loads 34
8.3.1 Blade Loads (as shown in Appendix A) 35
8.3.2 Shaft Loads (as shown in Appendix A) 35
8.3.3 Tower-Top (Yaw-Bearing) Loads (as shown in Appendix A) 35
8.3.4 Tower-Base Loads (as shown in Appendix A) 36
8.3.5 Substructure Loads (as shown in Appendix A) 36
8.4 Jacket – Extreme Conditions – Comparison of overall Maximum Loads 38
8.4.1 Blade Loads (as shown in Appendix A) 39
8.4.2 Shaft Loads (as shown in Appendix A) 39
8.4.3 Tower-Top (Yaw-Bearing) Loads (as shown in Appendix A) 39
8.4.4 Tower-Base Loads (as shown in Appendix A) 39
8.4.5 Substructure Loads (as shown in Appendix A) 39
9 Conclusions 40
9.1 Recommended Follow-On Studies 41
10 References 42
11 Appendix A: ULS Result Gallery 44

1 Nomenclature

ASE	Aero-Servo-Elastic
AHSE	Aero-Hydro-Servo-Elastic
COD	Co-directional (per IEC 61044-3 [4])
DLC	Design Load Case
ECM	Extreme Current Model (per IEC 61044-3 [4])
ESS	Extreme Sea State (per IEC 61044-3 [4])

EWLR	Extreme Water Level Reference (per IEC 61044-3 [4])
EWM	Extreme Wind Model (per IEC 61044-3 [4])
FC	Fully Coupled
FLS	Fatigue limit state
Hmax	Maximum wave height
Hs	Significant wave height
KYS	Keystone Engineering
MIS	Misaligned (per IEC 61044-3 [4])
M&N	Moffatt and Nichol
MSL	Mean sea level
NCM	Normal Current Model (per IEC 61044-3 [4])
NREL	National Renewable Energy Laboratory
NSS	Normal Sea State (per IEC 61044-3 [4])
NTM	Normal Turbulence Model (per IEC 61044-3 [4])
NWLR	Normal Water Level Reference (per IEC 61044-3 [4])
OD	Outer diameter
OEM	Original Equipment Manufacturer
OWT	Offshore Wind Turbines
RNA	Rotor-nacelle assembly
SC	Sequentially Coupled
t	Wall thickness
Tp	Peak spectral period
ULS	Ultimate limit state
z	z coordinate
1P	Rotor frequency
3P	Blade passing Frequency

2 Background

Offshore wind turbines (OWTs) are mounted on support structures that include a tower, a substructure, and the foundation to the seabed. Over 2,000 offshore wind turbines have been installed to date, mostly in the North Sea and the Baltic Sea in Europe, but the first U.S. offshore wind project began operation in 2016. Most of these operating OWTs are mounted on foundations that are rigidly fixed to the seabed in shallow water (0 – 50 m depth) using monopile, jacket, or gravity-base substructures. However, new technology is being developed that will allow floating wind turbines to operate in deeper water up to 1,000 m. Figure 1 shows a range of the most common types of substructures and concepts currently being considered.

Figure 1. Offshore wind substructure designs for varying water depths (Illustration by Josh Bauer, NREL)

The most common substructures are the monopile and the multimember lattice, or "jacket". Seventy-five percent of all offshore wind installations use monopiles (see Figure 2), which can be considered the baseline for offshore wind. Based on our market assessment of offshore wind projects that are under construction or that have announced design details, monopiles will remain the dominant substructure type, but jackets will increase from a 10% share to a 16% share in the next few years.

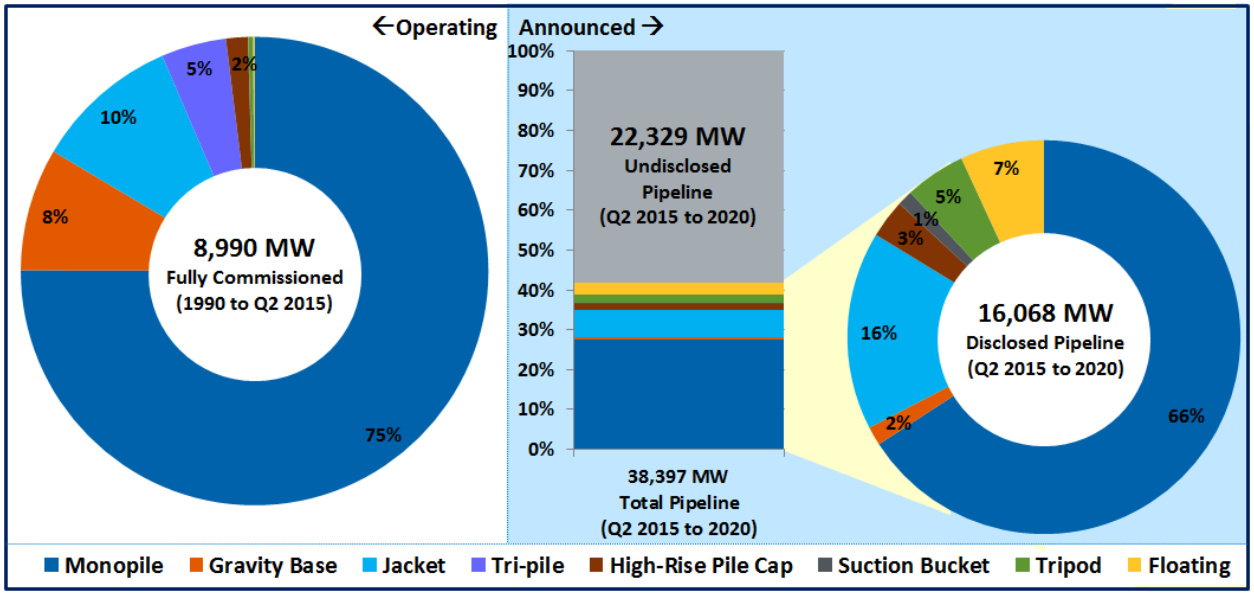

Figure 2 Global offshore wind substructure market share (figure credit NREL)

OWT substructures are subjected to a variety of loading during both normal operation and extreme events (e.g., faults, winter and tropical storms). These loads include those that occur directly on the substructure such as wave, current, and wind loads, and those that are transferred from the turbine and support tower. The load calculation for OWT systems is particularly challenging due to the rotor variable speed and turbulent inflow, the aero-elastic interaction of the blades and the wind field, the coupling between the Rotor Nacelle Assembly (RNA) and support structure, and the potential for significant dynamic amplification of these loads if the resulting frequencies are similar to any of the natural vibration frequencies of the RNA and support structure. This latter issue must be addressed carefully as the potential for resonant or near-resonant response of the OWT will lead to significantly greater loads. These amplified loads can result in large displacements during operation causing pre-mature shutdown, overload of structural components, and accelerated accumulation of fatigue damage.

The analysis of OWTs is conducted using design tools that have been validated under actual operating conditions to allow full design and type certification under IEC (International Electrotechnical Commission) standards and classification society guidelines. For OWTs, the analysis method must consider the aerodynamic/hydrodynamic loads and responses of the entire system (turbine, tower, substructure and foundation) coupled to the turbine control system dynamics. A *fully coupled* (turbine and support structure) *modelling approach* is more rigorous and allows for a thorough system optimization; however, intellectual property concerns can sometimes preclude this approach. In fact, turbine control system algorithms and turbine properties are not available within the public domain and often are not even made available to offshore substructure designers who work directly for the turbine manufacturers. This prevents engineering firms and contractors from directly performing an integrated, coupled analysis of the complete system.

In many cases, two separate analyses using different software tools and an information exchange may be necessary to design an offshore wind system. In the *sequentially coupled approach*, the turbine and

substructure designers will independently determine a reduced set of dynamic properties of their sub-systems, which is exchanged and included in their independent sub-system models. The turbine manufacturer then simulates the wind induced response at the tower support flange, considering the reduced model of the substructure and the hydrodynamic loads provided by the substructure designer. In turn, the substructure designer uses these tower base loads as inputs for the analysis of the substructure and its foundation (by adding aerodynamic and hydrodynamic loads to the sub-structure below the tower).

However, concerns exist that a sequentially coupled analysis could potentially reduce the quality and accuracy of the design process when compared to the fully coupled one. The industry, including turbine manufacturers, design firms, and regulatory agencies seek a better understanding of the impact of uncertainties introduced by a sequentially- vs. fully-coupled design approach.

Whereas the ability to conduct design optimization is limited to some degree with a sequentially coupled analysis method, the central questions are whether this approach can be adequate for design purposes, or if a significant amount of design related uncertainty is introduced. In fact, it could be hypothesized that because of a possible lack of convergence and/or less than ideal transfer of dynamic properties among different models, some structural modes important for the design might not get captured by this process.

In response to these questions, the National Renewable Energy Laboratory (NREL) proposed and was awarded a contract for research under BSEE's Solicitation Number E15PS00085. This report summarizes the work done under that solicitation, and which focused on the differences in ultimate load prediction between the fully coupled and the sequentially coupled modelling approach. The analysis was conducted through aero-hydro-servo-elastic simulations of OWTs on a monopile and on a jacket substructure; these two are the most common substructures and are expected to be sited in different water depths and to have significantly different dynamic behaviors.

The research team consisted of NREL and two subcontractors: Keystone Engineering (KYS), and Moffatt and Nichol (M&N); the team encompasses the most experienced modeling and engineering capabilities in the U.S. offshore wind industry today.

The main objective of the study was to illustrate the differences between the two approaches to design and analyze OWTs, and to provide guidelines for improved and expedited convergence. The results obtained by this study underline the need for a more in-depth investigation of the differences noted between the two modeling approaches: although predictions tend to closely agree for most load channels, some larger differences indicate that the sequentially coupled approach can be less conservative under certain circumstances and load cases than the fully coupled one, especially for substructure loads.

This report is organized as follows. Section 3 offers details on the actual analysis procedure used. Section 4 describes the geographical and metocean parameters of the sites selected for the study including data such as: directional joint probability of wind speed, wave height, wave periods, water depth, and soil characteristics. The sites were selected in light of current and proposed developments along the East Coast of the U.S.. The turbine parameters are also shown in the same Section. In Section 5, an overview

of the support structures is provided. Section 6.4 discusses the main assumptions in the simulations and the load cases and conditions analyzed; the initial verification among all employed models is given in Section 7. Key results are discussed in Section 8. Conclusions with recommended future steps are given in Section 9.

3 Definition of the Analysis Methods

As mentioned above, the goal of the study was to compare current-practice methodology in offshore wind turbine design, which calls for a sequentially-coupled approach, to the more rigorous fully-coupled approach, which entails computing simultaneous aerodynamics, hydrodynamics, structural-dynamics, and control system effects. Sections 3.1-3.2 discuss the details of the two methods used in this study. NREL played the role of the turbine Original Equipment Manufacturer (OEM), and the subcontractors focused on their respective substructure analyses (KYS on the jacket, and M&N on the monopile configuration). The goal was to compare the Ultimate Limit States (ULS) loads resulting from a semi-coupled analysis against those derived from a fully-coupled approach, as this can help assess potential issues with the load predictions from the sequentially coupled approach. NREL performed the fully-coupled analysis, and also acted as the turbine operator for the semi-coupled approach. Two load cases were selected (see Section 6.4): a power production and an extreme event load case.

NREL used FAST8, an aero-hydro-servo-elastic computer-aided-design tool widely used in both the research and industry communities (NREL, 2016). NREL modified FAST8's modules SubDyn (substructure structural dynamics) and ElastoDyn (turbine structural dynamics) to include pile stiffness effects and to allow for the introduction of superelement matrices at the tower-substructure interface.

KYS and M&N utilized SACS® (Bentley Systems) and EDP (Extended Design Program by Digital Structures Inc.), two offshore structural analysis and design tools well known and proven in the oil and gas industry to model the substructure and hydrodynamic loads in the semi-coupled approach.

Just like in a real-world case, this project was conducted with physical separation between turbine and substructure designers, giving rise to the challenges associated with the sequentially coupled modelling approach (e.g., different modelling tools, data exchange protocols). Therefore, the various models built in FAST8 and in the subcontractors' software had to be cross-verified to guarantee matching of fundamental structural and hydrodynamic characteristics. NREL provided the substructure geometric and structural definition above the mudline (together with FAST8's SubDyn/HydroDyn input files) and the turbine tower and RNA structural and inertial properties. Pile head stiffness matrices were supplied by KYS and M&N as input to NREL's fully-coupled simulations in order to achieve a realistic representation of the pile/soil interaction, similar to the one that is modeled in SACS® and EDP.

To limit potential sources of error, the simulations performed using both methods utilized the same wave surface profile, wind inflow, and linearized soil stiffness.

The turbine specific loads (e.g. tower base and blade root moments) were calculated by NREL's FAST simulations. FAST8 was run with a simplified substructure matrix representation and externally

generated substructure loads for the sequentially coupled approach, and with a complete SubDyn substructure model and internally generated hydrodynamic loads in the fully coupled approach. The substructure member loads were computed by KYS and M&N for the sequentially coupled approach, and by NREL for the fully coupled approach.

3.1 Sequentially Coupled Analysis

The sequentially coupled analysis method still is the most common design method used in the offshore wind industry for fixed-bottom systems such as jackets and monopiles. The aerodynamic and hydrodynamic loads are calculated separately by the turbine OEM and the foundation designer, respectively. Loads and dynamic stiffness data are transferred between the two parties at the tower bottom flange (the interface). This method allows for maximum control of each party's responsibility and of the respective Intellectual Properties, with no exchange of the details of the turbine and substructure designs. Inherent to the sequentially coupled approach is also a clear separation of design related liability issues.

A super-element representation of the substructure and foundation (i.e., 6x6 stiffness, mass and damping matrices) is created by the foundation designers (KYS and M&N in this study) and included in the aero-servo-elastic (ASE) simulations (e.g., FAST8 in this study) run by the turbine OEM (NREL in this study) to account for the response of the structure below the tower. The loading effects on the turbine and tower due to the hydrodynamic forcing on the substructure are provided by the foundation designers as an equivalent load vector (three forces and three moments) time history at the tower bottom flange. The super-element and associated equivalent hydrodynamic forcing at tower-base is a simplified method to account in the ASE simulations for the compliance, damping, and excitation of the substructure during loads analysis simulations of the wind turbine.

To calculate this time history, the foundation designers run finite-element dynamic simulations of the sub-structure and calculate the distributed wave loads, which are then reduced to tower base using the same reduction bias as was used to generate the super-element. Note that wind loads are not included in this step.

The last step of this method requires one more exchange of time variant loads. The coupled tower-base loads as calculated by the ASE simulations are then transferred back to the foundation designers, who, in turn, perform new load calculations, subjecting the substructure to the original hydrodynamic forcing as well as the newly received loads at the tower bottom flange.

In summary, the steps followed for the sequentially coupled approach performed in this study are:

a. KYS/M&N (substructure designers) run hydrodynamic simulations on their respective substructure and linearized foundation. No representation of the turbine is considered in these simulations (only the substructure/hydrodynamics are modeled here),
b. KYS/M&N provide to NREL (representing the OEM) equivalent loads (3 forces and 3 moments) at tower base in ASCII, time-series format,

c. KYS/M&N provide to NREL tower-based loads and equivalent stiffness, mass, and damping matrices (K,M,C [6x6] matrices) for a superelement, referenced at the tower base, which represents the properties of the substructure and foundation,
d. NREL runs a variety of FAST8 simulations that include flexible RNA and tower, aerodynamic loads, and a superelement representation of the substructure (K,M,C matrices). Equivalent loads at the tower base are injected into the simulations based on the data from KYS/M&N to simulate the effects of the substructure hydrodynamic loading on the remainder of the offshore wind turbine,
e. NREL passes the resulting tower base loads from the FAST simulation outputs to KYS and M&N,
f. M&N and KYS run new simulations with their models of the substructure and foundation adding the loads at tower base provided by NREL, which represent aerodynamic and inertia loads originating from the turbine,
g. NREL post-processes FAST results for loads in the main components of the RNA and tower, using the simulation data from step d,
h. KYS and M&N post-process their respective simulation results for loads and deflections in the substructure components.

This process is illustrated by Figure 3.

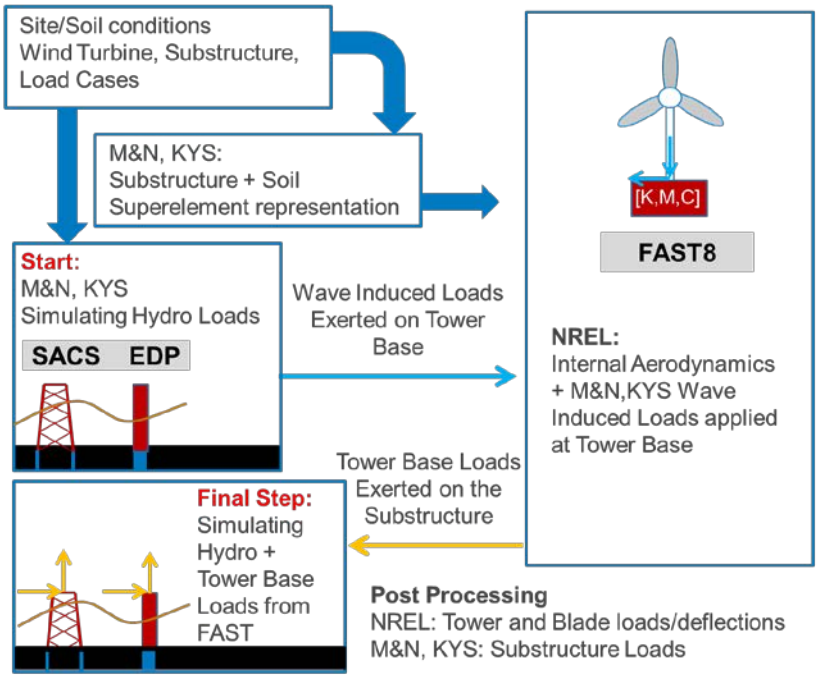

Figure 3. Schematics of the sequentially-coupled analysis method used in this study.

For an actual design application, KYS and M&N would assess their substructure design and potentially make adjustments to the wall thickness and geometry of the substructure. Once these adjustments are completed, the sequentially coupled analysis process will start over with step a). This process is repeated until the substructure design and the corresponding loads converge on a suitable solution.

Given the resource and time constraints associated with this project, only the one iteration (step a.) – h.)) was completed.

3.2 Fully Coupled Analysis

The fully coupled analysis method requires the use of an aero-hydro-servo-elastic (AHSE) computer-aided-engineering tool capable of simultaneously simulating aerodynamics, hydrodynamics, structural-dynamics, and control system effects on an offshore wind turbine. FAST8 is one such tool that was created by NREL and is publically available. In this study, we modeled the substructures (monopile and jacket) via FAST8's SubDyn module.

The fully coupled analysis only requires one entity (NREL in this study) to perform the AHSE simulations on the complete model of the offshore wind turbine, including RNA, tower, substructure, and foundation. The foundation is modeled by characteristic linear stiffness properties at the mudline as calculated by the substructure designers (KYS and M&N in this study). The fully coupled method is expected to yield more realistic load predictions, but also requires detailed design specifics on substructure and turbine to be exchanged by the various parties.

In summary, the steps followed for the fully coupled approach as performed in this study are:

i. KYS/M&N provide to NREL stiffness properties at the mudline ([6x6] stiffness matrix and apparent fixity pile properties)
j. KYS/M&N provide to NREL the wave elevation time series to calculate the hydrodynamic loads
k. NREL runs FAST simulations of the wind/wave DLCs considered, for the entire system: RNA, tower, substructure, and foundation, including aerodynamics, hydrodynamics, structural-dynamics and control system dynamics
l. NREL passes the resulting loads for the major components of the substructures to KYS and M&N for post-processing and comparison to the results from the sequentially-coupled approach
m. NREL post-processes loads for the major components of the turbine and RNA

This process is illustrated by Figure 4.

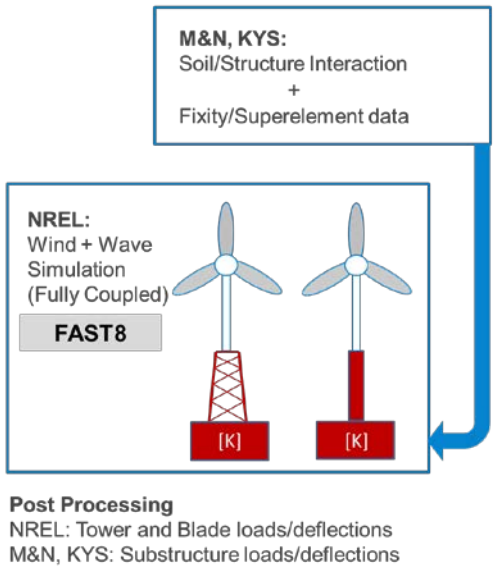

Figure 4. Schematics of fully-coupled analysis method.

Note that FAST8 was run with the same hydrodynamic and aerodynamic seeds as in the sequentially coupled analysis method to avoid artifacts in the comparison of the two methods. All the loads were extracted by NREL for the major components of both the turbine and substructure and compared to the sequentially-coupled method results.

4 Select Environmental and Turbine Parameters

4.1 Environmental Conditions

As mentioned above, two different OWT configurations were selected: the first configuration made use of a monopile, and therefore was suited for shallow waters (depths <30 m); the second configuration was based on a lattice substructure, or jacket, to be located in deeper waters (depths >50 m). Two suitable geographical sites were thus selected along the Eastern U.S. seaboard, where offshore wind development is currently taking place and wind energy areas have been leased. NREL proposed and BSEE approved the following two sites:

Table 1. Selected sites for the analysis.

Site No.	Location	Substructure Type	Actual Depth / Modeled Depth
1	Frying Pan Shoals, NC	Monopile	23.5 m / 20 m
2	Long Island, NY	Multimember (Jacket)	40.8 m / 50 m

4.1.1 Frying Pan Shoals (NOAA Buoy 41013):

The selected site for the monopile study is located within the proposed North Carolina Offshore Wind Call Area (Wilmington East) as announced by BOEM on August 11th 2014. The water depth and wave characteristics (given in Figure 7) correspond to the location of NOAA Buoy 41013 as seen in Figure 5.

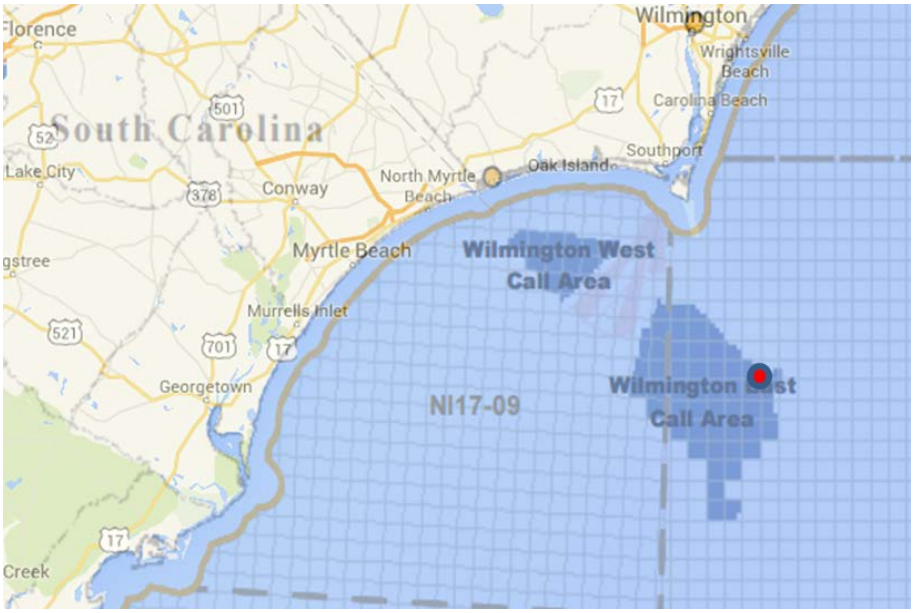

Figure 5. Location of NOAA Buoy 41013 within Wilmington East Call's area (indicated by the red dot).

4.1.2 Long Island Site (NOAA Buoy 44025):

The selected site for the multimember configuration is located within the New York lease area OCS-A 0512 announced by BOEM on March 15th 2017. The water depth and wave characteristics (given in Figure 8) correspond to the location of NOAA Buoy 44025 as seen in Figure 6.

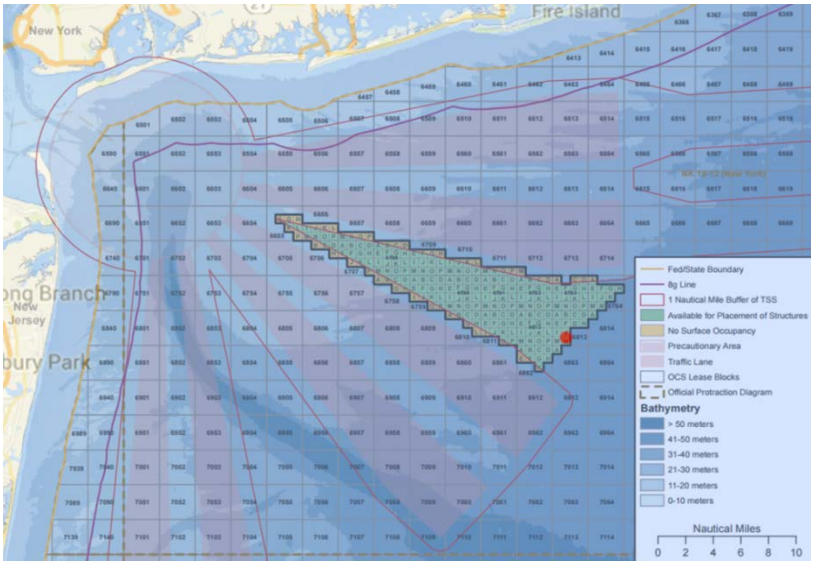

Figure 6. Location of NOAA Buoy 44025 within New York's offshore wind energy area (indicated by the red dot).

4.1.3 Overview of Metocean Conditions:

Since both locations coincide with NOAA buoys, detailed information regarding the wave and wind conditions is available in the public domain. Table 2 gives water depth and 50-yr significant and maximum wave-heights for both sites. This information is based on the analysis presented in (Damiani, Dykes, & Scott, 2016). Figure 7 shows the wave-height as a function of hub-height (90m above MSL) wind speeds at the North Carolina site; Figure 8 gives the same information for the Long Island site. In order to correlate wave height and wave period with hub-height wind speed, the NOAA buoy wind speed data has been extrapolated to hub-height (90m) using a vertical wind shear exponent of 0.1, which is often times used for offshore locations. The wave height and wave period data shown in Figure 7 and Figure 8 is based on binned measurement data from 1991-2000 for Long Island and 2003-2011 for Frying Pan Shoals.

Ocean currents were analyzed following the IEC standard (International Electrotechnical Commission, 2008) guidance for normal current model and extreme current model (more in Section 6.4), with both wind-driven near-surface currents, and subsurface currents. The former were aligned with the assumed wind directions, whereas the latter were assumed aligned with the wave propagation directions.

Table 2. 50-yr extreme metocean conditions at the two sites seleced for this study.

		50-yr 1-hr Wave		
Site Name	**NOAA BUOY #**	**Hs [m]**	**Tp_Hmax [s]**	**Hmax(*) [m]**
FRYING PAN SHOALS	41013	10.8	13.3	18.3
LONG ISLAND	44025	9.5	12.5	17.6

(*) Hmax was limited to the breaking wave height

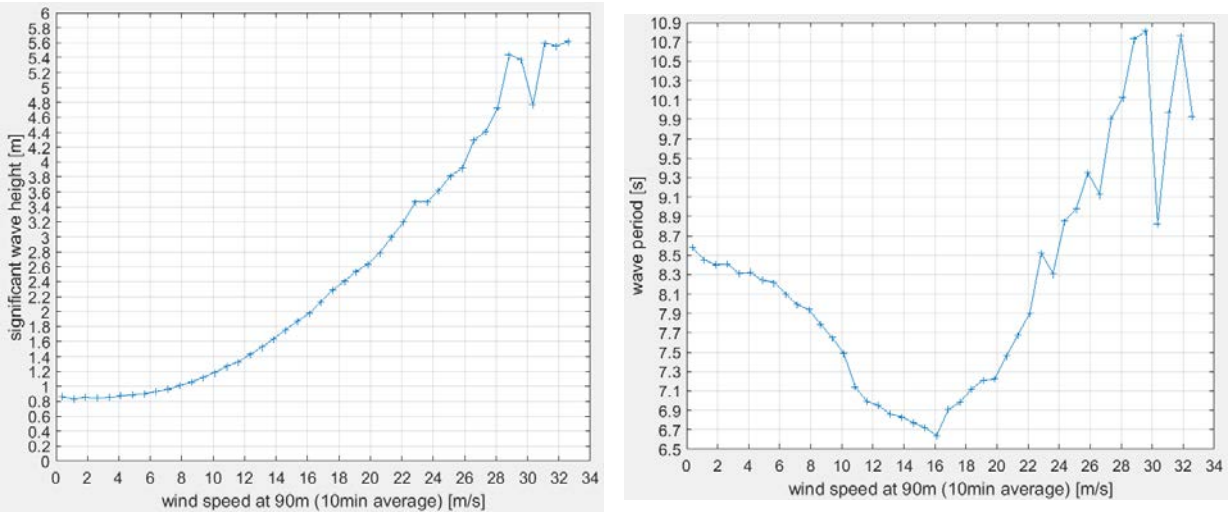

Figure 7. Significant wave height (left-hand side) and peak spectral period (right-hand side) as a function of wind speed at hub-height for the Frying Pan Shoals site.

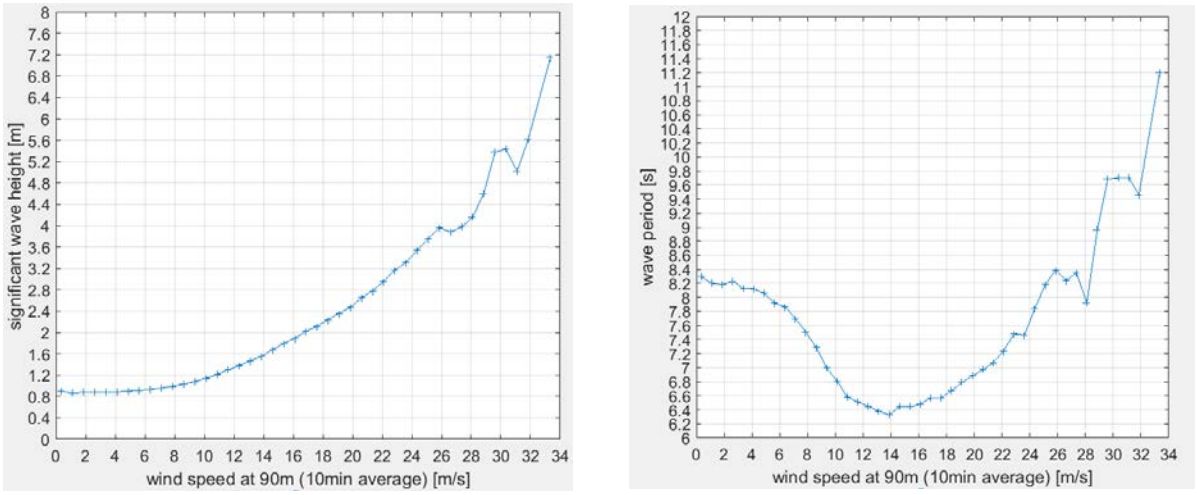

Figure 8. Significant wave height (left-hand side) and peak spectral period (right-hand side) as a function of wind speed at hub-height for the New York wind energy area site.

4.1.4 Characterization of Soil Conditions:

Unfortunately soil stratigraphic information was not publically available for the two sites of interest, therefore an approximate soil profile was used for both sites. This soil profile is representative of sand layers, with the least dense top layer (dynamically "softest" stiffness) being the largest contributor to the dynamic response of the system. The simplified stratigraphy profile is given in Table 3.

Moffatt & Nichol and Keystone Engineering calculated equivalent stiffness matrices at the pile heads (mudline) to be used both in their respective simulations as well as by NREL. The subcontractors further provided stiffness, mass, and damping matrices of the equivalent super-elements (substructure plus foundation effects) at the tower-base flange.

Table 3. Soil stratigraphy profile assumed for this study.

Depth [m]	Specific weight [kN/m^3]	Friction Angle [deg]
0-5	10	33
5-14	10	35
14-55.5	10	38.5

4.2 Wind Turbine Configuration

The NREL 5MW (Jonkman, Butterfield, Musial, & Scott, 2009) turbine was utilized for this study. The turbine key parameters are shown in Table 4. Note that the hub-height was maintained constant throughout the study, and therefore different towers were utilized for the monopile and the jacket substructures to account for different tower interface heights associated with the two substructures. In Table 4, the acceptable range of first eigenfrequencies is shown. That frequency band was used by the subcontractors as an aid in the design of the piling. The lower bound was calculated as 1.1 times the

upper limit 1P (rotor passing) frequency and the upper bound as 0.9 times the lower limit of the 3P (blade passing) frequency.

Table 4. Turbine key parameters.

Parameter	Value
Rating	5 MW
IEC Class	I-B
Rotor Configuration	Upwind, 3 blades
Control	Variable speed, collective pitch
Drivetrain	High-speed, multi-stage gearbox
Rotor/hub diameter	126m, 3m
Hub-height	90 m
Cut-in, rated, cut-out wind speeds	3 , 11.4, 25 m/s
Cut-in, rated, cut-out rotor speeds	6.9, 12.1 RPM
Rated tip speed	80 m/s
Overhang, shaft tilt, precone	5 m, 5°, 2.5°
Rotor mass	110, 000 kg
Nacelle mass	240,000 kg
Acceptable system 1st eigenfrequency range	(0.22 ; 0.31 Hz) Soft-stiff

5 Support Structure Definition

Two substructure designs were selected based on the availability of their design specifics as public domain data:

- The OC3 Monopile design (Jokman & Musial, 2010) was chosen as a good representation of the expected monopile response in shallow waters (<40 m water depths).
- The OC4 Jacket design (Popko, Vorprahl, Zuga, Kohlmeier, Jonkman, & Robertson, 2012) was chosen as a representative model of a multipile, multimember, lattice structure in transitional waters (40--60m water depths)

5.1 Overview of the Monopile Configuration

The OC3 monopile configuration is made up of a constant cross-section (outer diameter 6 m with a wall thickness of 0.060 m) which assumes a 36 m embedment length. The tower base connects at an elevation of 10 m above the mean-sea level (MSL).

The monopile extends from the tower base down to the mudline, which is at 20 m below MSL. Construction steel with a Young's modulus of 210×10^9 Pa, shear modulus of 80.8×10^9 Pa, and an effective density of 8,500 kg/m^3 was assumed as the main structural material. The value of 8,500 kg/m^3 is meant to be an increase above steel's typical value of 7,850 kg/m^3 in order to account for the secondary mass of paint, bolts, welds, and flanges not directly included in the engineering models used in this study.

The tower base diameter (6 m) and thickness (0.027 m) linearly taper to a top diameter of 3.87 m and a thickness of 0.019 m at a height of 87.6 m above MSL; the effective mechanical steel properties of the tower used in the DOWEC study, as given in Table 9 on page 31 of (Kooijman, Lindenburg, Winkelaar, & van der Hooft, 2003), were assumed. The resulting distributed support structure properties are given in Table 5. A detailed description of the OC3 Monopile can be found at (Jokman & Musial, 2010). Note that the OC3 transition piece was modeled as an integral part of the monopile, with no special arrangements or provisions for its analysis.

A structural damping ratio of 1% of critical was assumed.

Table 5. Distributed properties for the monopile and tower used in this study for the Frying Pan Shoals site.

Z MSL [m]	TMassDen [kg/m]	TwFAStiff [Nm^2]	TwSSStif [Nm^2]	TwGJStif [Nm^2]	TwEAStif [N]	TwFAIner [kg m]	TwSSIner [kg m]	TwFAcgOf [m]	TwSScgOf [m]
-56	9517.14	1.04E+12	1.04E+12	7.98E+11	2.35E+11	41979.2	41979.2	0	0
-20	9517.14	1.04E+12	1.04E+12	7.98E+11	2.35E+11	41979.2	41979.2	0	0
10	9517.14	1.04E+12	1.04E+12	7.98E+11	2.35E+11	41979.2	41979.2	0	0
10	4306.51	4.74E+11	4.74E+11	3.65E+11	1.06E+11	19205.6	19205.6	0	0
17.76	4030.44	4.13E+11	4.13E+11	3.18E+11	9.96E+10	16720	16720	0	0
25.52	3763.45	3.58E+11	3.58E+11	2.75E+11	9.30E+10	14483.4	14483.4	0	0
33.28	3505.52	3.08E+11	3.08E+11	2.37E+11	8.66E+10	12478.7	12478.7	0	0
41.04	3256.66	2.64E+11	2.64E+11	2.03E+11	8.05E+10	10689.2	10689.2	0	0
48.8	3016.86	2.25E+11	2.25E+11	1.73E+11	7.45E+10	9098.9	9098.9	0	0
56.56	2786.13	1.90E+11	1.90E+11	1.46E+11	6.88E+10	7692.7	7692.7	0	0
64.32	2564.46	1.59E+11	1.59E+11	1.23E+11	6.34E+10	6455.7	6455.7	0	0
72.08	2351.87	1.33E+11	1.33E+11	1.02E+11	5.81E+10	5373.9	5373.9	0	0
79.84	2148.34	1.10E+11	1.10E+11	8.43E+10	5.31E+10	4433.6	4433.6	0	0
87.6	1953.87	8.95E+10	8.95E+10	6.89E+10	4.83E+10	3622.1	3622.1	0	0

The geometry of the embedded portion of the monopile is given in Table 6. The pile was sized based on extreme loads calculated from maximum operational and parked load cases assuming the metocean conditions discussed above. M&N verified the capacity of the pile under maximum wave, current, and thrust from the turbine.

Table 6. Embedded pile geometry.

Depth below mudline [m]	OD [m]	t [m]
0-36	6	0.06

Finally a summary of the undistributed properties of the support structure is shown in Table 7.

Table 7. Undistributed properties for the support structure (monopile configuration).

Parameter	Value
Tower-Top Height above MSL	87.6 m
Tower-Base Height above MSL	10 m
Overall Mass	522,617 kg
C.G. location (w.r.t. mudline along tower centerline)	37.172 m
Structural Damping Ratio (all modes)	1%

5.2 Overview of the Jacket Configuration

A drawing of the OC4 Jacket (traditional four legged jacket with cross braces) is shown in Figure 9, which also highlights the monolithic transition piece (TP) used. The TP is a complex subcomponent of the support structure, which would require a dedicated study for its design and analysis, especially with regard to fatigue. Because the primary focus of this study lies on ULS analysis, the OC4 simplified model of the TP was deemed sufficient to highlight differences in the employed calculation methods. In future studies, the TP geometry should be defined with care and then an FLS analysis could be carried out by following the approaches indicated in this study (see also Section 3).

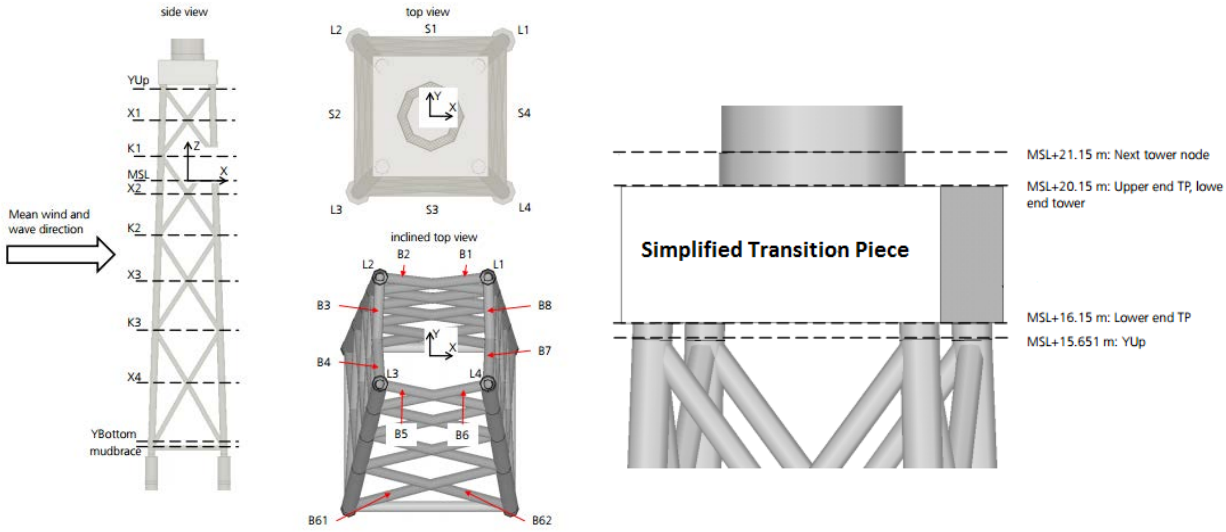

Figure 9. Overall schematic of the jacket and transition piece for the multimember substructure used in this study.

A detailed description of the OC4 Jacket can be found in (Vorprahl, Popko, & Kaufer, 2013). The tower distributed mass and stiffness properties are given in Table 8. The tower for this configuration has a base diameter of 5.6 m with a wall thickness of 0.032 m, whereas at the top the outer diameter is 4 m and the wall thickness is 0.03 m.

Table 8. Distributed properties for the tower on top of the Jacket.

Z MSL [m]	TMassDen [kg/m]	TwFAStiff [Nm^2]	TwSSStif [Nm^2]
20.15	4900.473	4.56E+11	4.56E+11
21.85	4900.473	4.44E+11	4.44E+11
25.25	4200.272	4.17E+11	4.17E+11
28.65	4057.18	3.91E+11	3.91E+11
32.05	3915.575	3.67E+11	3.67E+11
35.45	3770.476	3.42E+11	3.42E+11
38.85	3626.859	3.19E+11	3.19E+11
42.25	3477.86	2.97E+11	2.97E+11
45.65	3291.027	2.72E+11	2.72E+11
49.05	3102.113	2.48E+11	2.48E+11
52.45	3123.485	2.26E+11	2.26E+11
55.85	2969.644	2.07E+11	2.07E+11
59.25	2639.437	1.91E+11	1.91E+11
62.65	2517.769	1.76E+11	1.76E+11
66.05	2398.659	1.62E+11	1.62E+11
69.45	2282.134	1.49E+11	1.49E+11
72.85	2173.814	1.37E+11	1.37E+11
76.25	2344.182	1.42E+11	1.42E+11
79.65	2687.067	1.57E+11	1.57E+11
83.05	2971.055	1.69E+11	1.69E+11
86.45	3260.985	1.60E+11	1.60E+11
88.15	3260.985	1.55E+11	1.55E+11

The geometry of the piles is given in Table 9. The piles were sized based on extreme loads calculated from maximum operational and parked load cases assuming the metocean conditions discussed above. Similarly to what was done for the monopile by M&N, KYS verified the capacity of the pile under maximum wave, current, and thrust from the turbine.

Table 9. Embedded pile geometry.

Depth below mudline [m]	OD [m]	t [m]
0-55.5	2.082	0.06

6 Modeling Assumptions and Design Load Cases

6.1 Hydrodynamics

Because of the limited resource for this study, all models were analyzed in a ‘clean’ condition (no marine growth). Additionally, no “constrained” waves and no stretching were considered in this study. Wave stretching models provide a more realistic representation of the near-surface wave kinematics than

linear wave theory (Airy, 1841). However, different wave stretching schemes exist in the literature, and important differences exist in the various software implementations, which can give rise to significantly different structural responses (Rodenbusch & and Forristall, 1986). In order to minimize the effects of different hydrodynamics models on the results of the two investigated approaches to the analysis of offshore wind turbines, only linear wave (Airy) theory was considered. Constrained waves, which are large, deterministic waves embedded in a typical stochastic wave time-history profile were not included in this study for two reasons. First and foremost, constrained waves are thought to be most important for relatively static structures (such as oil and gas fixed-bottom platforms) and less for highly dynamic response machines such as wind turbines, where stochasticity is crucial. Second, this method suggested in (International Electrotechnical Commission, 2008) is computationally inefficient and requires extensive pre-processing time (Rainey & Camp, 2007), which was not available to this study. New and more efficient methods have recently been proposed in the literature. Future research could include this effect in this type of investigation.

6.2 Coordinate Systems, Load Channels and Substructure Nodes of Interest

Global and local coordinate systems were established at the beginning of the analysis and agreed upon by all team members (see Figure 10a).

For loads on the tower and monopile the global coordinate system, where the x-axis is aligned with the nominal wind direction, the z-axis points upward, and the y-axis is determined by right-hand rule. For the jacket members, a local coordinate system is also employed (see Figure 10b), with the z-axis along the member axis, the x-axis in the horizontal plane, and the y-axis is determined by right-hand rule.

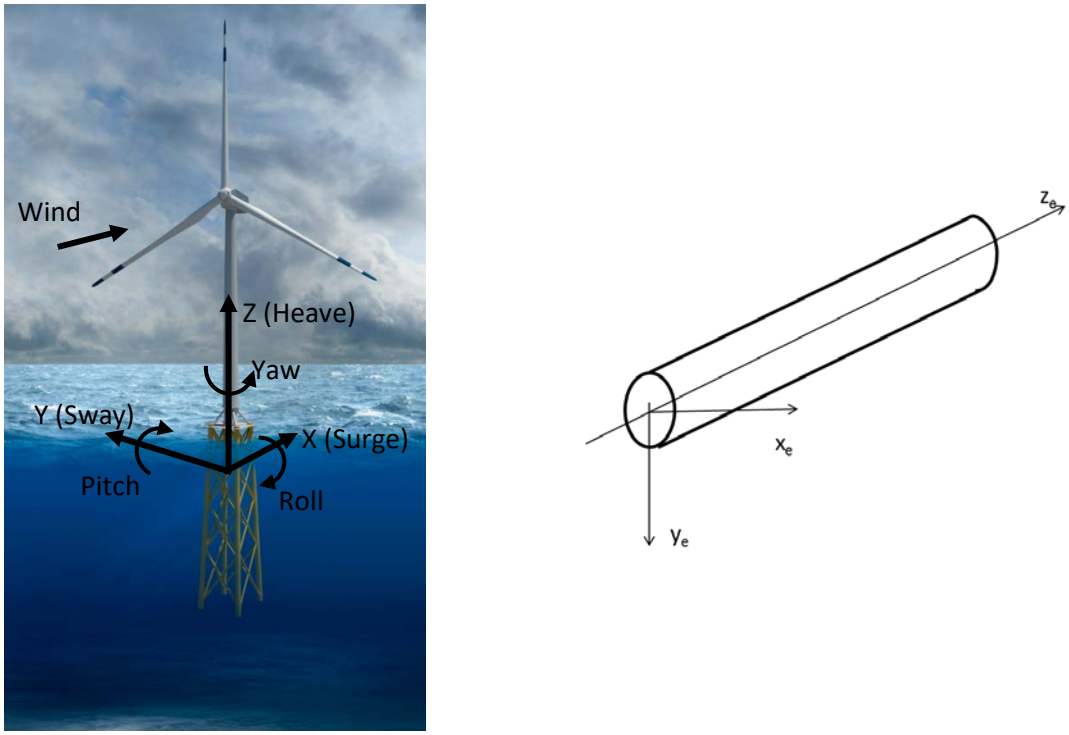

Figure 10. Global coordinate system (a) and local coordinate system for a typical structural member (b).

For blade loads, the coordinate system has the z-axis along the blade axis, the y-axis along the chord, and the x-axis is determined by right-hand rule (see Figure 11a). The low-speed shaft coordinate system has the x-axis aligned with the shaft axis, the z-axis pointing upward, and the y-axis is determined by right-hand rule (see Figure 11b).

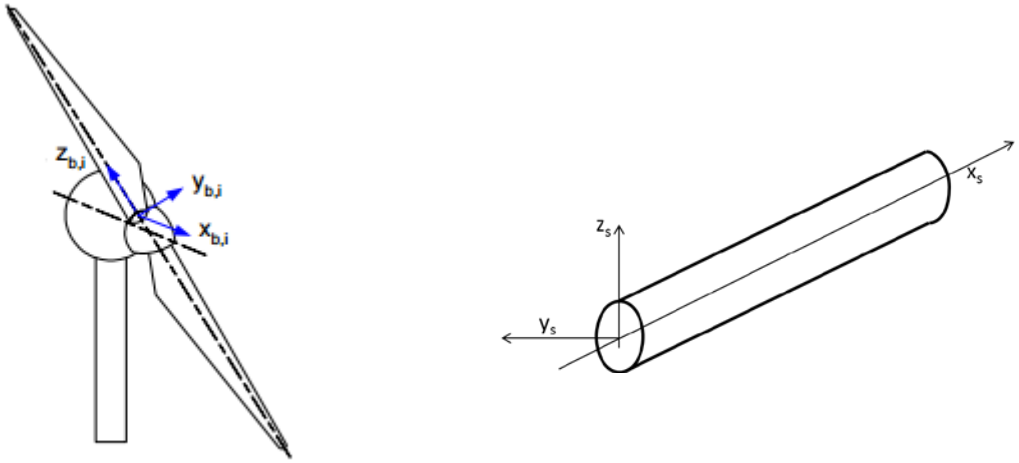

Figure 11. Blade (a) and shaft (b) local coordinate systems.

6.2.1 Load Channels

For the comparison between fully coupled and sequentially coupled approaches, we considered two sets of load channels, one for the RNA and tower, and one for the substructure.

The RNA and tower loads included: blade root loads, low speed shaft loads, tower-top (denoted as yaw-bearing) loads, and tower bottom loads (see also Table 10). For the blade root loads, we calculated shears (Fx, Fy) and bending moments (Mx, My) per the blade coordinate system. For completeness, we also included the axial force (Fz) and torsion (Mz), although these are not accounting for dynamic extensional effects and the torsional degree of freedom of the blades. These latter loads are, for typical rotor sizes and stiffness, relatively small and not driving the design. Nonetheless, future rotor blades (longer and slenderer) might present significant torsional and axial loads, and this aspect should be revised.

Shaft loads included bending moments (My, Mz, i.e. pitch and roll bending moments) per the coordinate system in Figure 11b. Yaw-bearing and tower base loads included three forces (Fx, Fy, Fz) and three moments (Mx, My, Mz) per the global coordinate system.

Table 10. RNA and tower load symbols.

Component	Load	Symbols used in the Graphs
Blade Root	Fx--Fz, Mx--Mz	BladeRootFx, BladeRootFy, BladeRootFz, BladeRootMx, BladeRootMy, BladeRootMz
Shaft	My, Mz	LSSMy, LSSMz
Yaw Bearing (Tower Top)	Fx--Fz, Mx--Mz	YawBearingFx, YawBearingFy, YawBearingFz, YawBearingMx, YawBearingMy, YawBearingMz
Tower Base	Fx--Fz, Mx--Mz	TowerBaseFx, TowerBaseFy, TowerBaseFz, TowerBaseMx, TowerBaseMy, TowerBaseMz

For the monopile, we compared the loads at the stations located at 0 m MSL (Mx, My), -10 m MSL (Mx, My), and mudline (Fx, Fy, Fz, Mx, My, Mz) per the global coordinate system.

Figure 12 and Table 11 show the selected nodes of the jacket where certain load components (per the member coordinate system) where extracted and compared between the two methods. K1L1 and K1L2 represent upper leg nodes (upwind and downwind, respectively), where axial forces were extracted for leg members 23 and 19; K4L2 and K4L1 represent lower leg nodes, where axial forces and bending moments were extracted for brace members 37, 41, 45, and 47; RL2 and RL1 represent pile head locations at the mudline (upwind and downwind, respectively), where all six components of internal loads were calculated.

Table 11. Nodes and members analyzed for the jacket, including what load components were considered.

Node	Member	Load	Symbols used in the Graphs
K1L2	23	Fz	K1L2
K1L1	19	Fz	K1L1
K4L2	41	Mx, My, Fz	K4L2_YZ
K4L2	47	Mx, My, Fz	K4L2_XZ
K4L1	37	Mx, My, Fz	K4L1_YZ
K4L1	45	Mx, My, Fz	K4L1_XZ
K5L2	33	Fz	K5L2
RL2	111	Fx--Fz, Mx--Mz	RL2
RL1	109	Fx--Fz, Mx--Mz	RL1

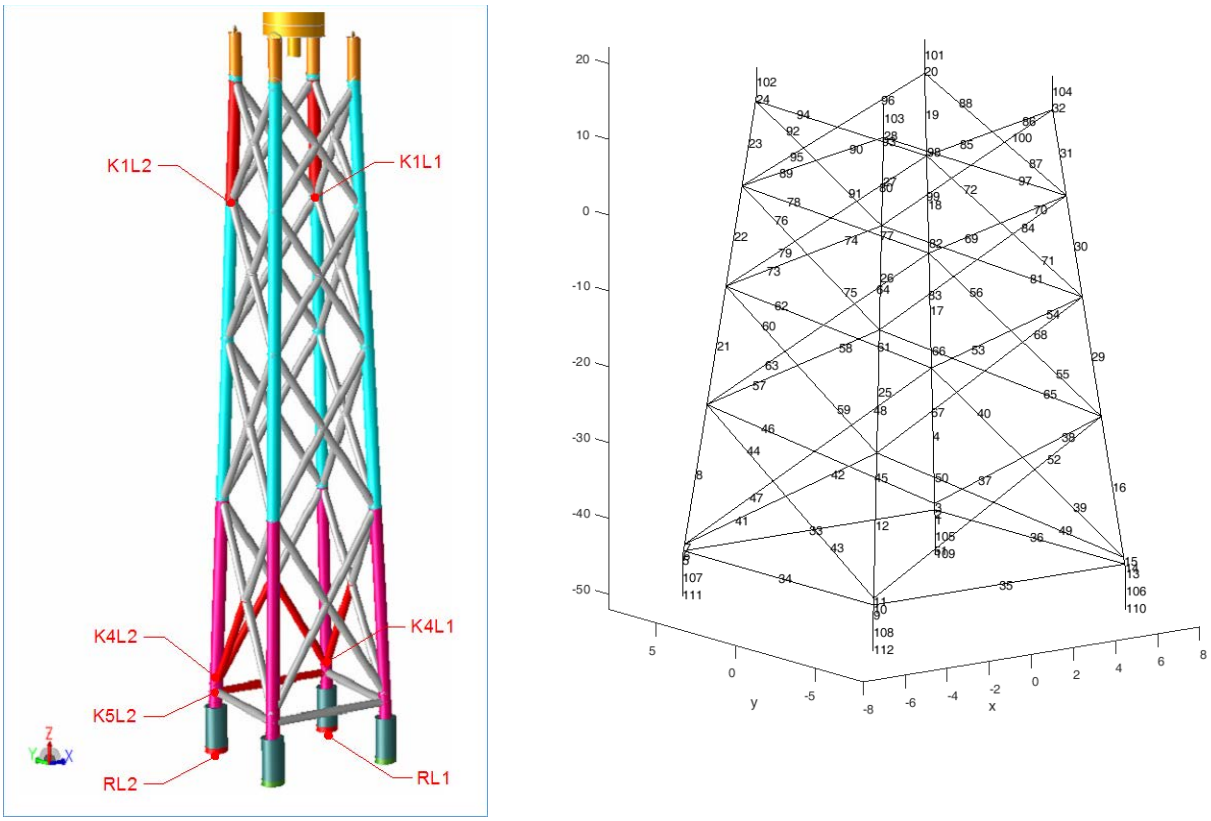

Figure 12. Nodes of interest for the jacket substructure from which loads were extracted and compared between the two approaches (left). Member numbers (right).

6.3 Exchange Data Format

All data was exchanged via either text (ASCII) or Excel files. Version control of all the files was implemented to account for modifications and iterations among all parties involved.

6.4 Design Load Cases

The DLCs presented in Table 12 are a subset of those prescribed by the IEC design standard 61400-3 (International Electrotechnical Commission, 2008); these DLCs are generally driving cases for OWT design and were selected for this study because they should provide sufficient information to emphasize differences in the methodology (fully coupled vs. sequentially coupled). Two main categories are selected: a power production set (DLC 1.1) and a parked (extreme event) set (DLC 6.1).

The selected wave conditions were based on the site specific conditions detailed in Section 4.1. The selected 50-year extreme wind speed for DLC 6.1a is based on the requirements for a Class I turbine as specified in the IEC-61400-1 standard. The selected sub-surface current speeds are based on ocean surface current data from NASA (NASA) and further discussions with the partners. The tidal conditions are based on the analysis in (Damiani, Dykes, & Scott, 2016) and further discussions with the partners. A JONSWAP spectrum was used for all simulations, with a shape factor of 3.3. The effective simulation length was set at 600 s; 150 s of transient time was discarded prior to the actual 600 s simulation output. During an actual industry project, at least 6 seeds would be considered to achieve a statistically sound representation of the entire wave spectrum. Given the limited resources allocated to this project,

only one seed was analyzed. However, since the nature of this project is focused on the identification of differences between the two modelling approaches and not on the development of an actual substructure design for a given site, a single seed was deemed sufficient. Subsurface currents were aligned with the wave direction, whereas surface currents were aligned with the wind direction. For the monopile, only the 0 degree wind direction was used, because of the axial symmetry of the structure. Further to note is the fact that the wave time series were generated by M&N and KYS and used by NREL for both the sequentially coupled and the fully coupled approach as direct inputs to the aero-hydro-servo-elastic software. To minimize potential issues related to different hydrodynamic modelling approaches, simple linear airy wave theory without any additional free surface treatment was used by all project partners.

In order to have a common nomenclature among all parties and to distinguish the results from various load cases, Table 13 and Table 14 show the identifiers used for the design load cases, together with the simulated key environmental parameter values.

Table 12. Load cases analyzed in this study.

DLC-1.1 (Normal power production):		
Wind model:	NTM	
Wind Speeds (WS):	12 m/s at hub height (90m)	
Wind Direction (WD):	0, 45	
Wave Model:	NSS	
	Jacket:	Hs=1.3410 m, Tp=6.4792 s
	Monopile:	Hs=1.3813 m, Tp=6.9695 s
Wave Direction:	0, 45, 90, 135	
Current Model:	NCM	
	Jacket:	Sub-surface current at still water level: 0.6 m/s
		Near-surface current (20 m reference depth): 0.0838 m/s
	Monopile:	Sub-surface current at still water level: 0.6 m/s
		Near-surface current (20 m reference depth): 0.0838 m/s
Tidal conditions: NWLR		
	Jacket:	0 m tidal offset
	Monopile:	0 m tidal offset
Sim. Length:	10min	
Max (*) number of simulations:	**1**WS x **2**WD x **4**Wave Direction = **8 (Jacket)**	
	1WS x **1**WD x **4**Wave Direction = **4 (Monopile)**	
DLC-6.1a (Parked with grid loss, 50 year extreme conditions):		
Wind model:	EWM Turbulent wind model	
Wind Speeds (WS):	50 m/s at hub height (90m)	
Wind Direction (WD):	0, 45 degrees	
Wave Model:	ESS	
	Jacket:	Hs=09.5 m, Tp=12.5 s
	Monopile:	Hs=10.8 m, Tp=13.3 s
Wave Orientations:	COD and MIS 90	
Current Model:	ECM	
	Jacket:	Sub-surface current at still water level: 1.2 m/s
		Near-surface current (20 m reference depth): 0.349 m/s

	Monopile:	Sub-surface current at still water level: 1.2 m/s Near-surface current (20 m reference depth): 0.349 m/s
Tidal conditions:	EWLR	
	Jacket:	+2.50m combined surge/tidal offset
	Monopile:	+1.25m combined surge/tidal offset
Sim. Length:	10min	
Yaw Misalignments [deg]:	0, 10	
Max (*) number of simulations:		**1**WS x **2** WD x **2** Wave Directions x **2**YawErrors = **8 (Jacket)** **1**WS x **1** WD x **2** Wave Directions x **2**YawErrors = **4 (Monopile)**

Table 13. Load cases Identifiers and key parameters for the monopile analysis.

Design Load Case	Identifier	Wind Speed, Vhub	Wave & Subsurface Current Direction	Yaw Error	Sea State	Significant Wave Height	Peak Spectral Period	Storm Surge
		[m/s]	[deg]	[deg]		[m]	[sec]	[m]
1.1	**A001**	12	0	0	NSS	1.3813	6.9695	0
1.1	**A002**	12	45	0	NSS	1.3813	6.9695	0
1.1	**A003**	12	90	0	NSS	1.3813	6.9695	0
1.1	**A004**	12	135	0	NSS	1.3813	6.9695	0
6.1a	**B001**	50	0	0	ESS	10.8000	13.3000	1.25
6.1a	**B002**	50	0	10	ESS	10.8000	13.3000	1.25
6.1a	**B003**	50	90	0	ESS	10.8000	13.3000	1.25
6.1a	**B004**	50	90	10	ESS	10.8000	13.3000	1.25

Table 14. Load cases Identifiers and key parameters for the jacket analysis.

Design Load Case	Identifier	Wind Speed, Vhub	Wind Direction	Wave & Subsurface Current Direction	Yaw Error	Sea State	Significant Wave Height	Peak Spectral Period	Storm Surge
		[m/s]	[deg]	[deg]	[deg]		[m]	[sec]	[m]
1.1	**A001**	12	0	0	0	NSS	1.341	6.4792	0
1.1	**A002**	12	0	45	0	NSS	1.341	6.4792	0
1.1	**A003**	12	0	90	0	NSS	1.341	6.4792	0
1.1	**A004**	12	0	135	0	NSS	1.341	6.4792	0
1.1	**A005**	12	45	0	0	NSS	1.341	6.4792	2.5
1.1	**A006**	12	45	45	0	NSS	1.341	6.4792	2.5
1.1	**A007**	12	45	90	0	NSS	1.341	6.4792	2.5
1.1	**A008**	12	45	135	0	NSS	1.341	6.4792	2.5
6.1a	**B001**	50	0	0	0	ESS	9.500	12.5000	2.5
6.1a	**B002**	50	0	0	10	ESS	9.500	12.5000	2.5

6.1a	**B003**	50	0	90	0	ESS	9.500	12.5000	2.5
6.1a	**B004**	50	0	90	10	ESS	9.500	12.5000	2.5
6.1a	**B005**	50	45	45	0	ESS	9.500	12.5000	2.5
6.1a	**B006**	50	45	45	10	ESS	9.500	12.5000	2.5
6.1a	**B007**	50	45	135	0	ESS	9.500	12.5000	2.5
6.1a	**B008**	50	45	135	10	ESS	9.500	12.5000	2.5

7 Model to Model Verification

Prior to initiating the load simulations for the selected DLCs, the team performed a set of dedicated analyses to verify that the respective models were consistent in terms of overall mass and inertial properties. This activity required extensive quality control activities by all parties and it was particularly time consuming as it required several iterations to arrive at a common basis among all models with several modifications to the inputs and assumptions (coordinate systems, retained degrees of freedom, member flooding, units, definition of wave, wind , current directions and profiles) among the various software programs. The first set of comparisons was done between the standalone SubDyn (FAST8's substructure structural dynamics module) and SACS/EDP. Mass, buoyancy, CG location, and eigenfrequencies of the substructures above the mudline were compared, while also considering stiffness effects at the pile heads. A brief summary of this initial validation step is given in Table 15 and Table 16. The difference in dry mass for the jacket is simply due to the way the transition piece is modeled in FAST8 (included as a lumped mass in the ElastoDyn module input and transparent to SubDyn) and in SACS (included in the jacket model), and was therefore expected and did not cause any issue. Eigenfrequencies were also assessed for the entire OWT, and in this case, the FAST8 results were post-processed via spectral analysis and compared to M&N's and KYS's model data (see Table 17).

Table 15. Comparison of overall inertial properties among different models.

Parameter	Monopile			Jacket		
	FAST	EDP	**Delta %**	FAST	SACS	**Delta %**
Tower Mass [kg]	237098	237001	0.04	216614	219800	-1.47
Tower Z-CG abv. SWL [m]	43.821	43.87	-0.11	50.55	49.83	1.43
RNA Mass [kg]	350000	350000	0.00	350000	350000	0.0001
RNA Z-CG abv. SWL [m]	89.571	89.57	0.00	89.57	89.57	0.0015
Substructure Mass (dry) [kg]	2.86E+05	285432	0.03	6.74E+05	6.86E+05	-1.80
Substructure Z-CG (dry) abv. SWL [m]	-5	-5	0.00	-21.90	-22.36	-2.08
Transition Piece Mass [kg]					666000	-
Overall Mass (dry) [kg]	8.73E+05	872433	0.02	1.24E+06	1.92E+06	-54.92
Submerged Volume [m^3]	5.65E+02	565.49	0.00	497.36	497.31	0.01
Ballasted Volume [m^3]	0.00E+00	0	0.00	199.59	199.55	0.02
Buoyant Volume [m^3]				297.77	297.76	0.00

Table 16. Comparison of First eigenfrequencies for monopile and jacket among different models.

	Monopile (Only Substructure)			Jacket (Only Substructure)		
Eigenfrequency [Hz]	FAST	EDP	**Delta %**	FAST	SACS	**Delta %**
	2.75E+00	2.76	-0.265	2.756	2.676	2.892
	2.75E+00	2.76	-0.265	2.756	2.676	2.888
	5.93E+00	5.93	0.019	5.004	5.25	-4.915
	1.63E+01	16.78	-2.976	5.413	-	-
	1.63E+01	16.78	-2.976	7.634	7.427	2.709

Table 17. Comparison of first eigenfrequencies for monopile- and jacket-based OWT systems among different models

	Monopile OWT			Jacket OWT		
Eigenfrequency [Hz]	FAST	EDP	**Delta %**	FAST	SACS	**Delta %**
	0.23	0.246	-7.052	0.3	0.3	-1.043
	0.24	0.246	-2.592	0.3	0.3	-1.542
	1.42	1.47	-3.5	0.94	0.9	4.213
	1.33	1.47	-10.511	0.93	0.91	1.798
				2.06	1.73	15.967

Overall differences were less than about 3%, except for eigenfrequencies above the fourth mode.

A second level of verification entailed comparing the dynamic response of NREL's FAST8 full OWT model to M&N's and KYS's models for a few simple cases. In fact, because the hydrodynamic loads were to be computed by M&N and KYS for the sequentially coupled approach and by NREL for the fully coupled approach, it had to be ensured that all team members utilized a consistent hydrodynamic modelling approach. A comparison of the hydrodynamic loads time series for a simple test case for Monopile and jacket are shown below in Figure 13-Figure 16.

For the monopile, we considered a power production case (e.g., A001) with a regular (sinusoidal) wave of 1.3813 m height and 6.9695 s period.

For the jacket we performed the verification on DLC A001-A003 and B001, B003, and B005.

As can be seen from Figure 13--Figure 16, relatively good agreement was achieved in the loads calculated in the substructures, which instilled confidence in both the overall calculation process and the hydrodynamic modeling assumptions.

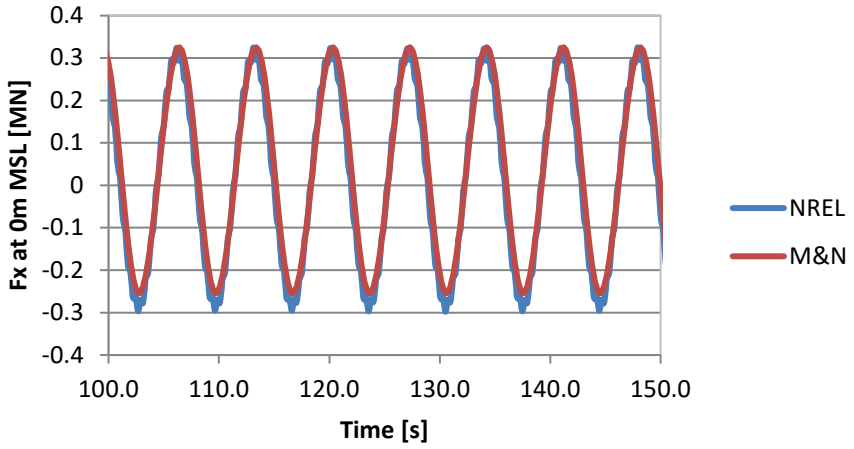

Figure 13. Monopile shear at MSL as calculated by NREL and M&N for a simple test case (H=1.3813 m, Tp=6.9695 s).

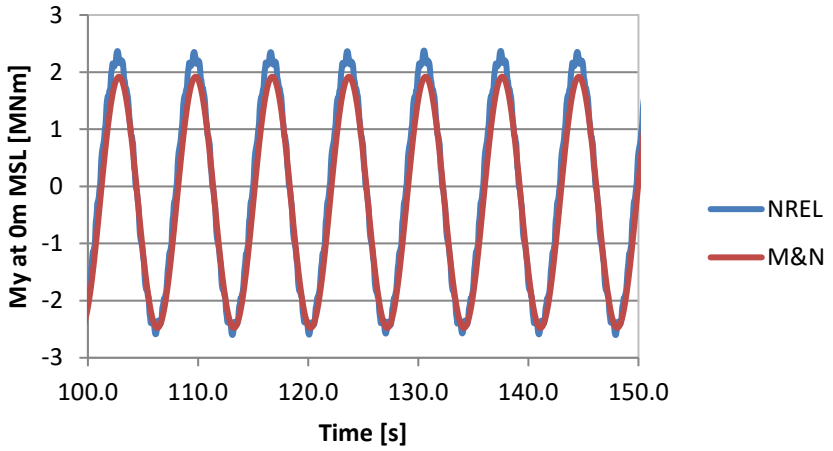

Figure 14 Monopile MSL overturning moment calculated by NREL and M&N for a simple test case (H=1.3813 m, Tp=6.9695 s).

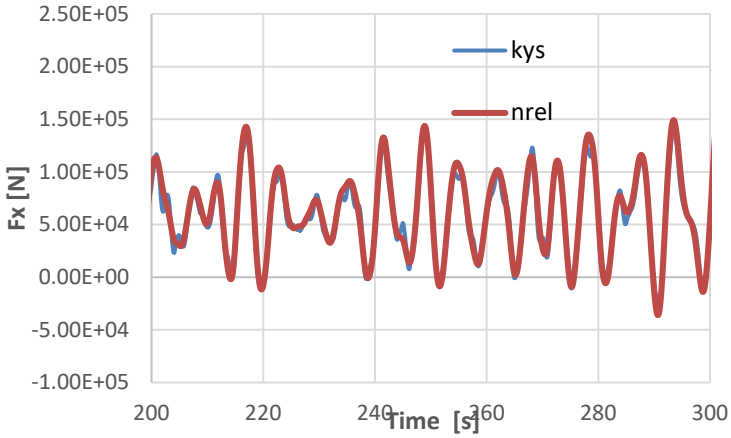

Figure 15. Equivalent hydrodynamic load Fx to be applied at tower-base for the verification case discussed in the text (same wave conditions as described for load case A002).

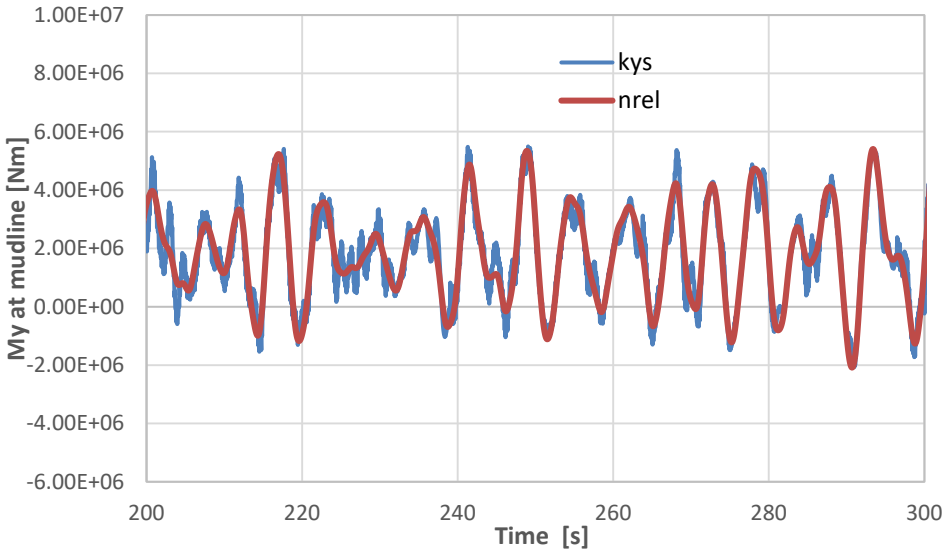

Figure 16. Overall moment reaction My at the mudline for the verification case discussed in the text (same wave conditions as described for load case A002).

8 Maximum Loads Comparison for ULS Load Cases

In this Section, we provide comments on the observed results for the maximum loads as calculated with the two approaches for various components and under the ULS DLCs listed in Table 12--Table 14. We separated the power production and the parked cases into two subsections for monopile and jacket OWT, respectively. For a complete gallery of the results in terms of calculated ULS loads and differences between fully coupled (FC) and sequentially coupled (SC) methods, the reader is referred to Appendix A. The symbols used in those graphs are explained in the previous Sections. In this Section, we also provide summary tables that compile the differences in *overall maxima* across all power-production and parked cases, respectively; the summary tables help assess whether one method is overall more conservative than the other for a specific load channel.

8.1 Monopile – Power Production – Comparison of overall Maximum Loads

Overall, very good agreement among the SC and FC results was observed (see Table 18, Table 19, Table 20). SC tends to give results that are more conservative than FC in most cases, which implies that the designs evaluated with the SC approach should at least be as safe as those that are verified via the more rigorous FC approach, though designs might therefore be over-conservative. Nonetheless, the FC approach is more conservative in several channels: shaft *LSSMy*, tower-top *YawBearingMx*, *YawBearingFy,* tower-base *TowerBaseFy, TowerBaseMx*. The large difference between FC and SC for *BladeRootMz* shown in Table 18 is related to an artifact in the *BladeRootMz* signal that is discussed below.

Table 18. Maximum turbine loads during power production (monopile), part1.

	BladeRootFx	BladeRootFy	BladeRootFz	BladeRootMx	BladeRootMy	BladeRootMz	LSSMy	LSSMz	YawBearingFx	YawBearingFy
Fully Coupled	395	245.4	860.1	6031	14020	3430	7303	6824	942.9	237
Sequentially Coupled	400.3	261.1	858.2	6093	14070	118.4	6837	6809	954.3	222.4
Delta (%)	1.3	6.4	-0.2	1.0	0.4	-96.5	-6.4	-0.2	1.2	-6.2

Table 19. Maximum turbine loads during power production (monopile), part 2.

	YawBearingFz	YawBearingMx	YawBearingMy	YawBearingMz	TowerBaseFx	TowerBaseFy	TowerBaseFz	TowerBaseMx	TowerBaseMy	TowerBaseMz
Fully Coupled	3566	5274	5653	5974	981.4	282.6	5900	23530	72470	5974
Sequentially Coupled	4328	5014	5842	6036	1012	271.8	7245	22120	72900	6036
Delta (%)	21.4	-4.9	3.3	1.0	3.1	-3.8	22.8	-6.0	0.6	1.0

Table 20. Maximum substructure loads during power production (monopile).

	MSL_Mx	MSL_My	Mx_10m_depth	My_10m_depth	Fx_mudline	Fy_mudline	Fz_mudline	Mx_mudline	My_mudline	Mz_mudline
Fully Coupled	25.9	81.9	28.9	91.9	1.4	0.6	8.7	33.8	103.4	6.0
Sequentially Coupled	24.6	82.3	27.7	92.2	1.4	0.6	9.7	32.3	104.0	6.0
Delta (%)	-4.8	0.6	-4.2	0.3	-2.8	-0.9	11.9	-4.5	0.6	0.1

8.1.1 Blade Loads (as shown in Appendix A)

The blade loads agree relatively well between FC and SC approaches (see Appendix A: ULS Result Gallery. The largest differences are in the Fy shear force (some 6% difference). The extremely large differences seen for the Mz maximum loads are caused by an artifact in the FC simulation that pushes the maximum values for this channel to unrealistic values. This issue is only observed for the monopile simulations during power production. A time series plot of the Mz signal is shown in Figure 17, where a single isolated spike in the signal is seen, and which is not accompanied by similar spikes in the other load channels investigated within this project. Also note that, as mentioned above, these results do not include the dynamic response of the blades along the torsional degree of freedom, as typical blades are very stiff in torsion.

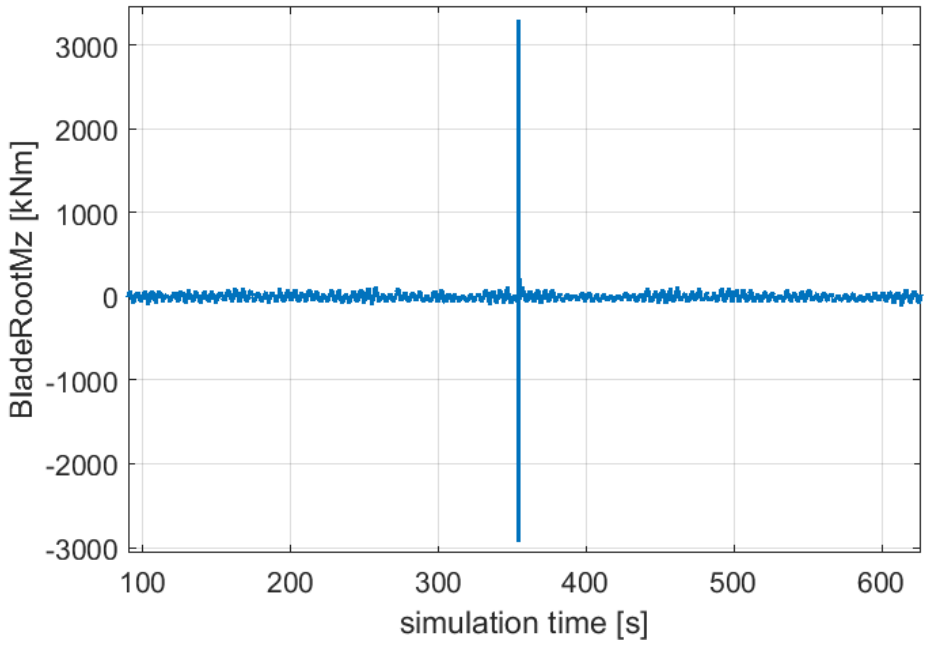

Figure 17. Typical time series of torsional moment at blade root as observed in our simulations.

8.1.2 Shaft Loads (as shown in Appendix A)

Relatively good agreement between FC and SC was also observed for the low speed shaft bending moments (differences on the order of ~6% and ~1% for My and Mz, respectively).

8.1.3 Tower-Top (Yaw-Bearing) Loads (as shown in Appendix A)

The largest differences for the yaw bearing loads are observed in the force aligned with global z. This is related to the fact that no significant damping in the z direction was specified for the SC approach. The lightly damped initial transient for the *YawBearingFz* signal is illustrated in Figure 18; it is responsible for the relatively large maximum loads for the SC approach and could be reduced through the selection of an appropriate linear damping coefficient. Other noticeable differences are observed for *YawBearingFy* (~10%) and *YawBearingMy* (~6%).

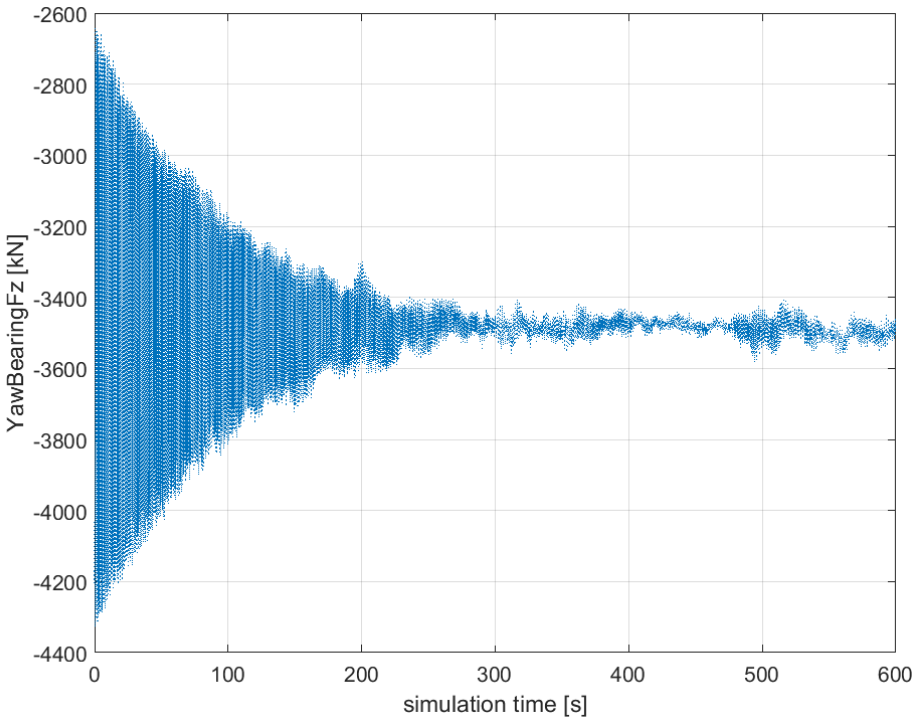

Figure 18. Typical time series of yaw bearing force along global z. Note the transient has not settled after more than 300 s (including 150 seconds of discarded data)

8.1.4 Tower-Base Loads (as shown in Appendix A)

Tower-base loads behaved similarly to what was seen for the tower-top loads. Relatively large differences in the *TowerBaseFz* signal are due to an insufficiently damped initial transient oscillation, whereas differences around 10% in the *TowerBaseFy* shear were noted.

8.1.5 Substructure Loads (as shown in Appendix A)

For the substructure loads, differences amounted to some 5% for the bending moments about the global x-axis and approximately 10% for the shear force in x-direction at the mudline. SC and FC loads for the mudline shear force in the y-direction differed up to 30% for certain wind/wave orientations.

8.2 Monopile – Extreme Conditions – Comparison of overall Maximum Loads

Overall, the differences between the SC and FC monopile results were larger for the extreme load cases than for the power production cases. Even more importantly, the FC approach seems to be more conservative for the majority of the analyzed channels for DLCs B001—B004. A comparison of the *overall* maximum turbine and tower loads for all parked DLCs (B001-B004) (see Tables Table 21Table 22) shows agreement within 10% between SC and FC; in Table 23, for the respective substructure loads, the calculated relative errors are on the order of 13%, with the SC less conservative than the FC approach.

Table 21. Maximum turbine loads during extreme conditions (monopile), part1.

	BladeRootFx	BladeRootFy	BladeRootFz	BladeRootMx	BladeRootMy	BladeRootMz	LSSMy	LSSMz	YawBearingFx	YawBearingFy
Fully Coupled	98.71	347.2	177.1	9991	1969	152.5	4570	5709	514.7	779.4
Sequentially Coupled	97.91	349.3	186	10030	2102	148.3	4705	5453	507.6	818.1
Delta (%)	-0.8	0.6	5.0	0.4	6.8	-2.8	3.0	-4.5	-1.4	5.0

Table 22. Maximum turbine loads during extreme conditions (monopile), part2.

	YawBearingFz	YawBearingMx	YawBearingMy	YawBearingMz	TowerBaseFx	TowerBaseFy	TowerBaseFz	TowerBaseMx	TowerBaseMy	TowerBaseMz
Fully Coupled	3429	2697	3941	6086	1057	860.9	5764	65050	62680	6086
Sequentially Coupled	3526	2842	3943	5661	1008	893.8	5981	69260	58550	5661
Delta (%)	2.8	5.4	0.1	-7.0	-4.6	3.8	3.8	6.5	-6.6	-7.0

Table 23. Maximum substructure loads during exteme conditions (monopile).

	MSL_Mx	MSL_My	Mx_10m_depth	My_10m_depth	Fx_mudline	Fy_mudline	Fz_mudline	Mx_mudline	My_mudline	Mz_mudline
Fully Coupled	72.9	72.7	83.9	89.0	3.5	3.6	8.6	113.6	111.7	6.1
Sequentially Coupled	78.0	67.6	88.4	80.4	3.5	3.2	8.5	101.9	97.0	5.7
Delta (%)	7.0	-7.0	5.4	-9.7	0.5	-12.7	-1.2	-10.3	-13.2	-7.5

8.2.1 Blade Loads (as shown in Appendix A)

For the simulated extreme conditions with a parked turbine, differences between SC and FC blade root loads were larger than what was observed during the power production cases, namely: *BladeRootFx*: ~5%, *BladeRootFz*: ~5%, *BladeRootMy*: ~10%. Note that the load spike observed in the *BladeRootMz* signal during the power production conditions did not occur in the parked simulations.

8.2.2 Shaft Loads (as shown in Appendix A)

Compared to the power production case, the parked case showed larger differences (~10%) for *LSSMz* between FC and SC results.

8.2.3 Tower-Top (Yaw-Bearing) Loads (as shown in Appendix A)

For the yaw bearing loads, larger differences compared to the power production case can be observed for: *YawBearingFx* ~4%, *YawBearingMz* ~20%. A consideration similar to what stated for the blade torsion must be emphasized. The torsional degree of freedom of the tower was not included in the calculations, as normally towers are pretty stiff in torsion, and the torsional moment is not a design driver.

8.2.4 Tower-Base Loads (as shown in Appendix A)

Similar levels of differences between FC and SC results were observed for both the yaw bearing loads and the tower base loads. The largest difference (~20%) at tower base was seen in the *TowerBaseMz* (torsional moment).

8.2.5 Substructure Loads (as shown in Appendix A)

The differences between FC and SC substructure loads were larger than for the power production cases. Bending moments differed by about 10% between FC and SC results (compared to about 5% for the power production case). Even larger differences in mudline shear forces (*Fx_mudline* ~200% and *Fy_mudline* ~150%) were noted for the parked case.

The mudline shear forces are highly influenced by hydrodynamic loads, which points to potential differences between M&N and NREL in terms of hydrodynamic load application. Further investigation is needed here.

Note that the comparison of the overall maximum substructure loads for all analyzed parked cases (B001-B004) shown in Table 23 states differences between FC and SC beyond 10%.

8.3 Jacket – Power Production – Comparison of overall Maximum Loads

Turbine loads were well captured by the SC method when compared to the FC results, and the differences were smaller than for the monopile configurations. For several wind/wave direction combinations the FC approach appears to yield more conservative results than the SC approach, especially for the *YawBearingFx*, *YawBearingFy,* and *TowerBaseFy* load channels.

A comparison of the maximum turbine loads over all analyzed power production load cases (A001-A008) yielded differences between SC and FC below 5% (see Table 24--Table 25). Table 26 and Table 27 show lager differences (up to 60%) for the member loads, but the SC approach appears to be conservative for all the member load channels analyzed.

Table 24. Maximum turbine loads during power production (jacket), part1.

	BladeRootFx	BladeRootFy	BladeRootFz	BladeRootMx	BladeRootMy	BladeRootMz	LSSMy	LSSMz	YawBearingFx	YawBearingFy
Fully Coupled	392.6	246.8	837	6114	14190	206.6	6186	7097	892.3	646.2
Sequentially Coupled	396.4	246.1	836	6122	14200	203.1	6225	7350	874.5	622.5
Delta (%)	1.0	-0.3	-0.1	0.1	0.1	-1.7	0.6	3.6	-2.0	-3.7

Table 25. Maximum turbine loads during power production (jacket), part2.

	YawBearingFz	YawBearingMx	YawBearingMy	YawBearingMz	TowerBaseFx	TowerBaseFy	TowerBaseFz	TowerBaseMx	TowerBaseMy	TowerBaseMz
Fully Coupled	3562	7287	5993	5259	894.6	656.3	5692	47220	60680	5259
Sequentially Coupled	3560	7234	6019	5141	910.2	637.1	5691	47410	60700	5141
Delta (%)	-0.1	-0.7	0.4	-2.2	1.7	-2.9	0.0	0.4	0.0	-2.2

Table 26. Maximum substructure loads during power production (jacket), part1.

	K1L1_FZ	K1L2_FZ	K5L2_FZ	RL1_FZ	RL1_FY	RL1_FX	RL1_MZ	RL1_MY	RL1_MX	RL2_FZ	RL2_FY	RL2_FX	RL2_MZ
Fully Coupled	6643	2427	249.8	9225.0	290.1	370.8	224.2	1974.0	1434.0	3232.0	297.1	380.6	1512.0
Sequentially Coupled	6660	2599	271.2	9568.3	414.8	467.5	342.4	2301.3	1954.2	3629.8	387.8	478.5	1870.6
Delta (%)	0.3	7.1	8.6	3.7	43.0	26.1	52.7	16.6	36.3	12.3	30.5	25.7	23.7

Table 27. Maximum substructure loads during power production (jacket), part2.

	RL2_MY	K4L1_XZ_FZ	K4L1_XZ_MY	K4L1_XZ_MX	K4L1_YZ_FZ	K4L1_YZ_MY	K4L1_YZ_MX	K4L2_XZ_FZ	K4L2_XZ_MY	K4L2_XZ_MX	K4L2_YZ_FZ	K4L2_YZ_MY	K4L2_YZ_MX
Fully Coupled	1965.0	755.8	65.1	82.3	800.4	69.6	69.9	563.9	55.1	66.4	557.1	52.4	58.2
Sequentially Coupled	2303.7	922.0	81.9	106.9	921.6	99.5	88.2	713.2	88.9	96.6	597.7	79.4	90.0
Delta (%)	17.2	22.0	25.9	29.9	15.1	42.9	26.2	26.5	61.4	45.6	7.3	51.7	54.8

8.3.1 Blade Loads (as shown in Appendix A)

The blade root loads agreed very well with about 1% difference between FC and SC results.

8.3.2 Shaft Loads (as shown in Appendix A)

About a 4% difference between FC and SC results can be observed for the *LSSMz* (shaft yawing moment).

8.3.3 Tower-Top (Yaw-Bearing) Loads (as shown in Appendix A)

The largest differences in yaw-bearing loads were found for the *YawBearingFy* (~15%) and the *YawBearingFx* (~3%) shear signals for specific load cases.

8.3.4 Tower-Base Loads (as shown in Appendix A)

The differences at tower-base are consistent with those noted at tower top.

8.3.5 Substructure Loads (as shown in Appendix A)

Focusing on the substructure member loads, the SC approach appears to predict maximum loads that are +20% larger than the corresponding values computed based on the FC approach. The best agreement between SC and FC is found for *K1L1_FZ* and *RL1_FZ* (differences below 5%).

With the exception of *K1L1_FZ*, *RL1_FZ*, and *K4L2_YZ_FZ* during certain wind/wave orientations, the SC approach proved to be more conservative for the substructure loads.

The relatively good agreement of the turbine maximum loads and the relatively large over prediction of substructure member maximum loads by the SC approach is in line with what was reported in (Seidel & Ostermann, 2009). Power spectra of the *RL1_Fx* and *RL1_Fy* (pile head shears) are shown in Figure 19 and Figure 20. The large peaks around 1.7 Hz in the KYS (SC) response coincide with the first global torsion mode (reported at 1.73 Hz by KYS). This mode appears to be significantly under predicted by the FC approach. This higher order global mode is exciting local member deformations that are not predicted by the FC modelling approach. According to (Seidel & Ostermann, 2009) this excitation during the recovery run is of artificial nature and leads to a significant overestimation of the local member loads. In the sequentially coupled analysis, the global torsion mode was not accurately represented in the FAST simulation due to the applied reduction scheme. In the subsequent recovery run, the tower base loads from FAST were used as input to the substructure design tool (EDP/SACS) possibly overexciting higher-order modes, such as the global torsion mode at around 1.7 Hz.

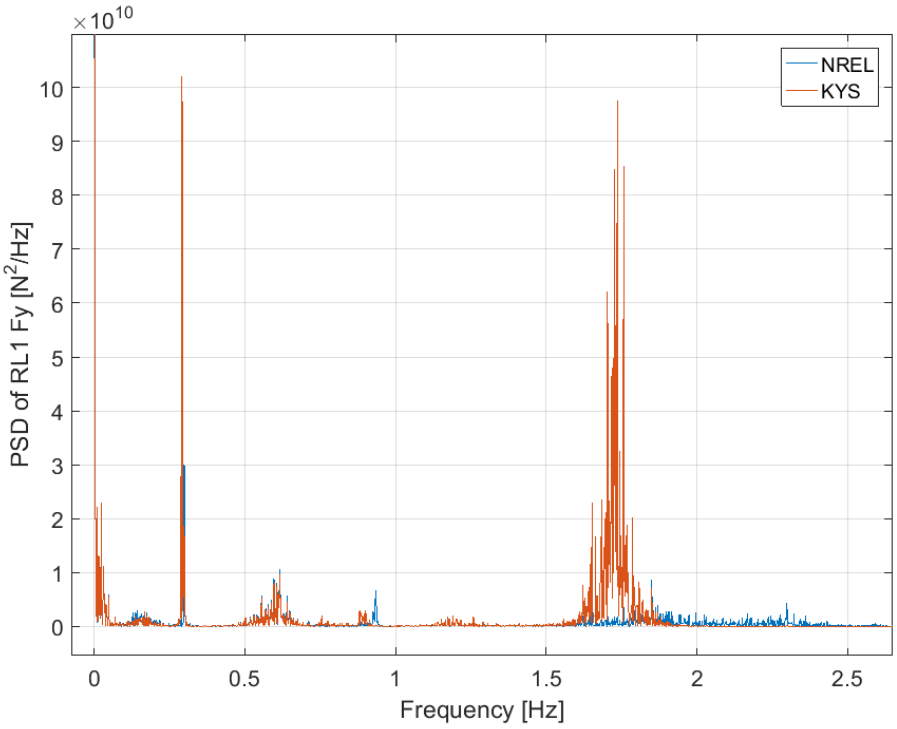

Figure 19. Power spectral density (PSD) plot of the pile head shear *RL1_Fy* as calculated by NREL and KYS.

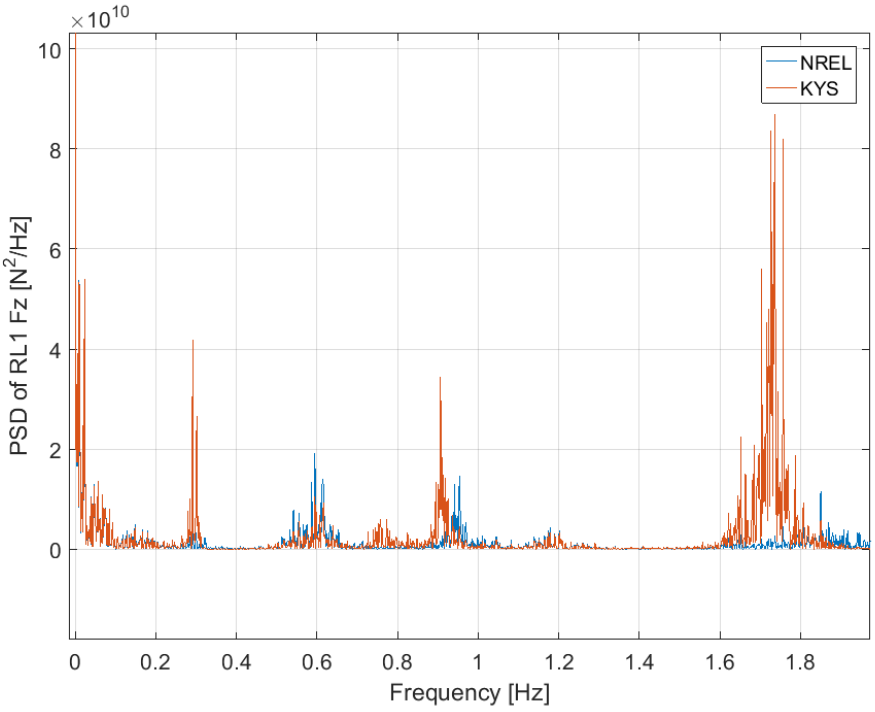

Figure 20. Power spectral density (PSD) plot of the pile head normal force *RL1_Fz* as calculated by NREL and KYS.

8.4 Jacket – Extreme Conditions – Comparison of overall Maximum Loads

The differences in the results from SC and FC approaches are larger under parked DLCs than under the power-production ones. As for the maximum turbine loads, the FC and the SC approaches alternately predicted higher (more conservative) loads, depending on the load channel and wind/wave direction combination. Compared to the power production case, however, the SC approach appears to be less conservative under extreme condition DLCs. By comparing the overall maxima across all parked cases, the maximum difference in turbine loads (Table 28--Table 29) amounted to ~13%, and with the SC method showing less conservative results. For the respective substructure loads (Table 30--Table 31), differences on the order of 30--40% were noted with SC being less conservative, whereas one load channel (K5L2_FZ) showed the overall largest difference (~50%) with FC returning lesser values than SC.

Table 28. Maximum turbine loads during extreme conditions (jacket), part1.

	BladeRootFx	BladeRootFy	BladeRootFz	BladeRootMx	BladeRootMy	BladeRootMz	LSSMy	LSSMz	YawBearingFx	YawBearingFy
Fully Coupled	89.34	160.4	178.8	5413	1869	151.5	4872	5942	502.4	893.1
Sequentially Coupled	83.72	159.1	179.2	5340	1807	147.8	4933	6118	464.2	805.7
Delta (%)	-6.3	-0.8	0.2	-1.3	-3.3	-2.4	1.3	3.0	-7.6	-9.8

Table 29. Maximum turbine loads during extreme conditions (jacket), part2.

	YawBearingFz	YawBearingMx	YawBearingMy	YawBearingMz	TowerBaseFx	TowerBaseFy	TowerBaseFz	TowerBaseMx	TowerBaseMy	TowerBaseMz
Fully Coupled	3382	3347	3547	7035	585.5	962.7	5511	65830	37240	7035
Sequentially Coupled	3381	2891	3507	7080	505.8	852.5	5507	58860	34520	7080
Delta (%)	0.0	-13.6	-1.1	0.6	-13.6	-11.4	-0.1	-10.6	-7.3	0.6

Table 30. Maximum substructure loads during extreme conditions (jacket), part1.

	K1L1_FZ	K1L2_FZ	K5L2_FZ	RL1_FZ	RL1_FY	RL1_FX	RL1_MZ	RL1_MY	RL1_MX	RL2_FZ	RL2_FY	RL2_FX	RL2_MZ
Fully Coupled	5019	4491	377	10440	913.0	916.2	295.5	4482.0	4321.0	12350.0	922.7	924.8	4351.0
Sequentially Coupled	5075	4472	573	11705	1089	990.1	278.4	4784.7	5256.3	7660.0	1206.5	960.7	5752.1
Delta (%)	1.1	-0.4	51.9	12.1	19.3	8.1	-5.8	6.8	21.6	-38.0	30.8	3.9	32.2

Table 31. Maximum substructure loads during extreme conditions (jacket), part2.

	RL2_MY	K4L1_XZ_FZ	K4L1_XZ_MY	K4L1_XZ_MX	K4L1_YZ_FZ	K4L1_YZ_MY	K4L1_YZ_MX	K4L2_XZ_FZ	K4L2_XZ_MY	K4L2_XZ_MX	K4L2_YZ_FZ	K4L2_YZ_MY	K4L2_YZ_MX
Fully Coupled	4503.0	1786.0	69.0	226.9	1881.0	130.6	226.9	1867.0	89.5	222.9	1798.0	104.0	219.7
Sequentially Coupled	4564.2	1930.4	71.1	279.7	1389.6	89.6	264.4	1600.0	89.2	231.8	1641.0	63.1	293.0
Delta (%)	1.4	8.1	3.1	23.3	-26.1	-31.4	16.5	-14.3	-0.3	4.0	-8.7	-39.3	33.4

8.4.1 Blade Loads (as shown in Appendix A)

For the blades, the most prominent differences are observed in the shear *BladeRootFx* (~6%) and *BladeRootMy* moment (~10%).

8.4.2 Shaft Loads (as shown in Appendix A)

The differences between SC and FC shaft loads increased as well going to extreme condition DLCs (, e.g., ~5% for *LSSMy* and ~14%for *LSSMz*).

8.4.3 Tower-Top (Yaw-Bearing) Loads (as shown in Appendix A)

At tower top, differences between SC and FC *YawBearingFx*, *YawBearingMx*, *YawBearingMy* and *YawBearingMz* exhibited values of about 15%.

8.4.4 Tower-Base Loads (as shown in Appendix A)

Similar differences were noted for the corresponding tower-base load channels.

8.4.5 Substructure Loads (as shown in Appendix A)

Just as for RNA and tower loads, the overall differences between SC and FC member loads are larger than what was observed for the power production case. Whereas the member loads were conservatively calculated by the SC approach for the power production case, for the parked conditions the FC approach produced the more conservative estimates in many cases. A time series plot of *K4L1_XZ_MY* (bending moment in the bottom brace, Figure 21a) illustrates that the frequency content between SC and FC appears to be similar. However the difference in mean value between the two signals eventually causes the differences in maximum loads, with FC being the more conservative solution. This difference in mean value was not observed for the corresponding load channel during power production (see Figure 21b). Further analysis is needed to clear this point, but it was outside the scope of this project.

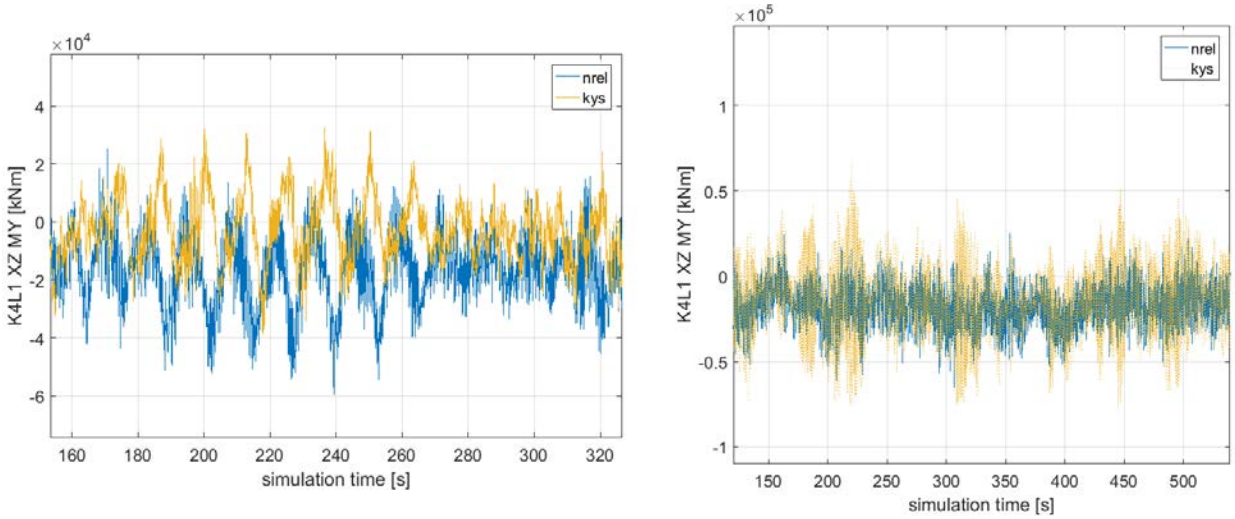

Figure 21. Time series plot of bending moment in brace member 45 for a parked DLC (a) and a power production DLC (b), as calculated by NREL and KYS.

9 Conclusions

A study was conducted for BSEE to assess the impact of sequentially coupled modelling approaches on the ULS loads and therefore eventually on the design of offshore wind turbines. The SC approach is commonly used in the industry as it avoids sharing proprietary information between different design groups (turbine OEM and substructure designers), but reservations exist concerning its ability to capture all the important dynamic coupling aspects associated with OWTs. In this study, we compared results in terms of maximum ULS loads as predicted from power production and parked (extreme event) case simulations when using either SC or FC methods. Whereas the comparison is quite involved and significant details exist for the various component load channels, a few general statements can be made.

For the turbine RNA and tower, very good agreement between the two methods was seen during the analyzed power production cases. Larger differences were observed for the extreme condition cases as compared to operational cases. The overall level of differences in turbine loads during extreme conditions was larger for the jacket-based OWT (~5%-20%) than for the monopile-based OWT (~5%-10%). For power production conditions, the larger differences in turbine loads were observed for the monopile OWT (~%5-10%), whereas for the jacket OWT results showed relatively small differences (~1%-5%).

For the monopile loads, the ultimate bending moments under power production DLCs agree within about 5% between SC's and FC's results, whereas the shear forces at mudline exhibited some larger differences (~10%-30%). For the extreme condition DLCs, these differences increase (~10% for bending moments and +100% for shear forces at mudline). This could potentially be related to issues in the hydrodynamic load definition/application and should be investigated further. The SC approach does not consistently return more conservative load estimates for the monopile.

For the jacket member loads under power production DLCs, the SC approach appears to be generally overestimating the ULS loads (+20%). A frequency domain analysis of substructure member load signals demonstrated that the SC coupled approach showed more contributions from higher-order global deformation modes. This is consistent with the data presented in (Seidel & Ostermann, 2009) which identifies the SC approach as overly conservative due to the artificial excitation of these higher-order modes. For the extreme condition DLCs, the differences in jacket loads are larger (+40%) than what was observed for the power production DLCs, and the SC approach produced less conservative estimates in several instances. A potential discrepancy in member mean loads between FC and SC approaches during parked DLCs needs to be further investigated.

When considering the maximum load values across all operational cases (A001-A008), the RNA and tower loads were found to be within 3% and 6% for the jacket and the monopile configuration, respectively. When considering the maximum load values across all parked cases (B001-B008), the RNA and tower loads were within 13% and 7% for the jacket and the monopile configuration, respectively, and with the SC results being less conservative than the FC results. For the substructure loads across all power-production cases, results showed differences up to 60% for the jacket members, and with the SC approach overestimating the loads; the monopile maximum loads were in close agreement (6-11%) and with no clear over/underestimation by any particular method. Across all the parked cases (B001—B008),

one jacket member load channel was overestimated by ~50% under SC, whereas several other member loads were underestimated up to 39% when compared to FC; the monopile loads were underestimated by up to 11% by the SC method.

Some of these differences can have important consequences on the design of the support structures, with potentially either overdesigned or underdesigned components, and should be further investigated. It can be stated, however, that including the modal content of the hydrodynamic forces in the SC aeroelastic simulations which can be accomplished using larger superelement matrices that include modal degrees of freedom, could further improve the agreement between SC and FC modelling approaches.

This study highlighted how the SC approach requires a thorough and time intensive model verification, a rigorous data exchange protocol, and an extensive and critical quality control. Also for this reason, the SC method limits the opportunity for design optimization. The FC approach, on the other hand, is more direct and rigorous, but, often times, not as practical due to the division of responsibility and intellectual property.

Our findings yield some significant differences that require further investigation in order to address any remaining concern regarding the practicability of the sequentially coupled analysis method for the design of offshore wind systems. More analysis is needed to allow for a clear identification of the sources of the observed differences and to devise potential mitigation strategies.

9.1 Recommended Follow-On Studies

Given the level of differences observed between fully coupled and sequentially coupled modelling approach, the authors would recommend further follow-on studies that focus on the characterization and the mitigation of the observed differences.

Future research should expand the results to FLS load cases, and potentially other load cases for ultimate loads, including constrained wave cases.

Further and targeted calibration efforts are required to minimize possible errors due to the utilization of different software packages.

Expanding the substructure superelement to include additional model degrees of freedom (Craig-Bampton method) may help to reduce the observed differences.

To compare the effect of the observed differences in load predictions on structural weight, a complete design iteration could be performed.

Furthermore, the effects of higher order hydrodynamics should be assessed, and larger and more flexible turbine models should be employed to verify the effects on the RNA loads.

There has been some evidence that the importance of a coupled analysis may become even more important for floating substructures. The industry for floating offshore wind substructures is just getting started with only five commercial floating offshore wind turbines operating today, but the pipeline for tracking this development indicates that a commercial industry may be forming in the next five years.

The effort to assess this issue for floating offshore wind substructures is beyond the scope of this project, but it is recommended that it be studied in future research.

10 References

Airy, G. (1841). *Tides and waves.* London: Encyclopaedia Metropolitana.

Damiani, R., Dykes, K., & Scott, G. (2016). A comparison study of offshore wind support structures with monopiles and jackets for U.S. waters. *The Science of Making Torque from Wind.* Munich, Germany: TORQUE.

International Electrotechnical Commission. (2008). IEC 61400-3 Wind Turbines - Part : Design Requirements for Offshore Wind Turbines. Geneva, Switzerland: IEC.

Jokman, J., & Musial, W. (2010). *Offshore Code Comparison Collaboration (OC3) for IEA Task 23 Offshore Wind Technology and Deployment (NREL/TP-500-48191).* Golden, CO: NREL.

Jonkman, J., Butterfield, W., Musial, W., & Scott, G. (2009). Definition of a 5-MW Reference Wind Turbine for Offshore System Development. Golden, CO: NREL.

Kooijman, H., Lindenburg, C., Winkelaar, D., & van der Hooft, E. (2003). *DOWEC 6 MW PRE-DESIGN Aero-elastic modelling of the DOWEC 6 MW pre-design in PHATAS.* DOWEC-F1W2-HJK-01-046/9.

NASA. (n.d.). *Ocean Surface Currents (OSCAR)*. Retrieved 4 10, 2016, from http://oceanmotion.org/html/resources/oscar.htm

NREL. (2016, July 27). *NWTC Information Portal*. Retrieved May 24, 2017, from FAST v8: https://nwtc.nrel.gov/FAST8

Popko, W., Vorprahl, F., Zuga, A., Kohlmeier, M., Jonkman, J., & Robertson, A. e. (2012). Offshore Code Comparison Collaboration Continuation (OC4), Phase I - Results of Coupled Simulation of Offshore Wind Turbine with Jacket Support Structure. *International Offshore and Polar Engineering Conference* (pp. Vol. 1, pp. 337-346). Rhodes, Greece: International Society of Offshore and Polar Engineers (ISOPE).

Rainey, P., & Camp, T. (2007). Constrained non-linear waves for offshore wind turbine design. *Journal of Physics*.

Rodenbusch, G., & and Forristall, G. (1986). An Empirical Model for Random Directional Wave Kinematics Near the Free Surface. *Offshore Technology Conference.* Houston, TX.

Seidel, M., & Ostermann, F. (2009). Validation of Offshore Load Simulations Using Measurement Data from the DOWNVInD project. *European Offshore Wind Conference.* Stockholm, Sweden.

Vorprahl, F., Popko, W., & Kaufer, D. (2013). *Description of a basic model of the 'UpWind Reference Jacket' for code comparison in the OC4 Project under IEA Wind Annex 30.* Bremerhaven, Germany: Fraunhofer IWES.

11 Appendix A: ULS Result Gallery

Monopile – Turbine Loads – Power Production

Blade Root Loads:

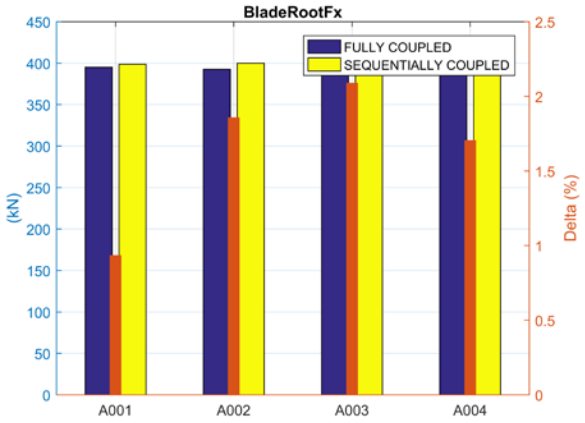

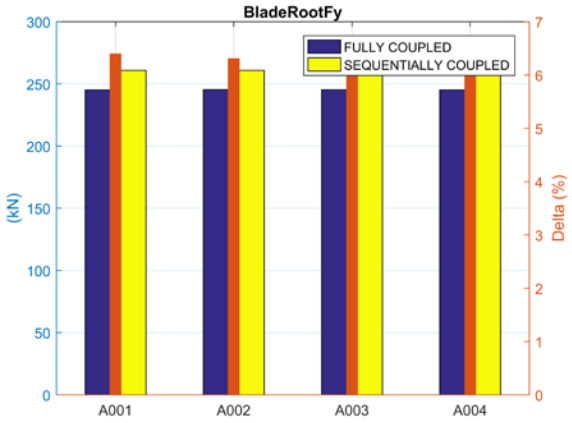

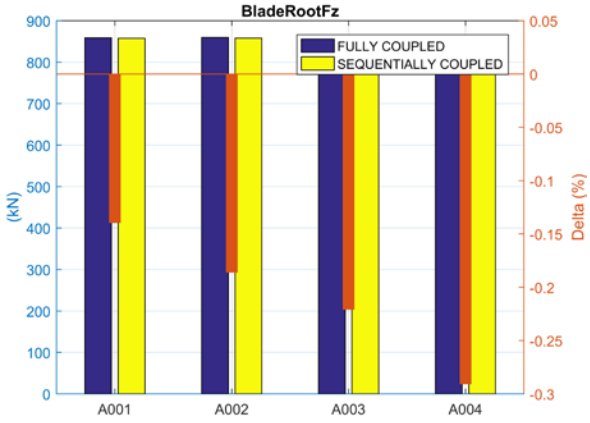

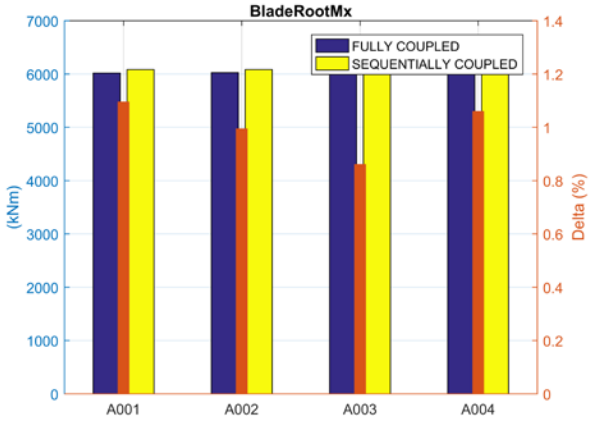

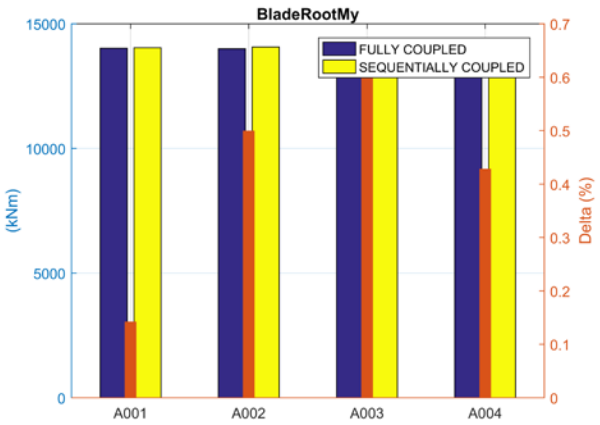

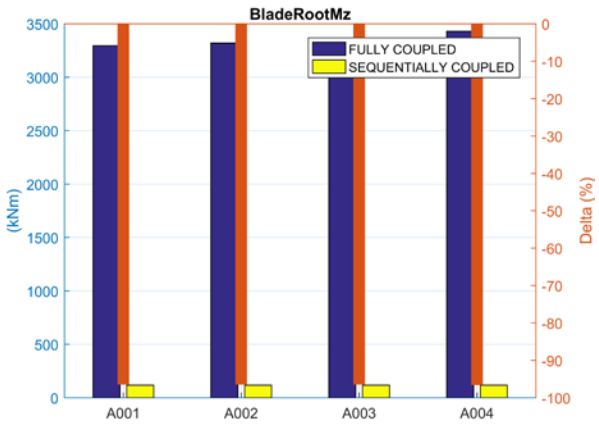

Low Speed Shaft Loads:

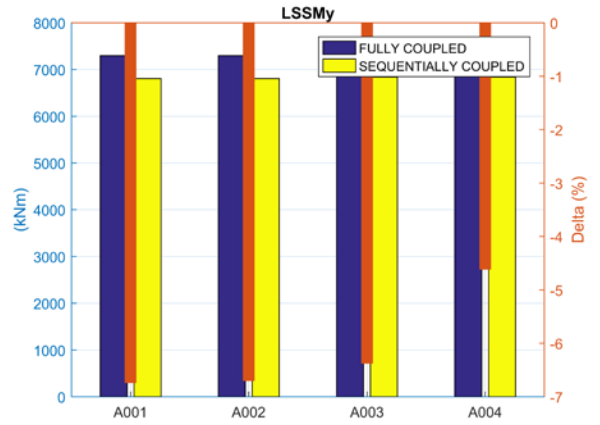

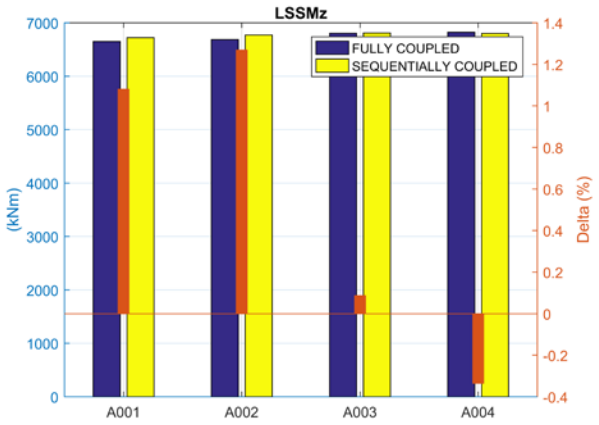

Yaw Bearing Loads:

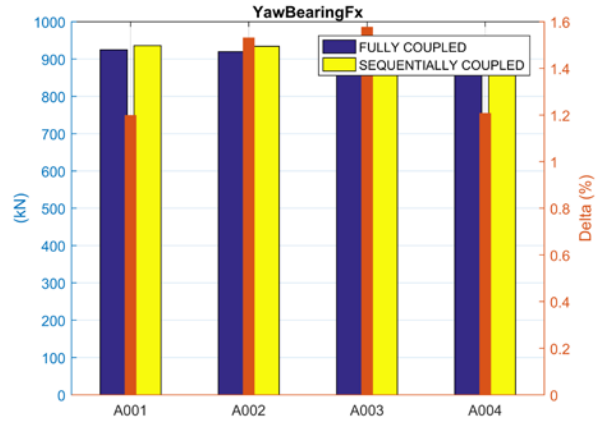

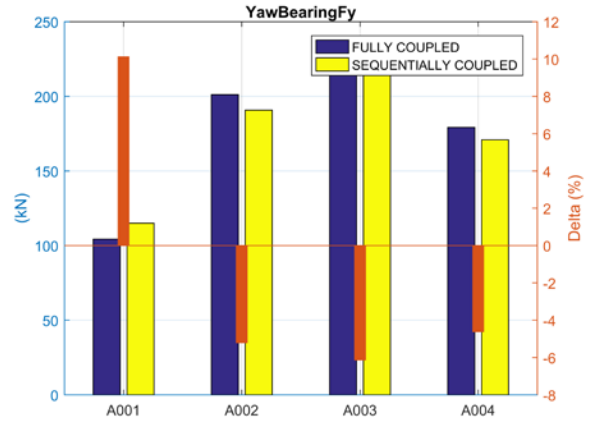

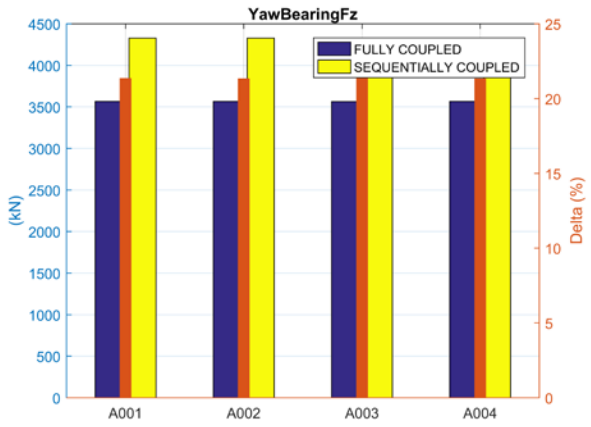

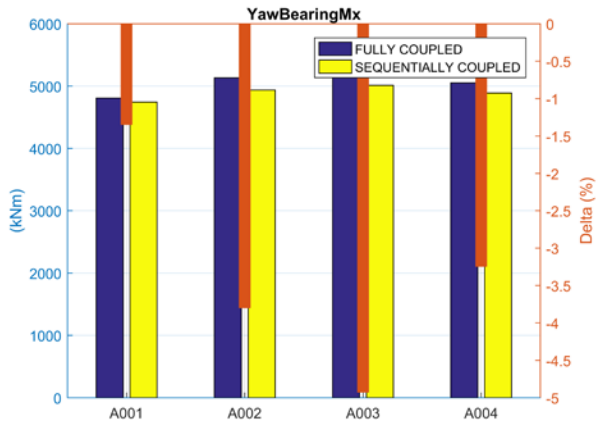

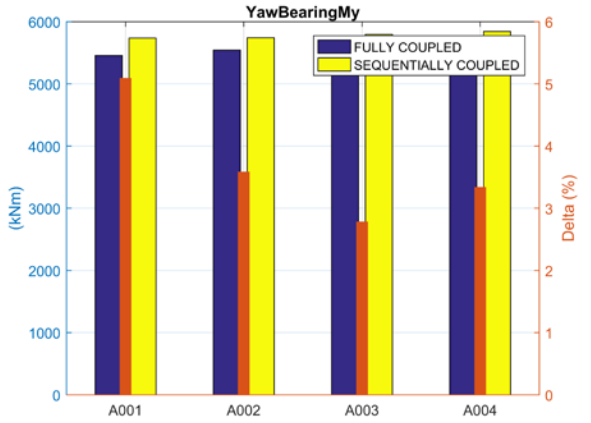

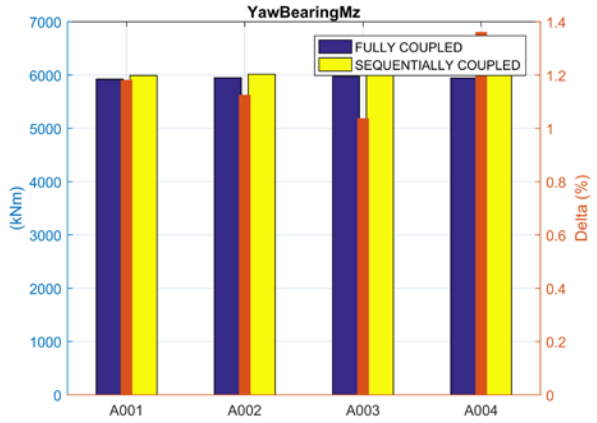

Tower Base Loads:

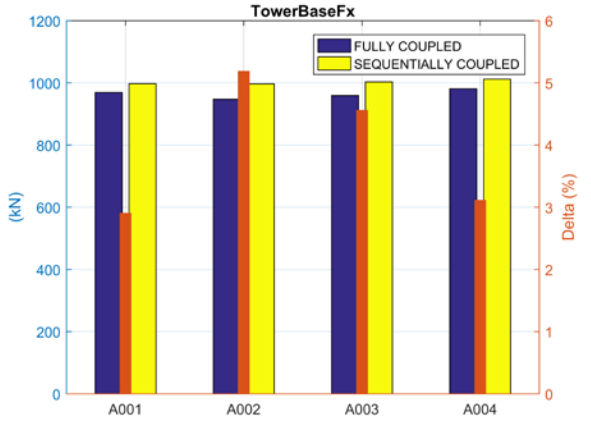

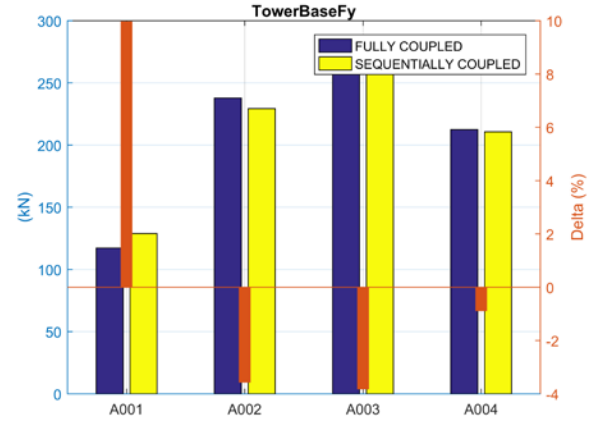

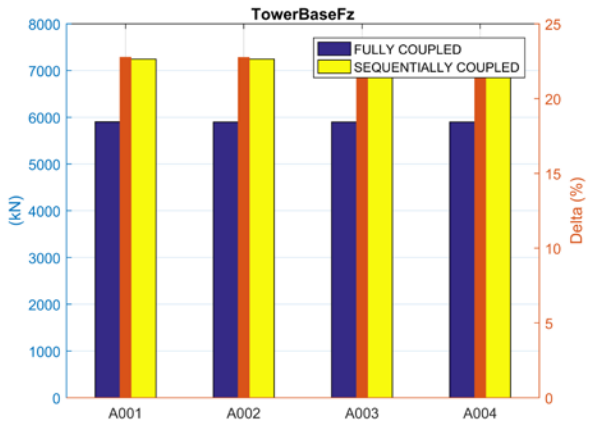

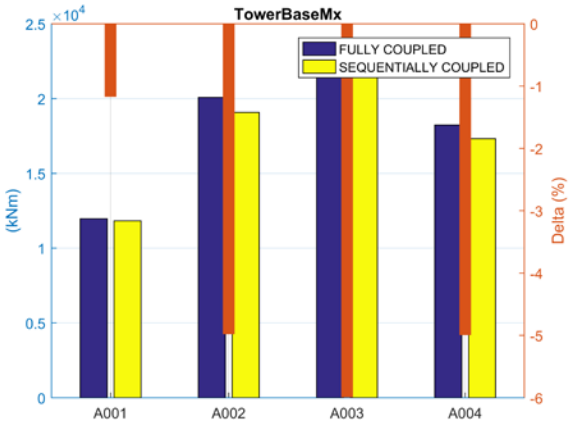

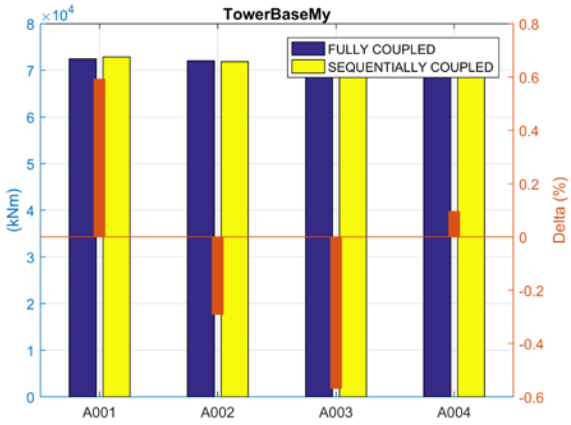

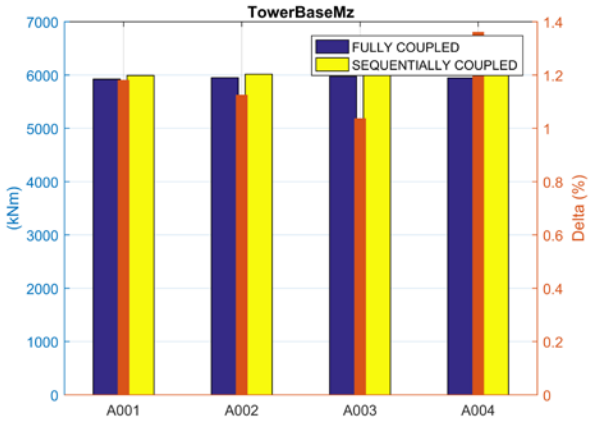

Monopile – Substructure Loads – Power Production

Bending Moments at mean sea level:

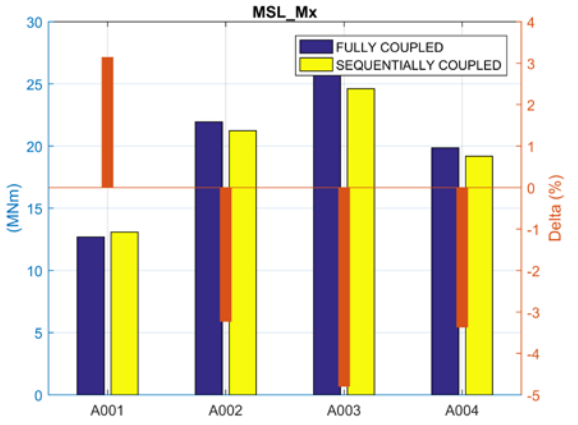

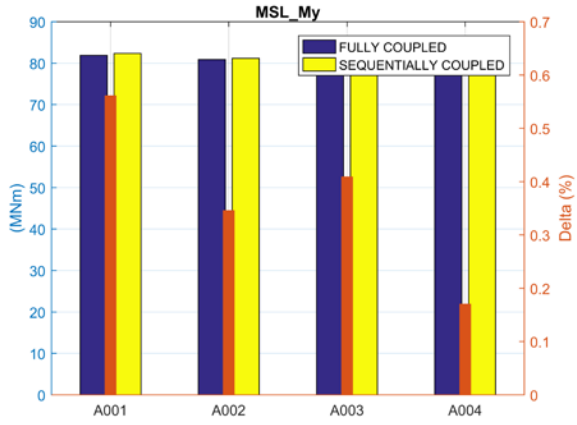

Bending Moments at 10m water depth:

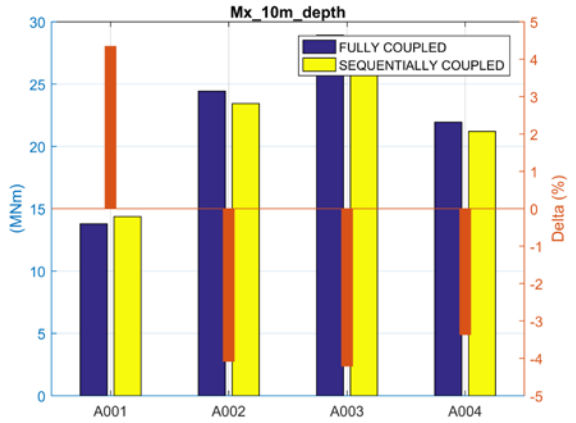

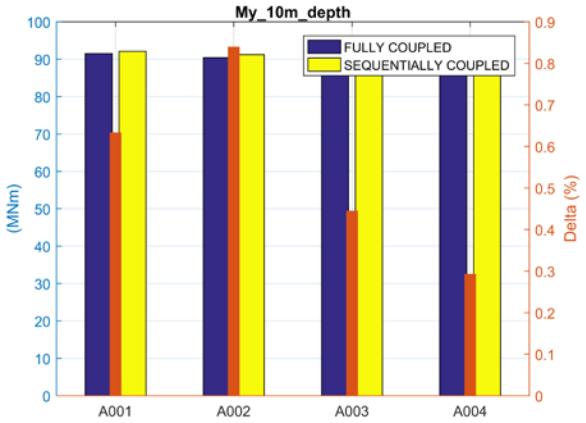

Pile loads at mudline:

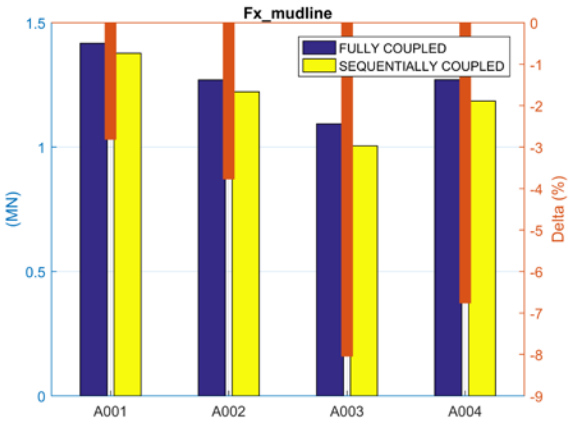

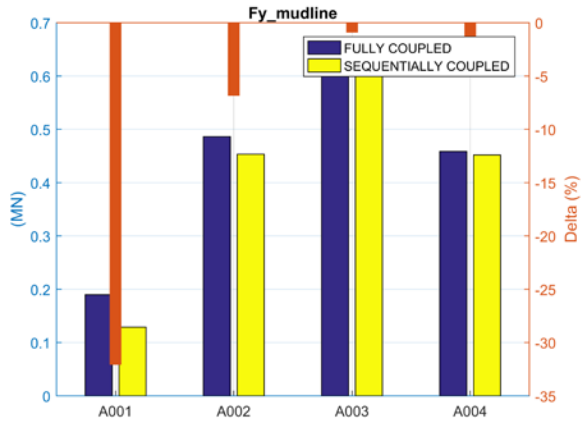

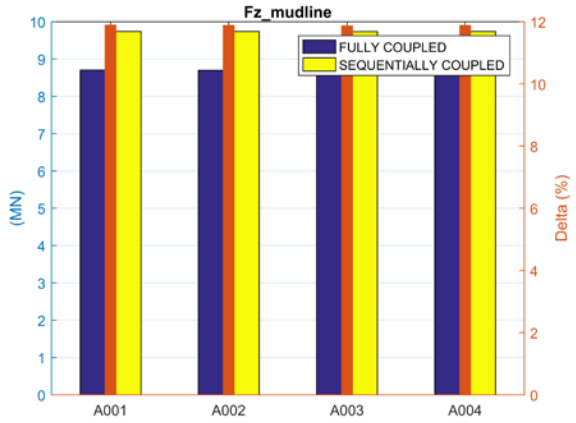

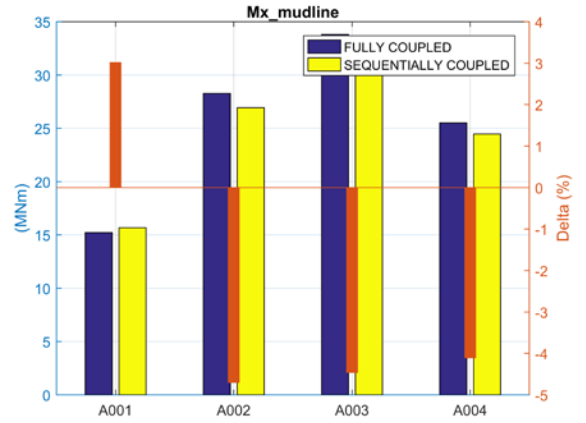

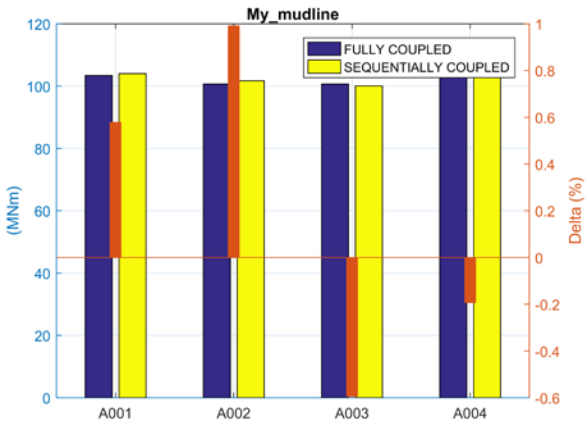

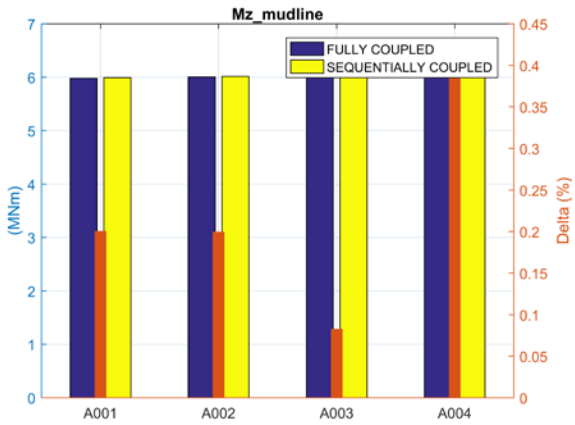

Monopile – Turbine Loads – Extreme Conditions

Blade Root Loads:

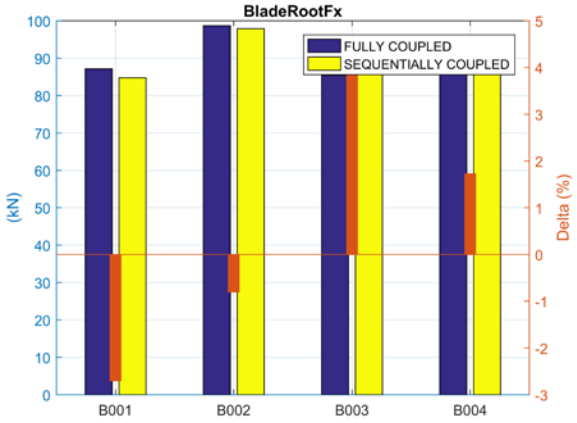

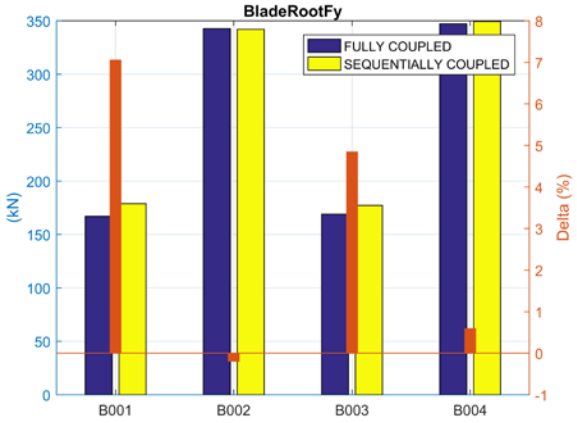

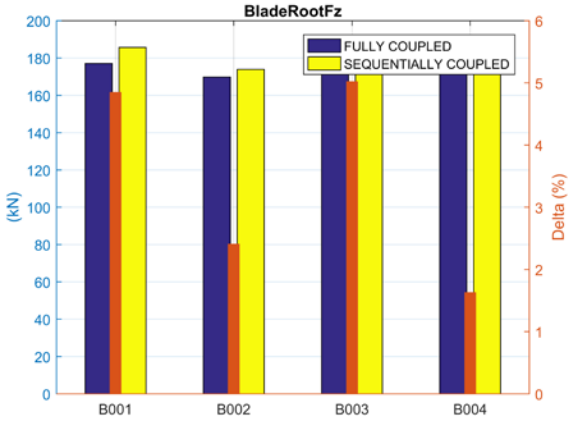

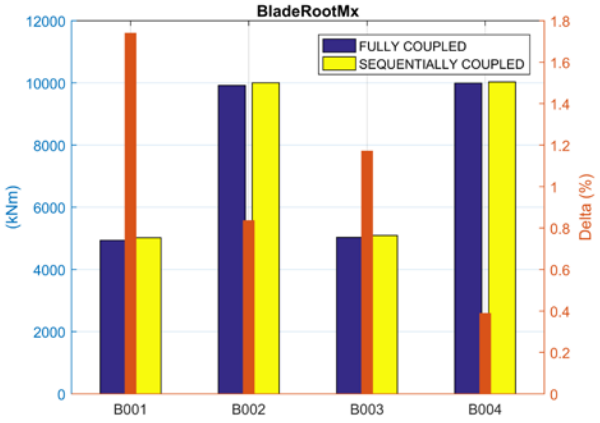

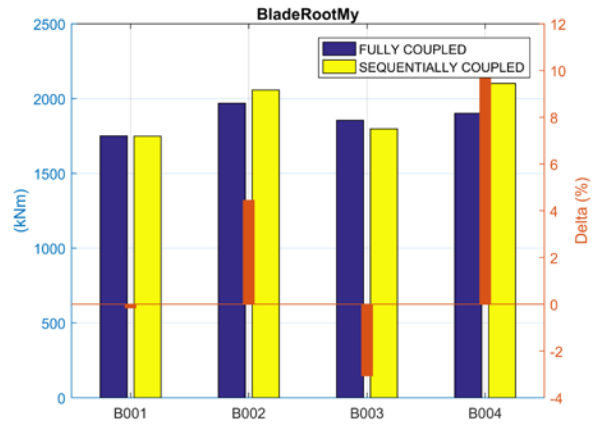

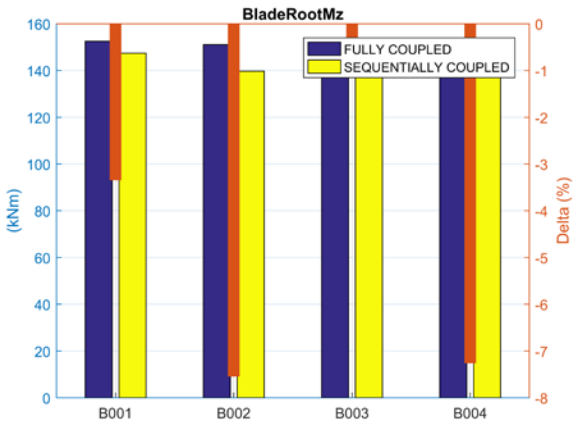

Low Speed Shaft Loads:

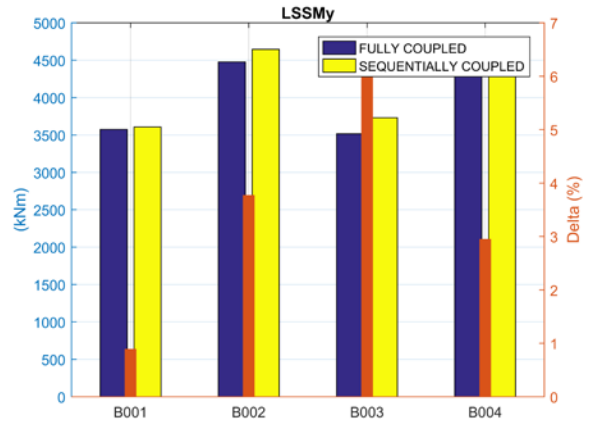

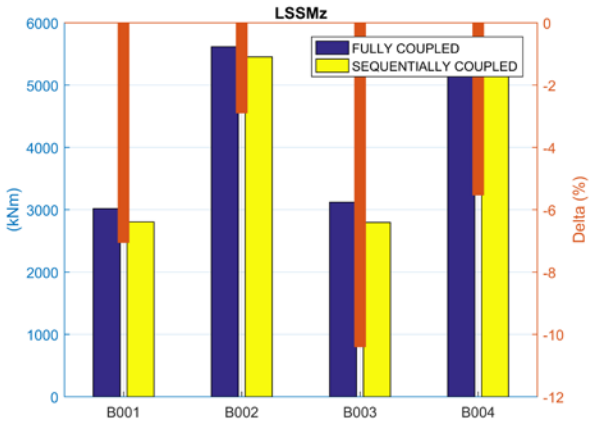

Yaw Bearing Loads:

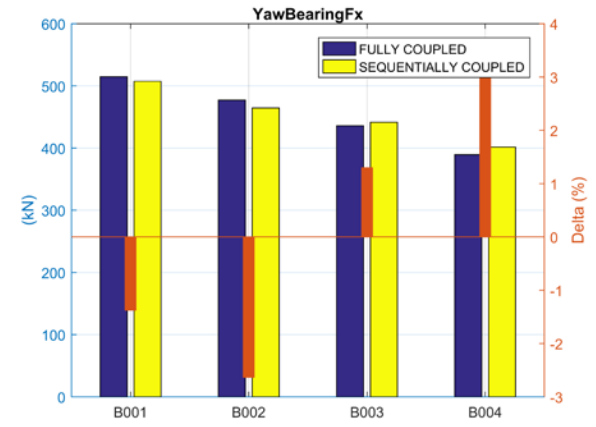

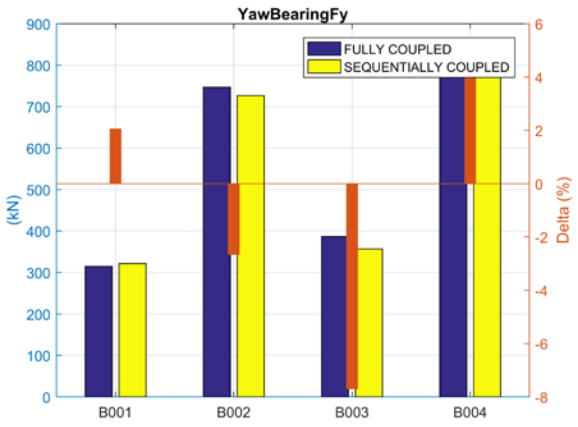

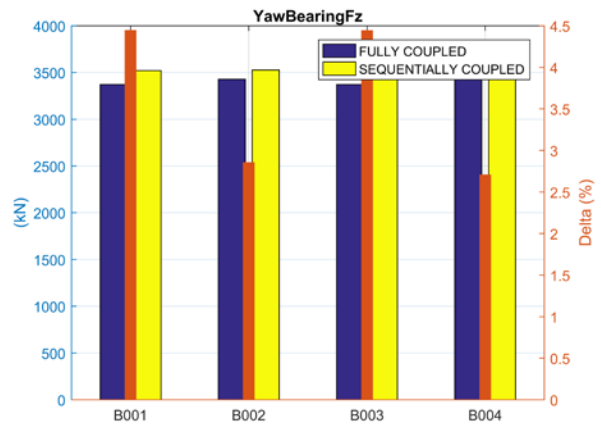

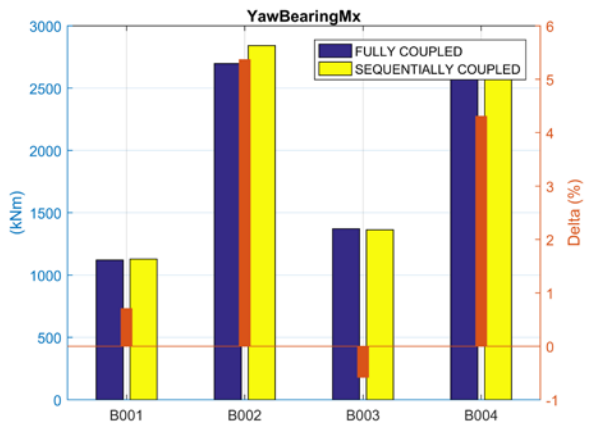

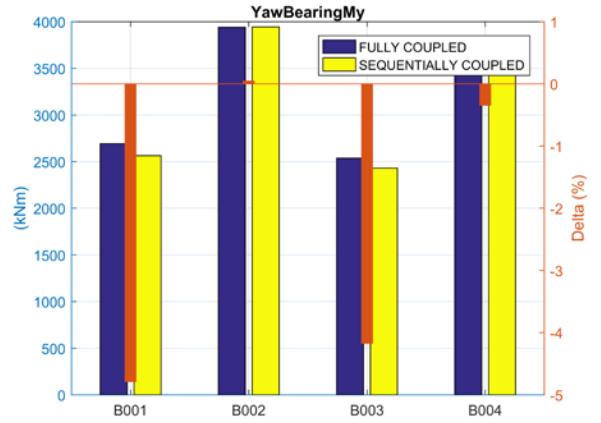

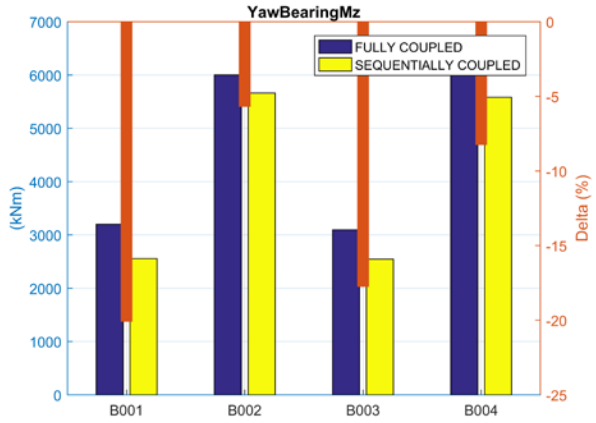

Tower Base Loads:

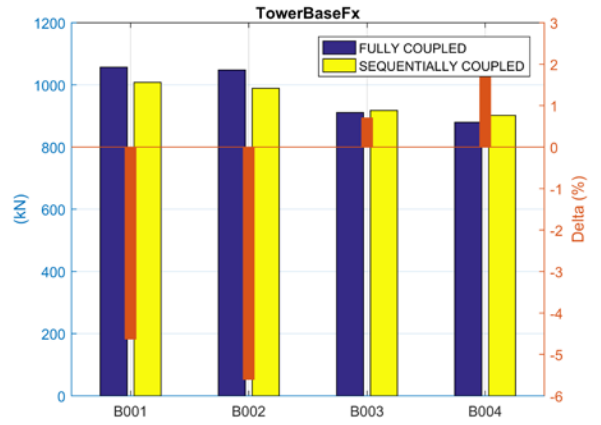

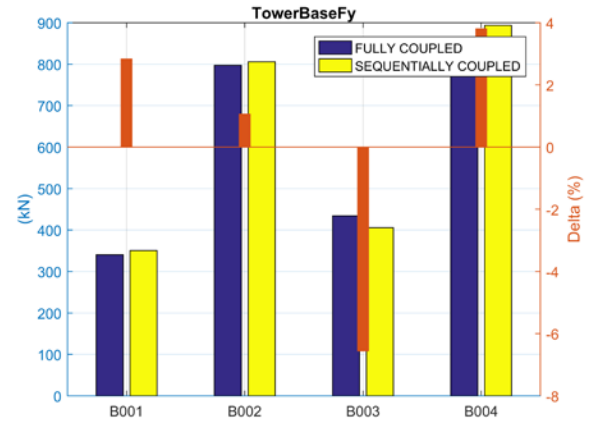

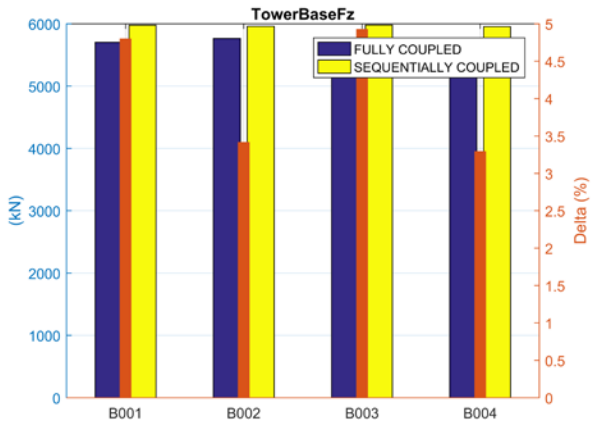

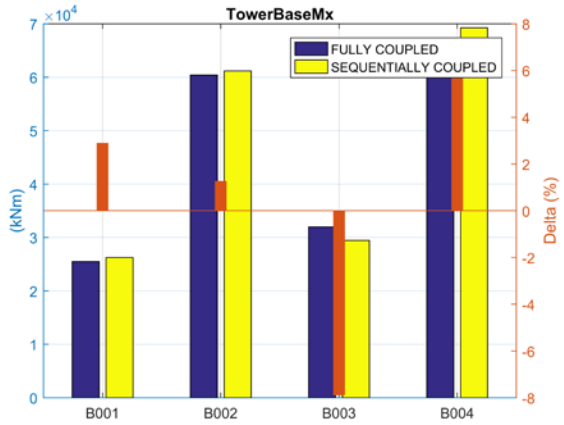

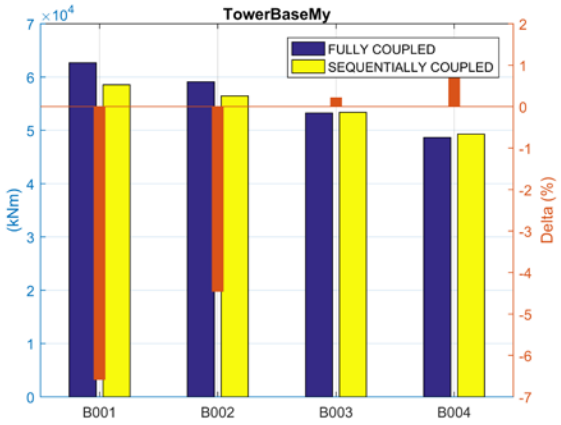

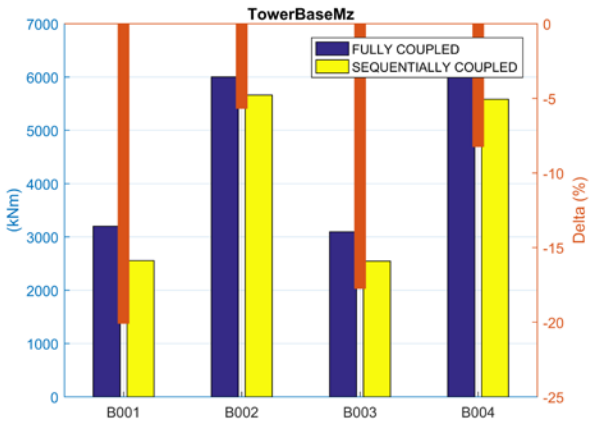

Monopile – Substructure Loads – Extreme Conditions

Bending Moments at mean sea level:

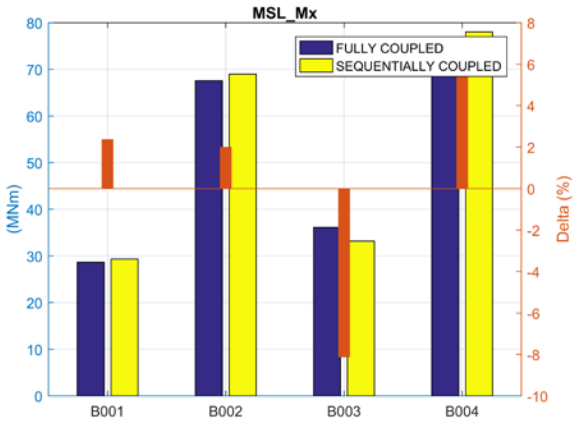

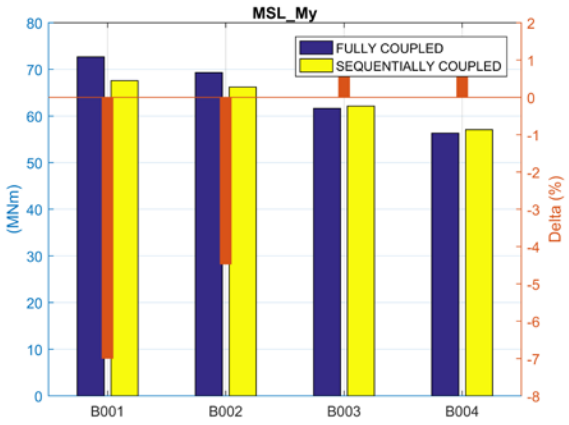

Bending Moments at 10m water depth:

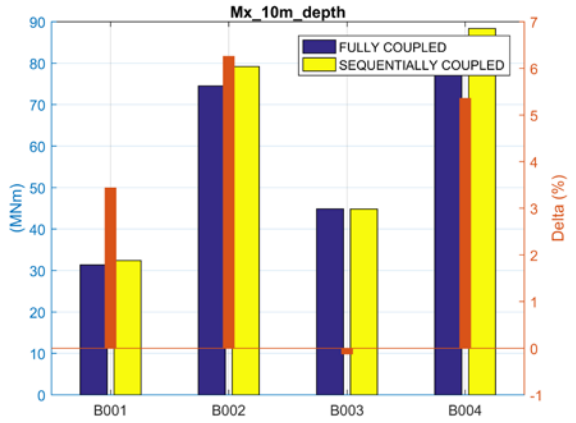

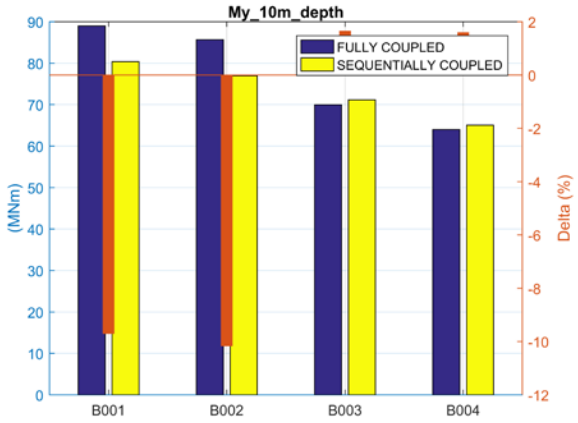

Piled loads at mudline:

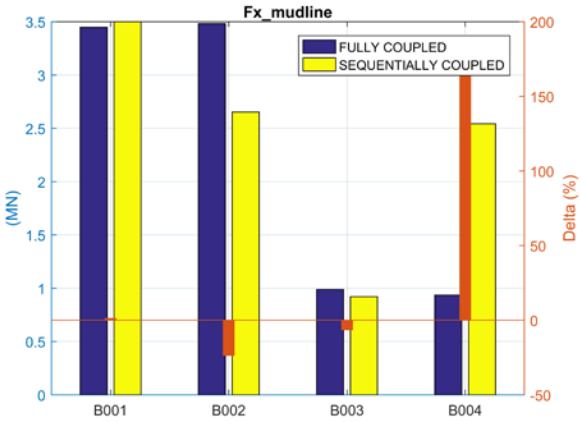

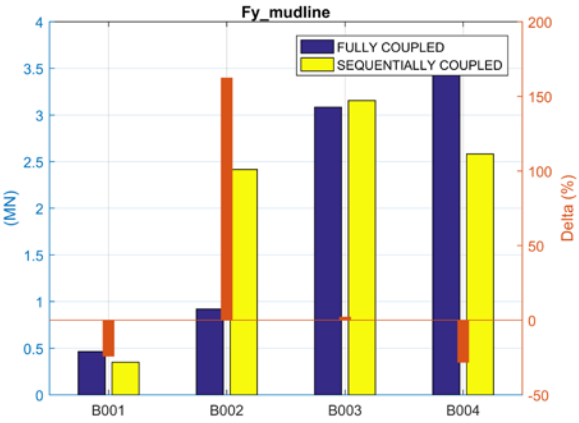

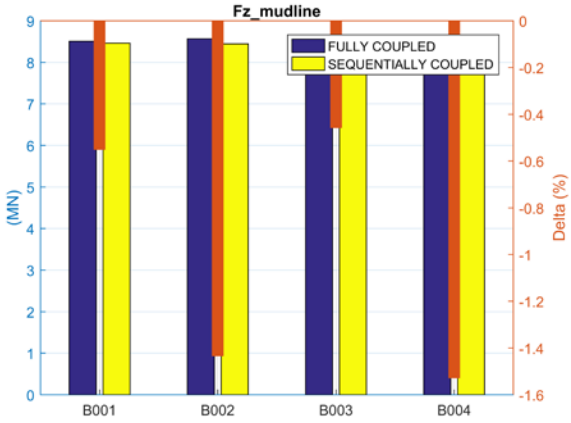

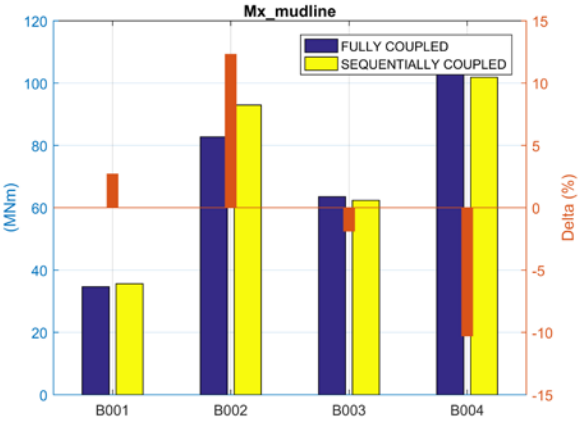

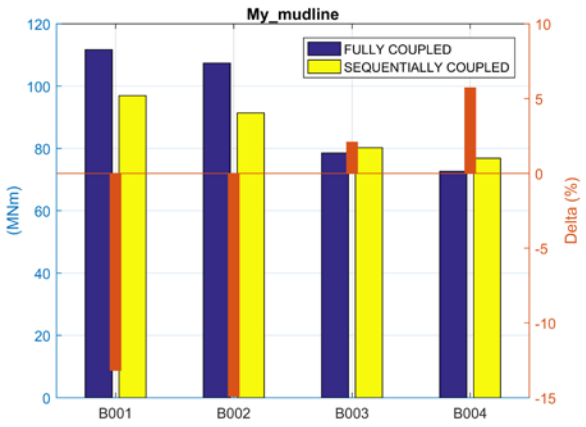

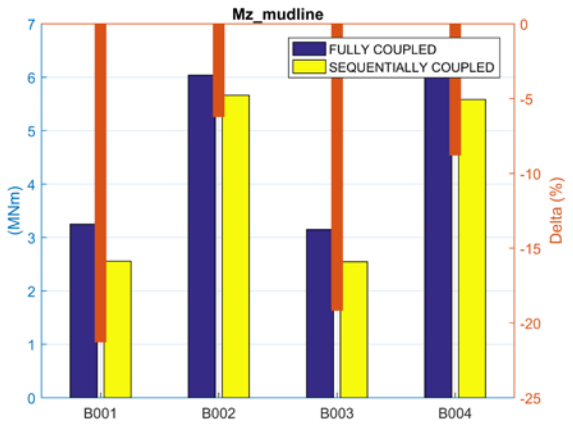

Jacket – Turbine Loads – Power Production

Blade Root Loads:

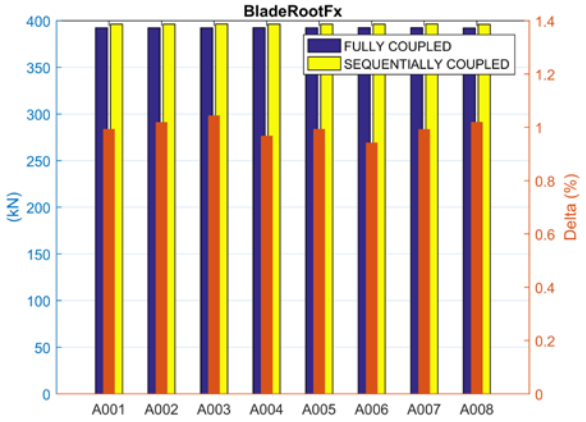

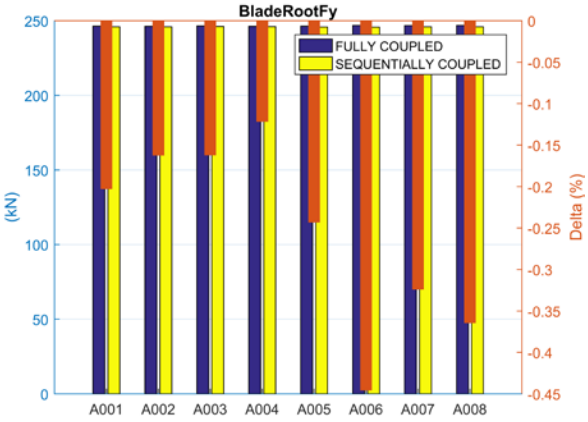

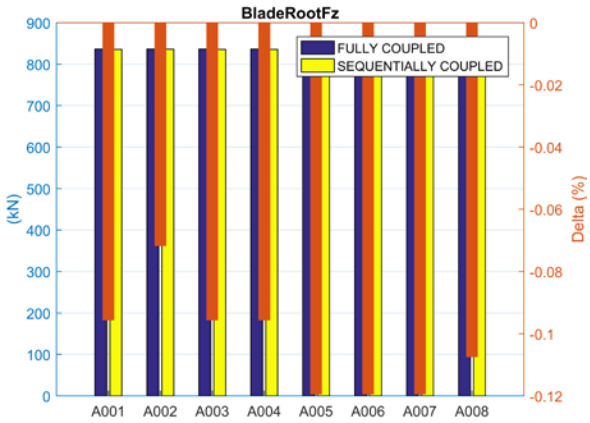

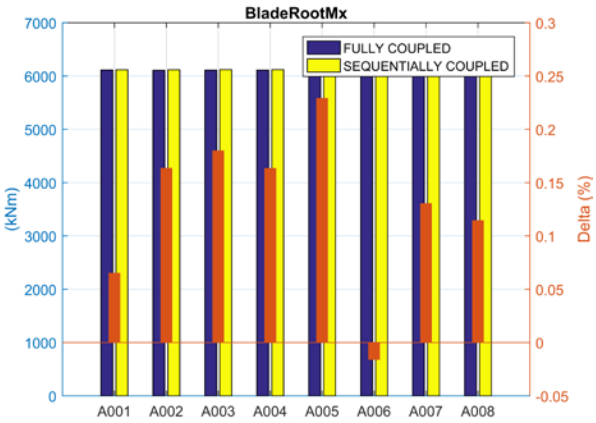

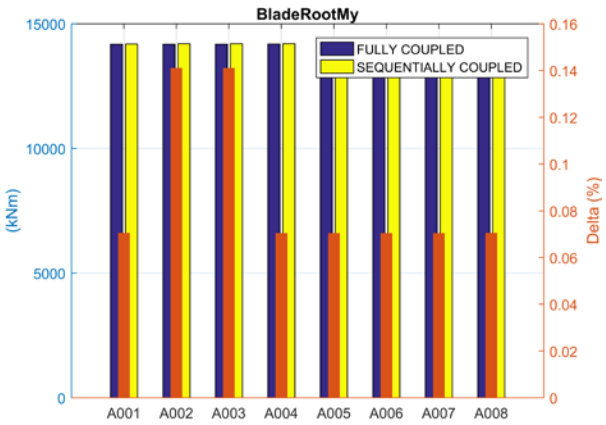

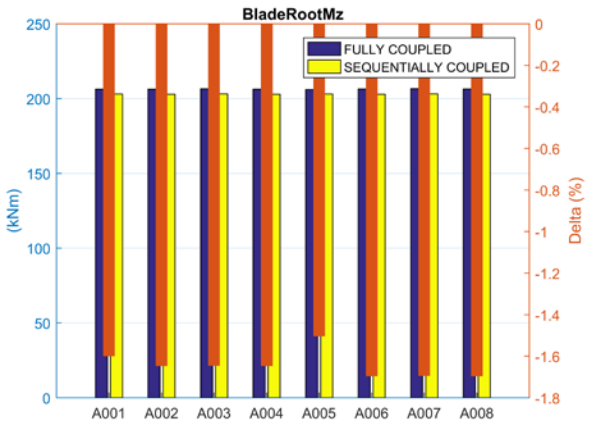

Low Speed Shaft Loads:

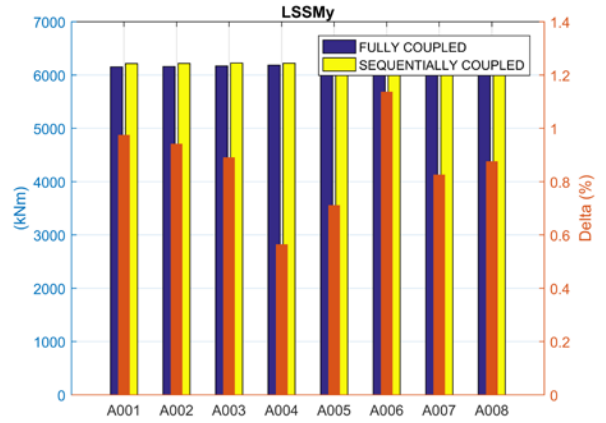

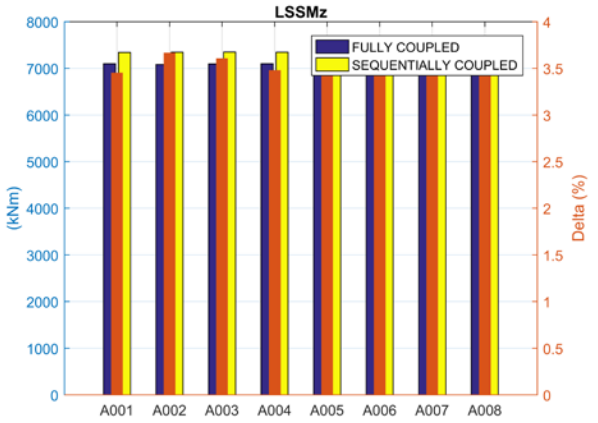

Yaw Bearing Loads:

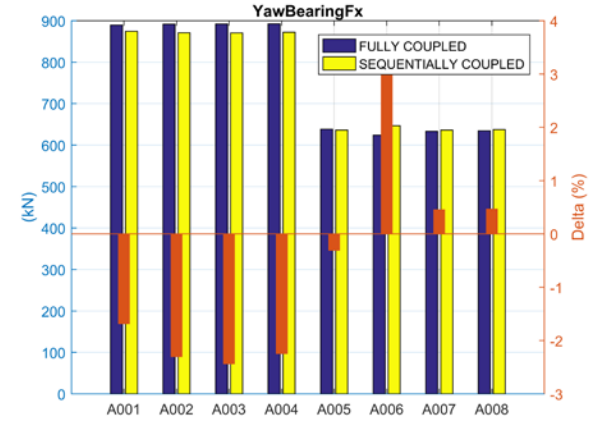

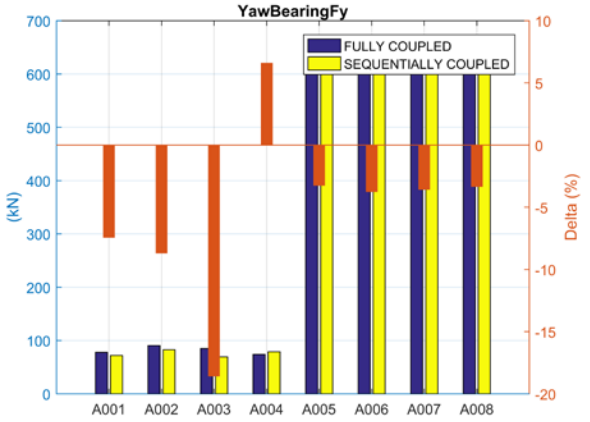

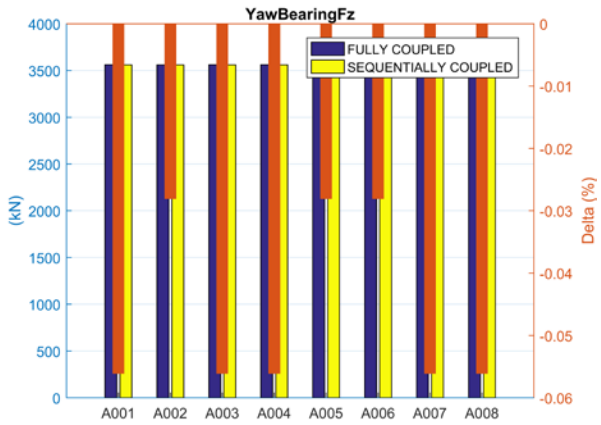

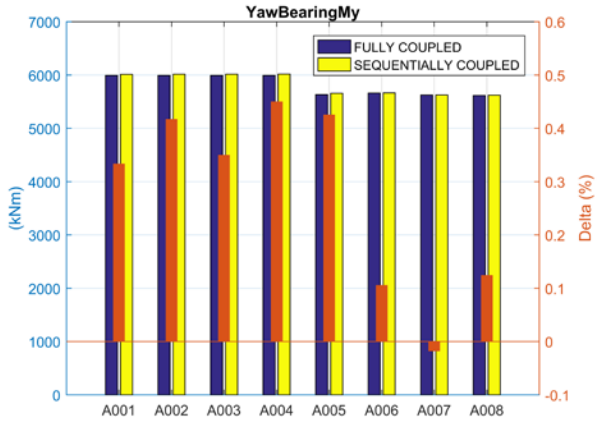

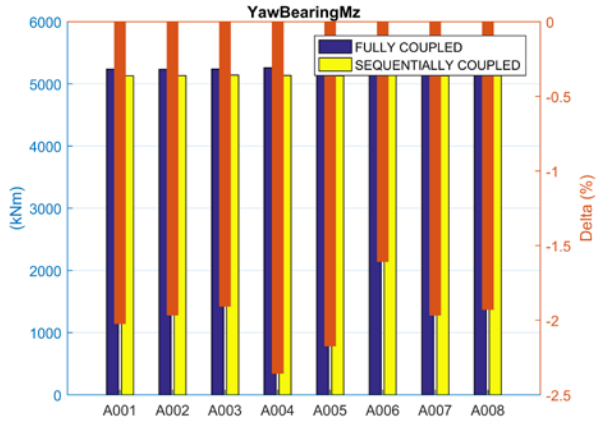

Tower Base Loads:

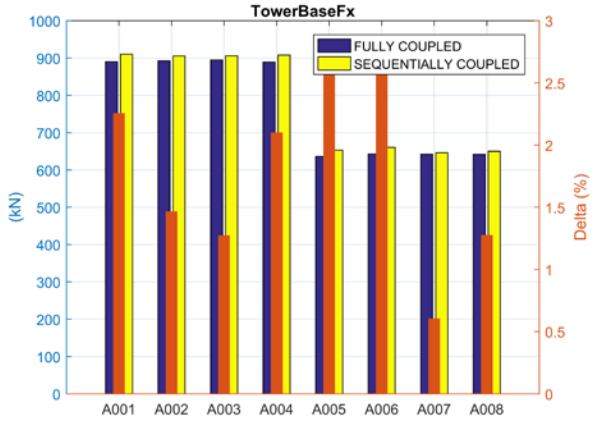

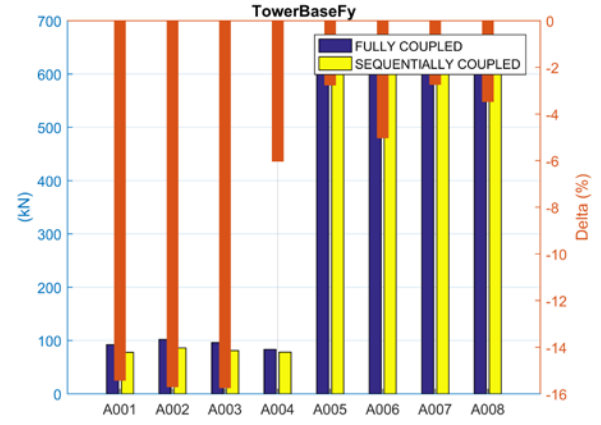

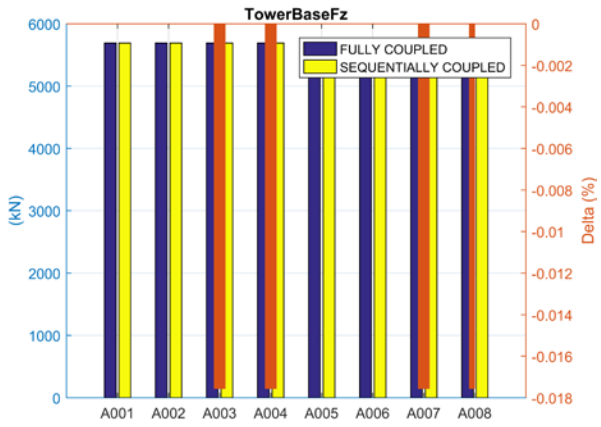

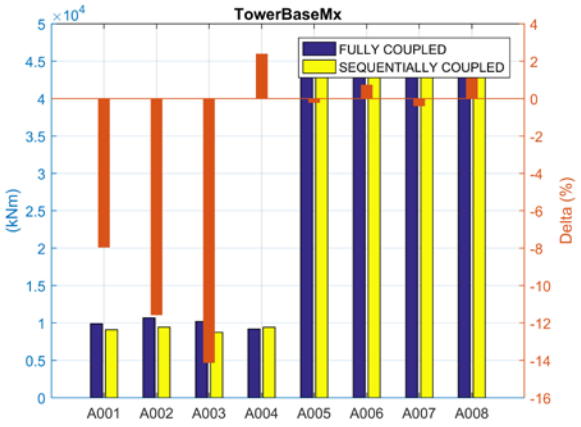

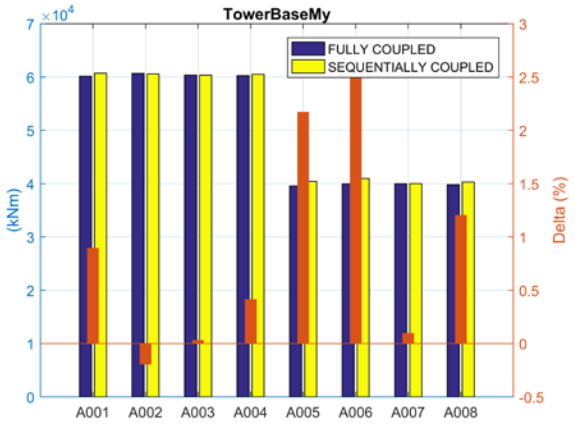

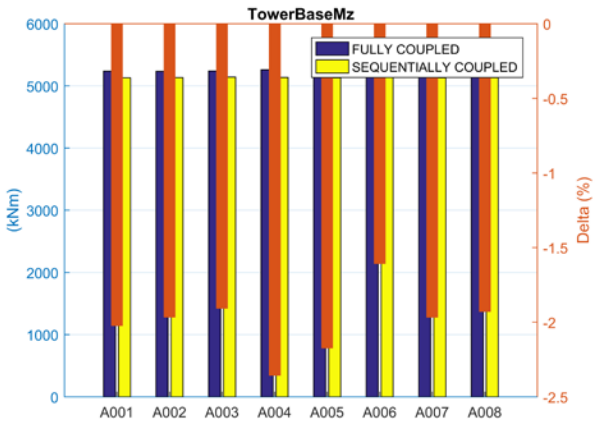

Jacket – Substructure Loads – Power Production

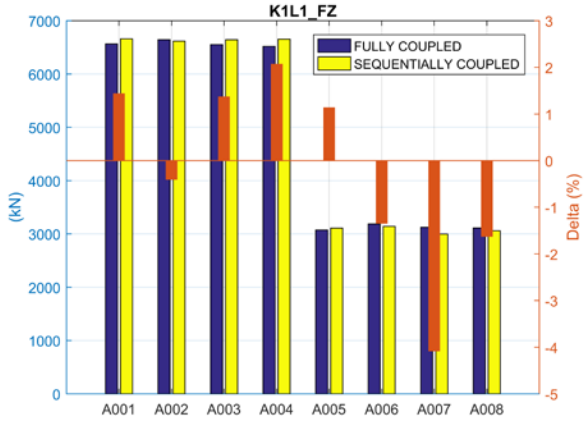

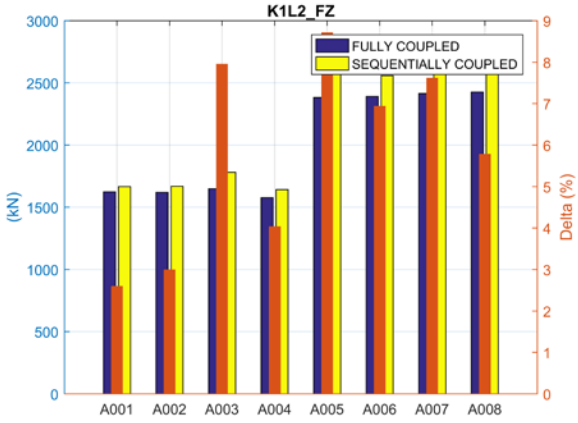

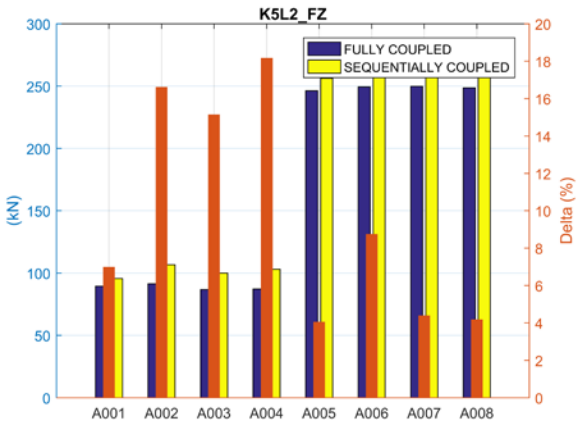
K5L2_FZ
FULLY COUPLED
SEQUENTIALLY COUPLED
(kN)
Delta (%)
A001
A002
A003
A004
A005
A006
A007
A008

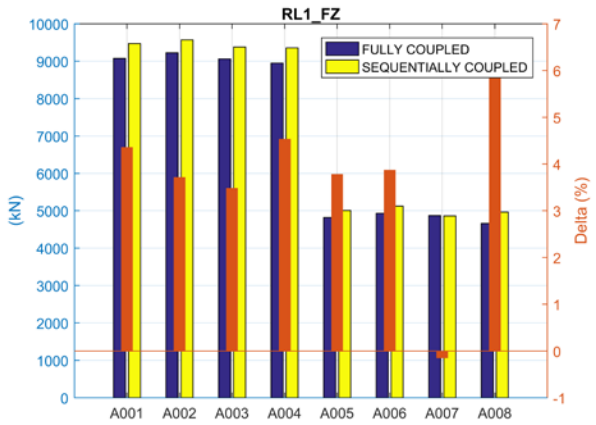
RL1_FZ
FULLY COUPLED
SEQUENTIALLY COUPLED
(kN)
Delta (%)
A001
A002
A003
A004
A005
A006
A007
A008

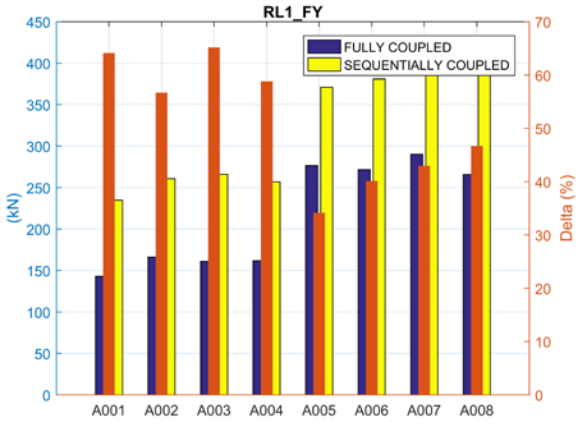
RL1_FY
FULLY COUPLED
SEQUENTIALLY COUPLED
(kN)
Delta (%)
A001
A002
A003
A004
A005
A006
A007
A008

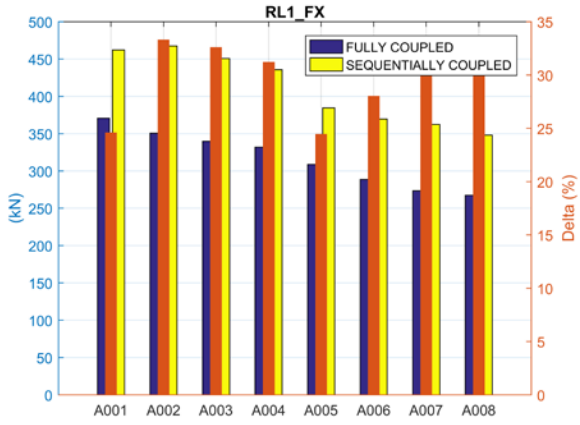
RL1_FX
FULLY COUPLED
SEQUENTIALLY COUPLED
(kN)
Delta (%)
A001
A002
A003
A004
A005
A006
A007
A008

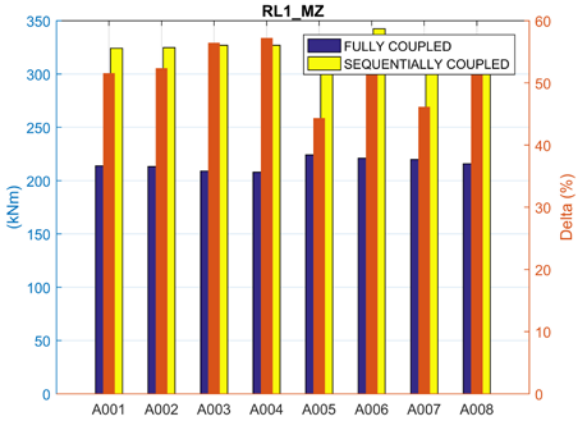
RL1_MZ
FULLY COUPLED
SEQUENTIALLY COUPLED
(kNm)
Delta (%)
A001
A002
A003
A004
A005
A006
A007
A008

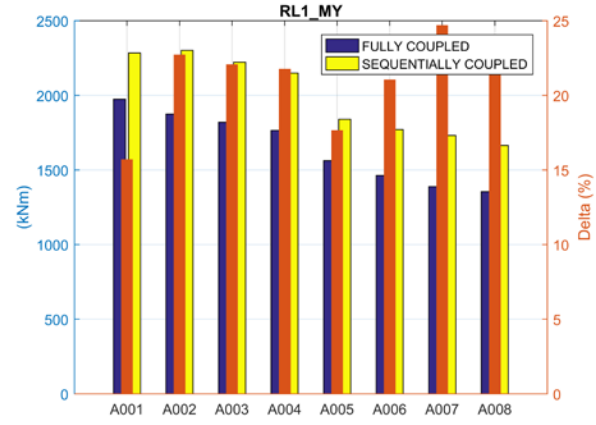
RL1_MY
FULLY COUPLED
SEQUENTIALLY COUPLED
(kNm)
Delta (%)
A001
A002
A003
A004
A005
A006
A007
A008

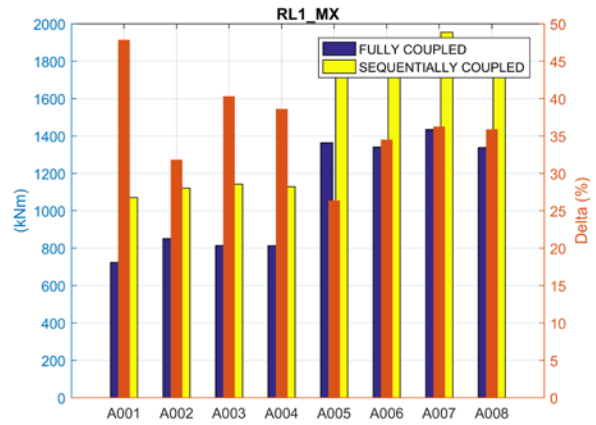
RL1_MX
FULLY COUPLED
SEQUENTIALLY COUPLED
(kNm)
Delta (%)
A001
A002
A003
A004
A005
A006
A007
A008

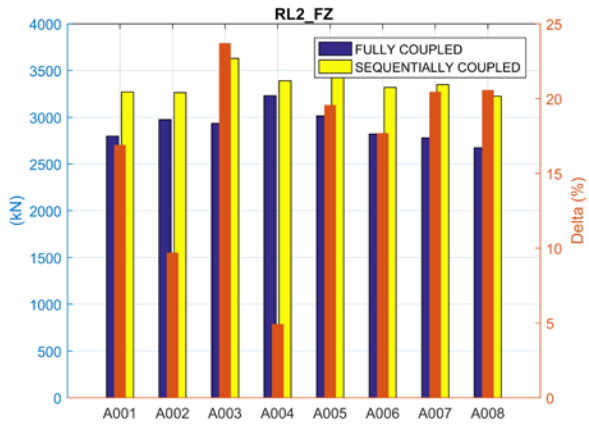
RL2_FZ
FULLY COUPLED
SEQUENTIALLY COUPLED
(kN)
Delta (%)
A001
A002
A003
A004
A005
A006
A007
A008

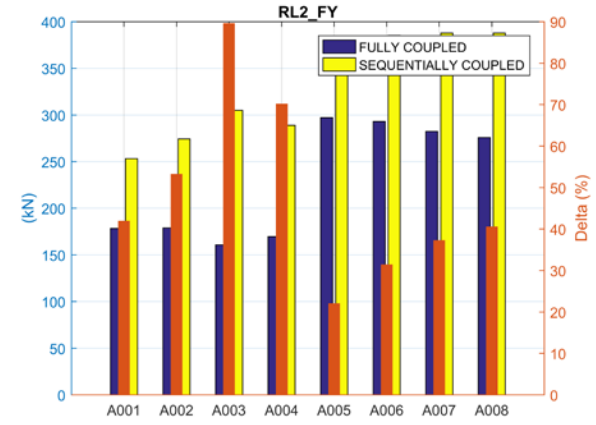
RL2_FY
FULLY COUPLED
SEQUENTIALLY COUPLED
(kN)
Delta (%)
A001
A002
A003
A004
A005
A006
A007
A008

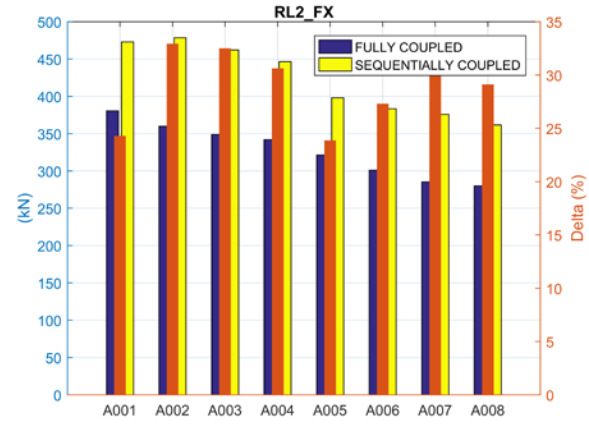
RL2_FX
FULLY COUPLED
SEQUENTIALLY COUPLED
(kN)
Delta (%)
A001
A002
A003
A004
A005
A006
A007
A008

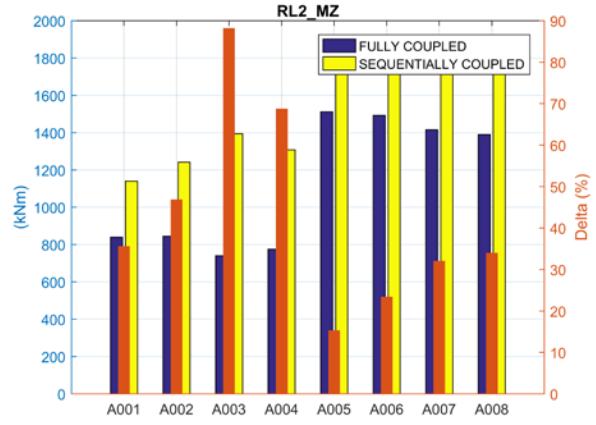
RL2_MZ
FULLY COUPLED
SEQUENTIALLY COUPLED
(kNm)
Delta (%)
A001
A002
A003
A004
A005
A006
A007
A008

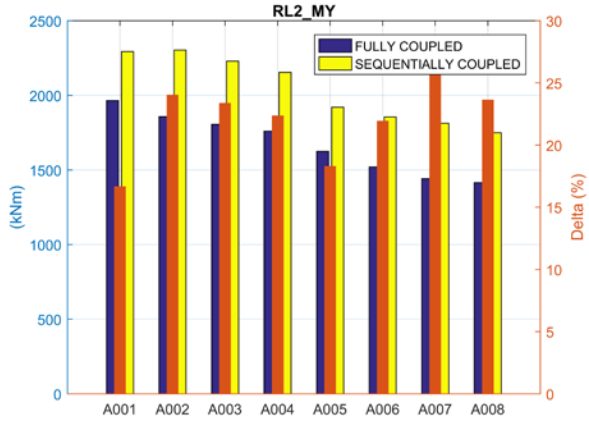
RL2_MY
FULLY COUPLED
SEQUENTIALLY COUPLED
(kNm)
Delta (%)
A001
A002
A003
A004
A005
A006
A007
A008

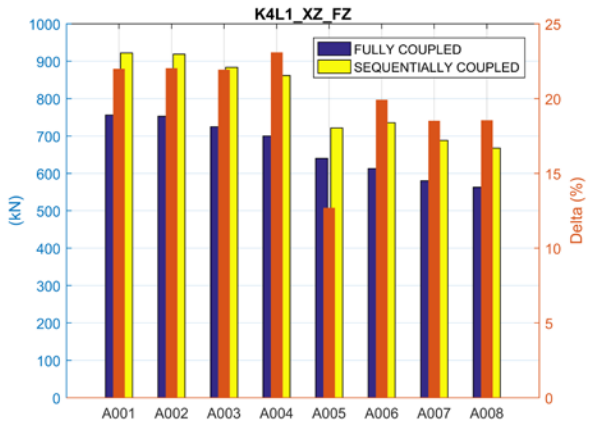
K4L1_XZ_FZ
FULLY COUPLED
SEQUENTIALLY COUPLED
(kN)
Delta (%)
A001 A002 A003 A004 A005 A006 A007 A008

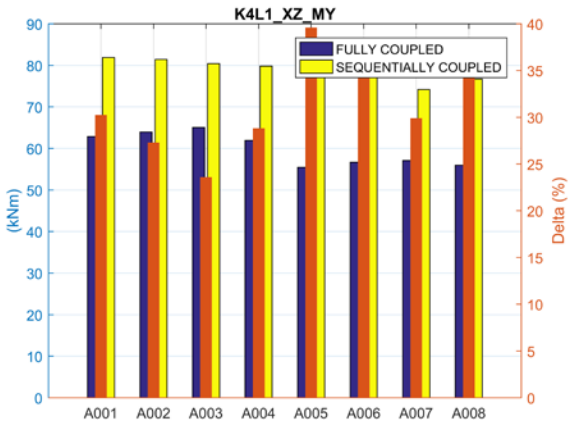
K4L1_XZ_MY
FULLY COUPLED
SEQUENTIALLY COUPLED
(kNm)
Delta (%)
A001 A002 A003 A004 A005 A006 A007 A008

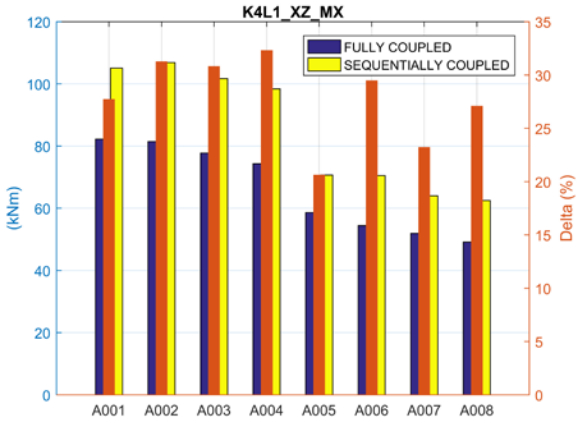
K4L1_XZ_MX
FULLY COUPLED
SEQUENTIALLY COUPLED
(kNm)
Delta (%)
A001 A002 A003 A004 A005 A006 A007 A008

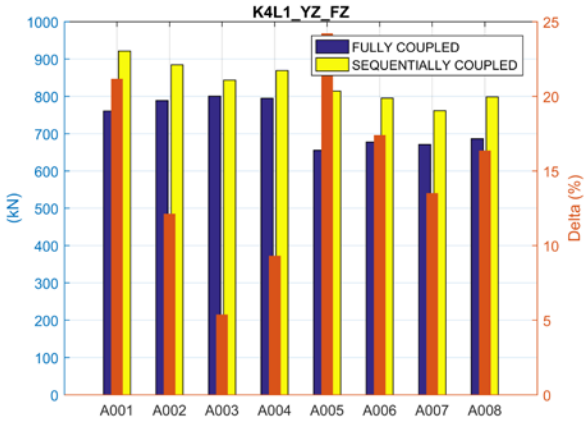
K4L1_YZ_FZ
FULLY COUPLED
SEQUENTIALLY COUPLED
(kN)
Delta (%)
A001 A002 A003 A004 A005 A006 A007 A008

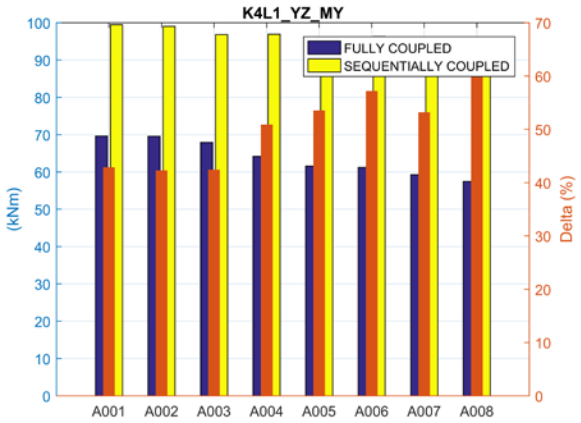
K4L1_YZ_MY
FULLY COUPLED
SEQUENTIALLY COUPLED
(kNm)
Delta (%)
A001 A002 A003 A004 A005 A006 A007 A008

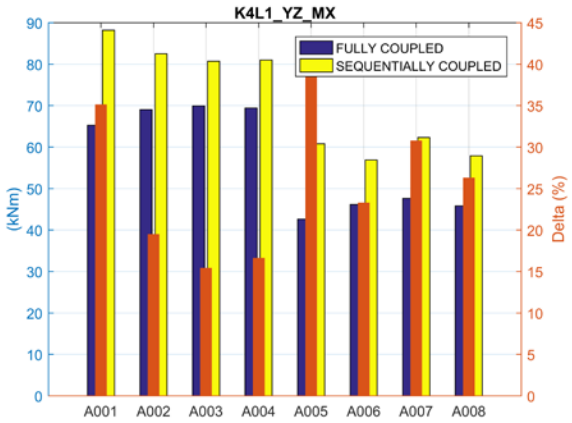
K4L1_YZ_MX
FULLY COUPLED
SEQUENTIALLY COUPLED
(kNm)
Delta (%)
A001 A002 A003 A004 A005 A006 A007 A008


K4L2_XZ_FZ
FULLY COUPLED
SEQUENTIALLY COUPLED
(kN)
Delta (%)
A001
A002
A003
A004
A005
A006
A007
A008

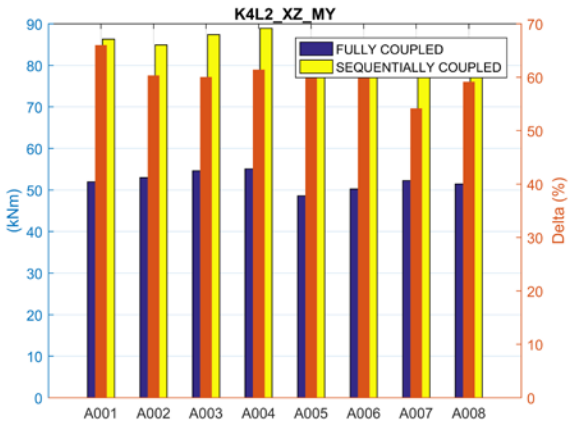
K4L2_XZ_MY
FULLY COUPLED
SEQUENTIALLY COUPLED
(kNm)
Delta (%)
A001
A002
A003
A004
A005
A006
A007
A008

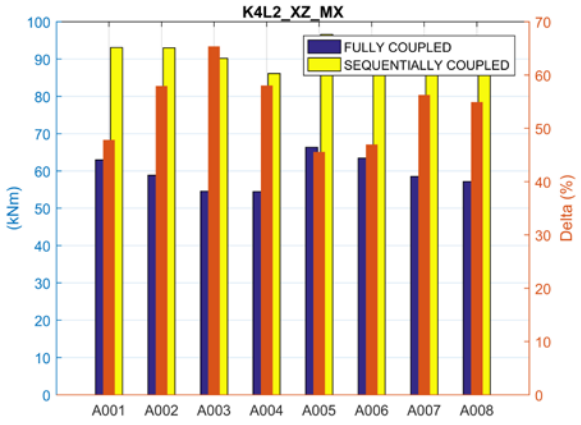
K4L2_XZ_MX
FULLY COUPLED
SEQUENTIALLY COUPLED
(kNm)
Delta (%)
A001
A002
A003
A004
A005
A006
A007
A008

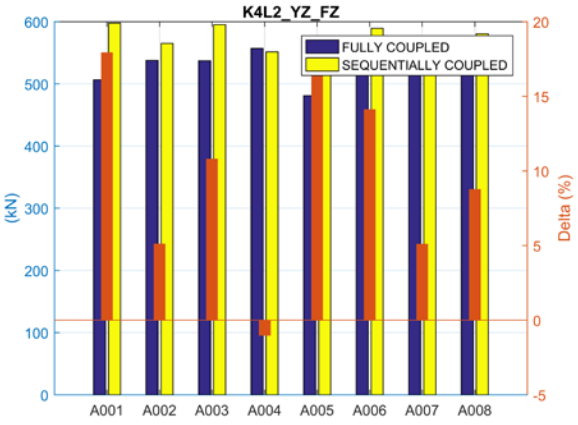
K4L2_YZ_FZ
FULLY COUPLED
SEQUENTIALLY COUPLED
(kN)
Delta (%)
A001
A002
A003
A004
A005
A006
A007
A008

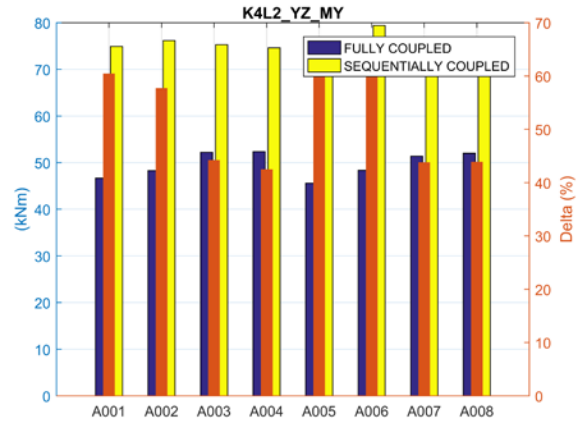
K4L2_YZ_MY
FULLY COUPLED
SEQUENTIALLY COUPLED
(kNm)
Delta (%)
A001
A002
A003
A004
A005
A006
A007
A008

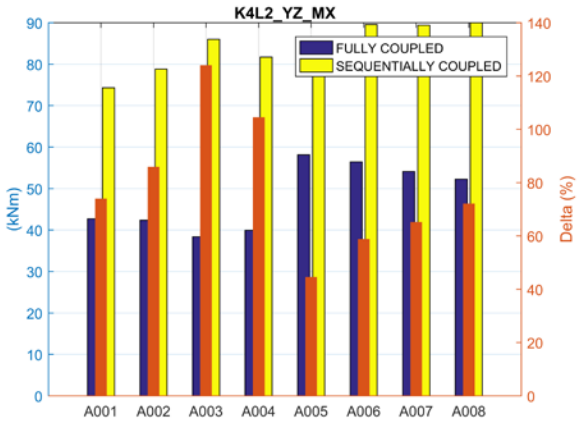
K4L2_YZ_MX
FULLY COUPLED
SEQUENTIALLY COUPLED
(kNm)
Delta (%)
A001
A002
A003
A004
A005
A006
A007
A008

Jacket – Turbine Loads – Extreme Conditions

Blade Root Loads:

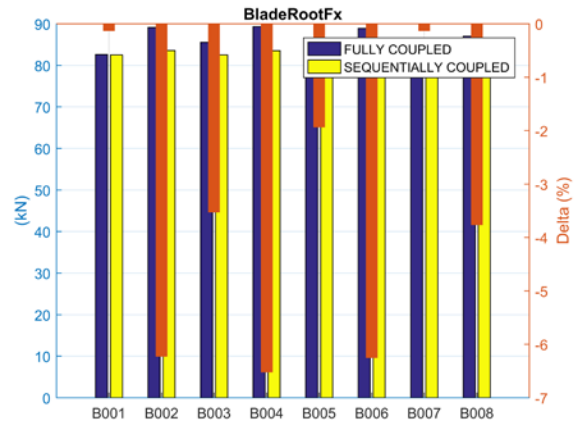

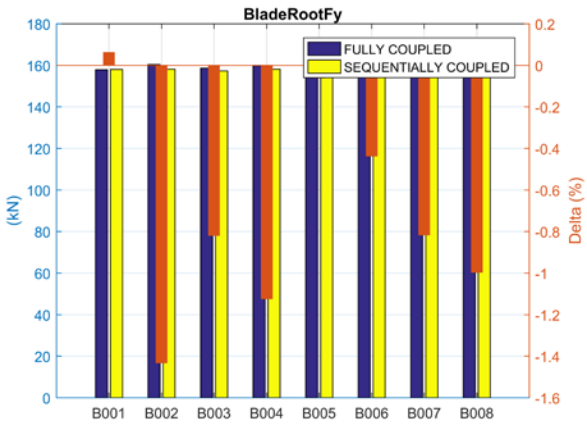

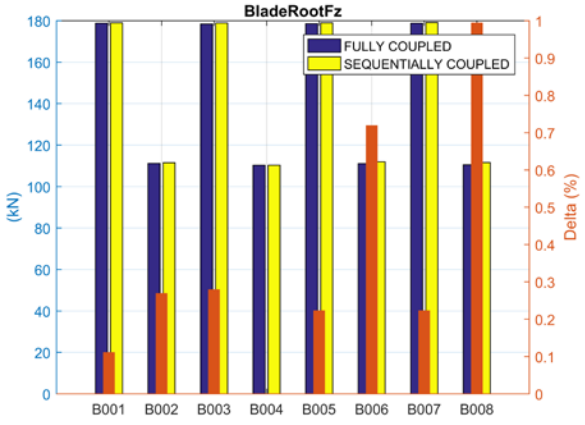

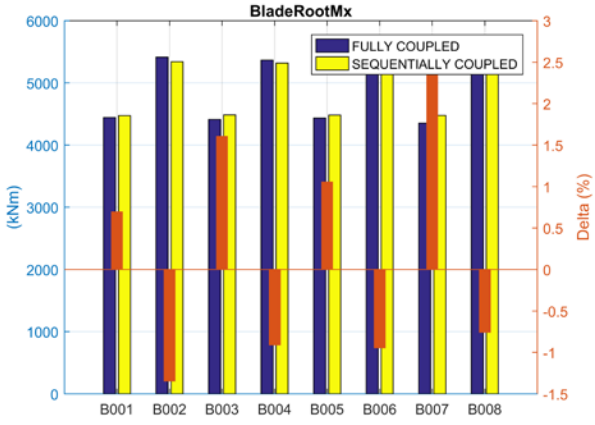

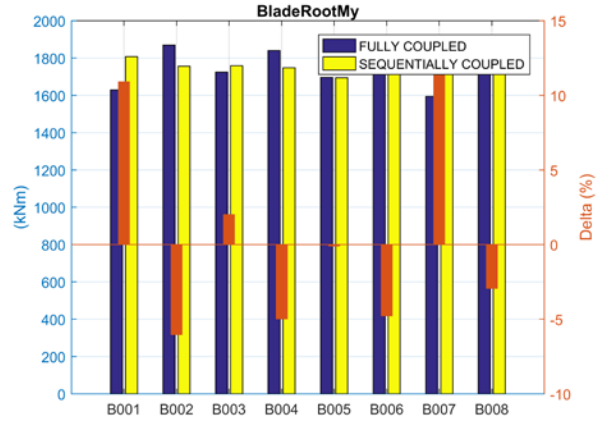

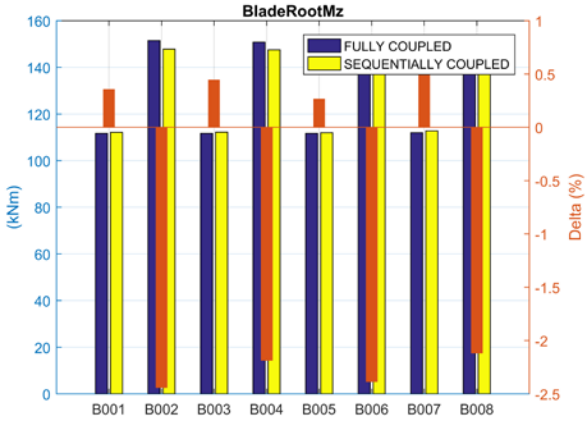

Low Speed Shaft Loads:

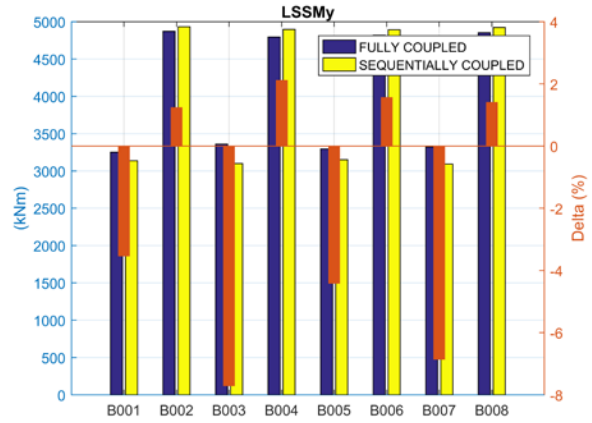

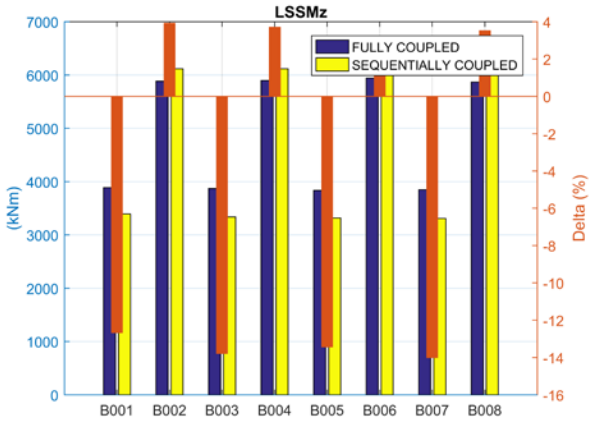

Yaw Bearing Loads:

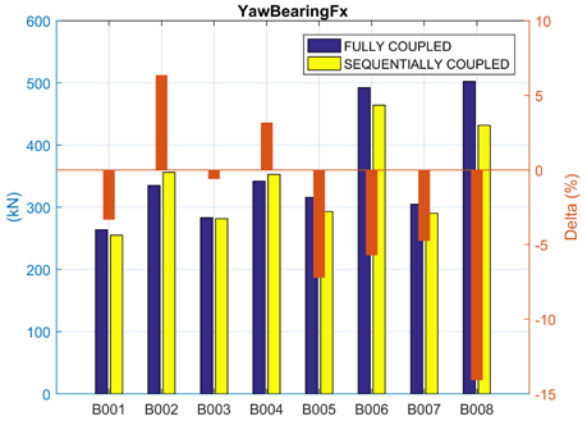

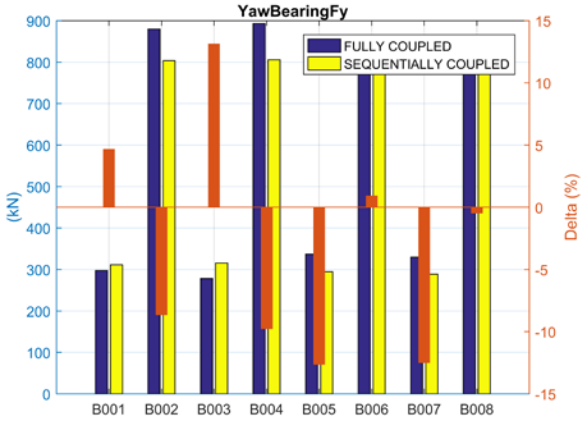

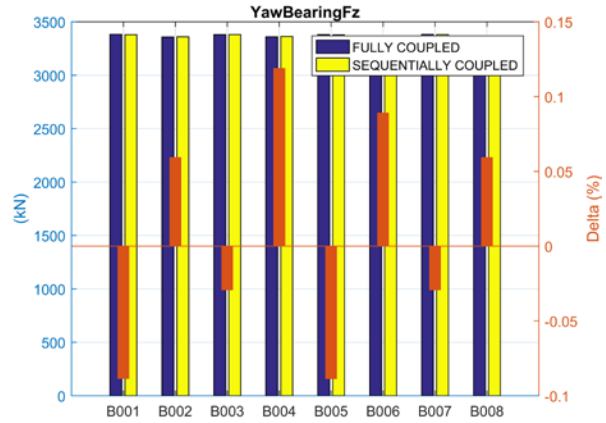

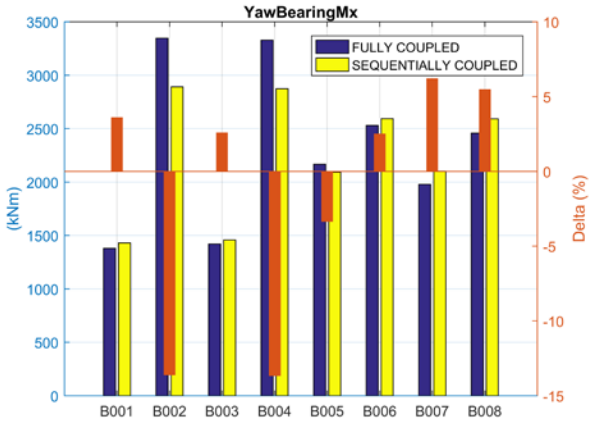

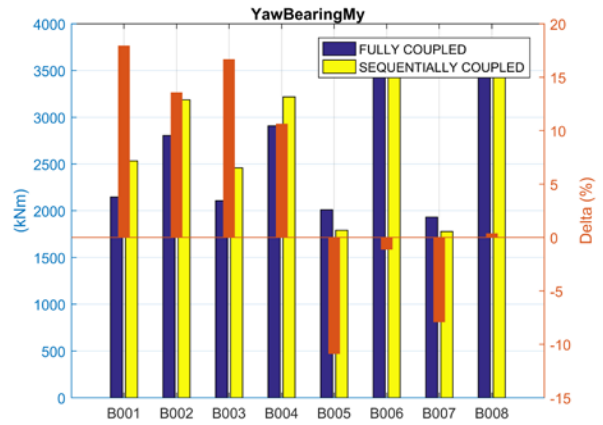

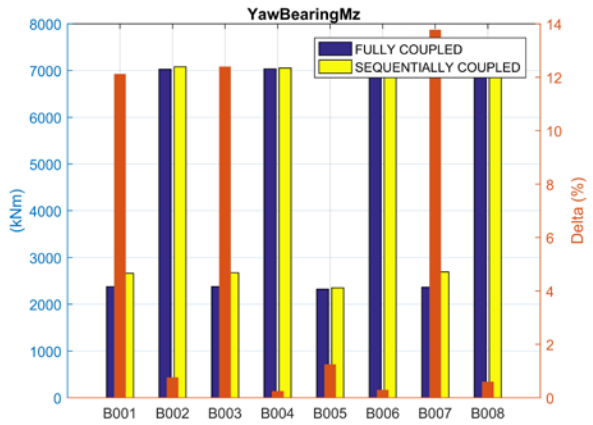

Tower Base Loads:

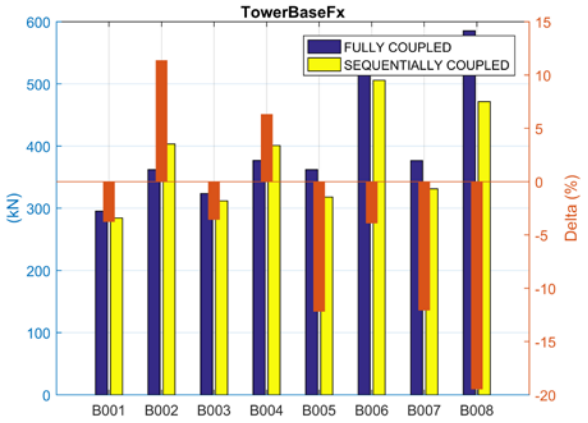

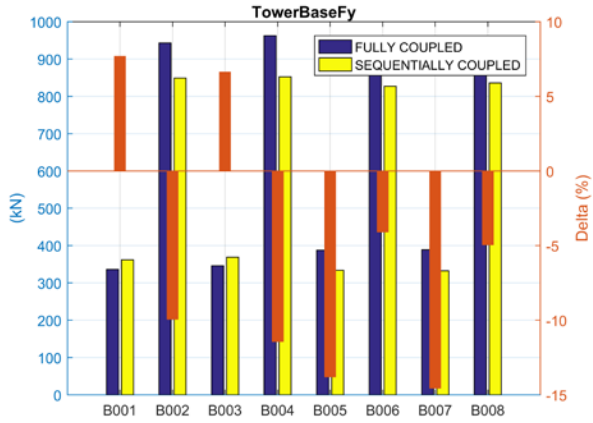

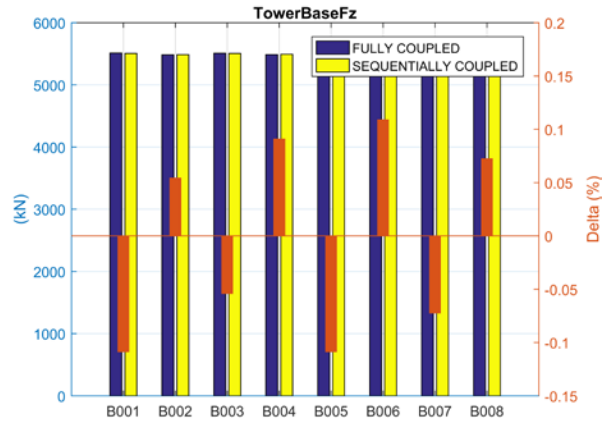

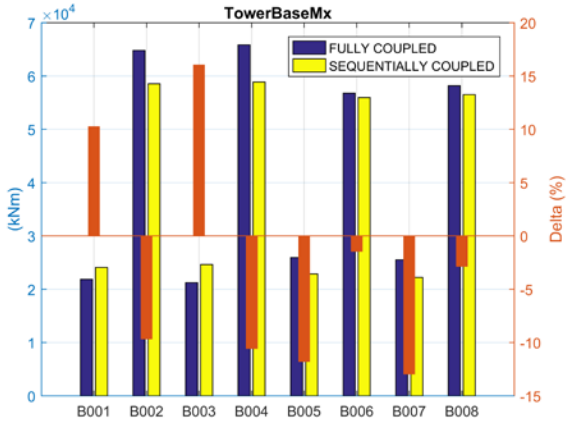

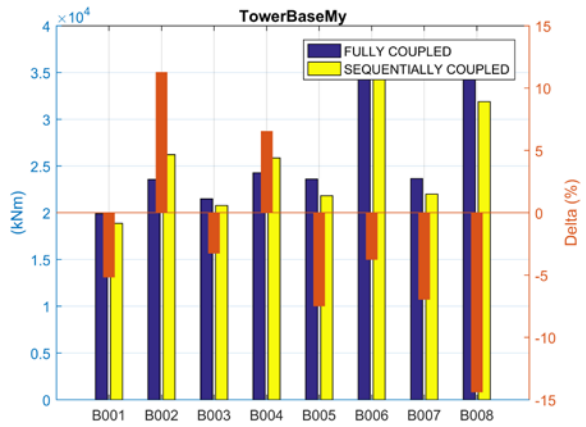

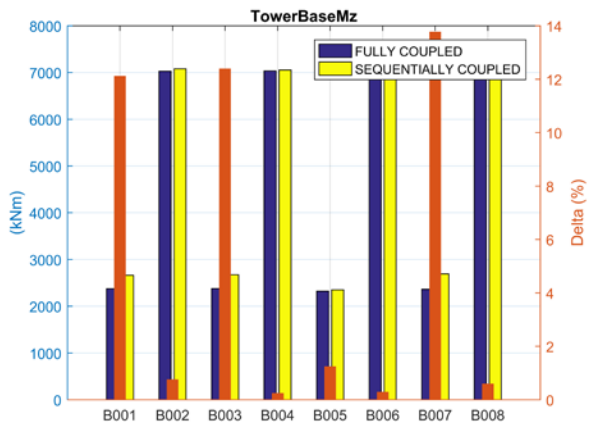

Jacket – Substructure Loads – Extreme Conditions

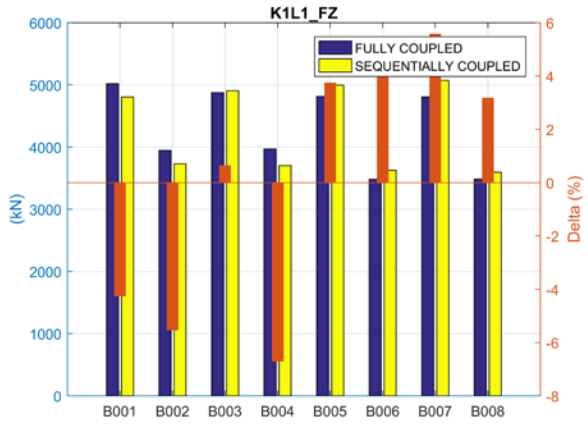

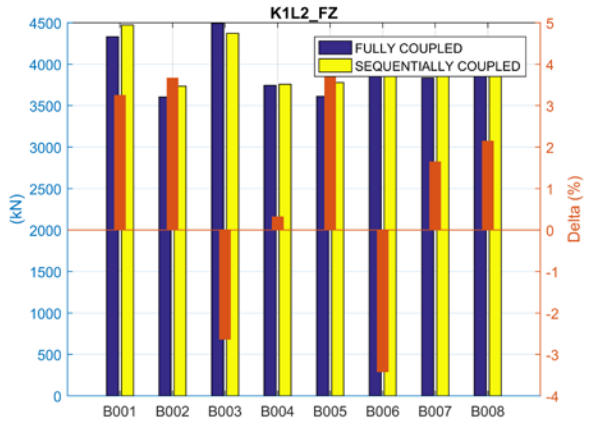

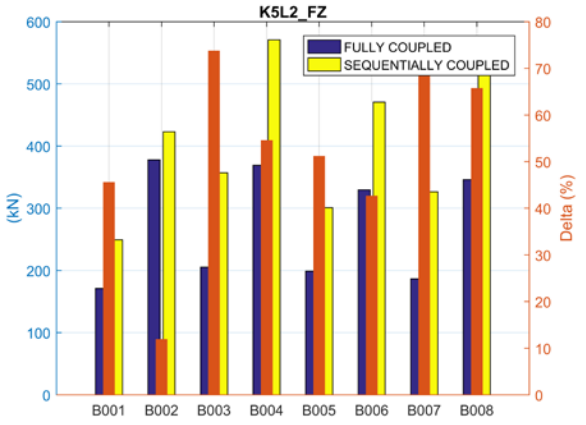

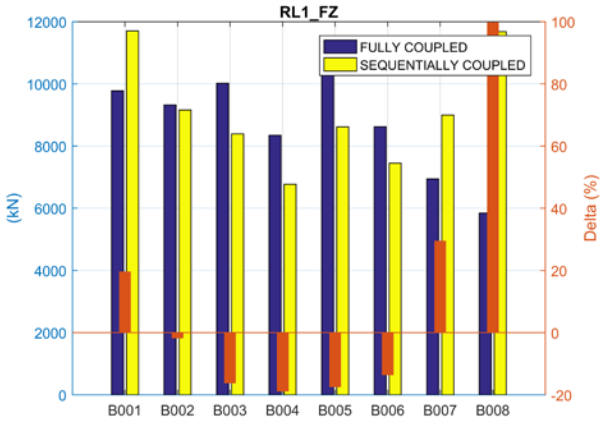

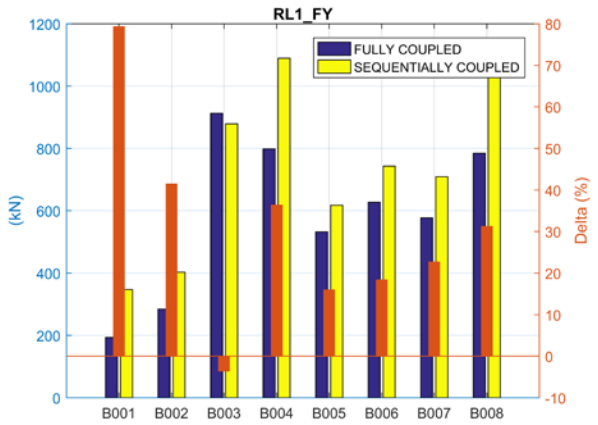
RL1_FY
FULLY COUPLED
SEQUENTIALLY COUPLED
(kN)
Delta (%)
B001
B002
B003
B004
B005
B006
B007
B008

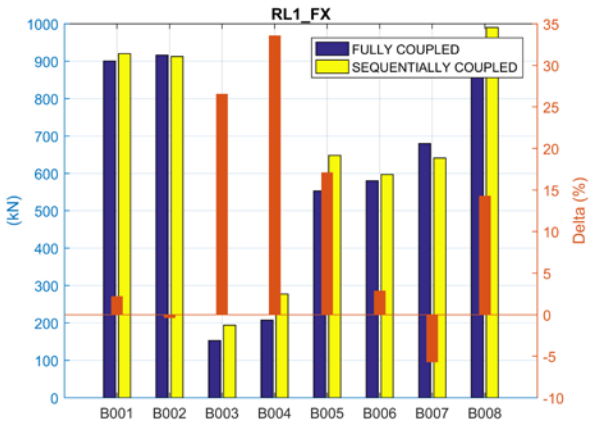
RL1_FX
FULLY COUPLED
SEQUENTIALLY COUPLED
(kN)
Delta (%)
B001
B002
B003
B004
B005
B006
B007
B008

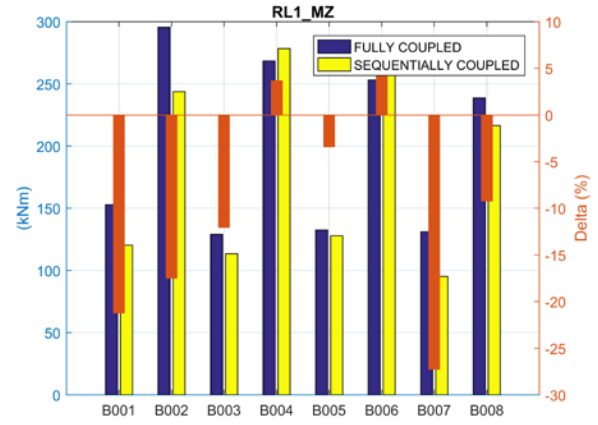
RL1_MZ
FULLY COUPLED
SEQUENTIALLY COUPLED
(kNm)
Delta (%)
B001
B002
B003
B004
B005
B006
B007
B008

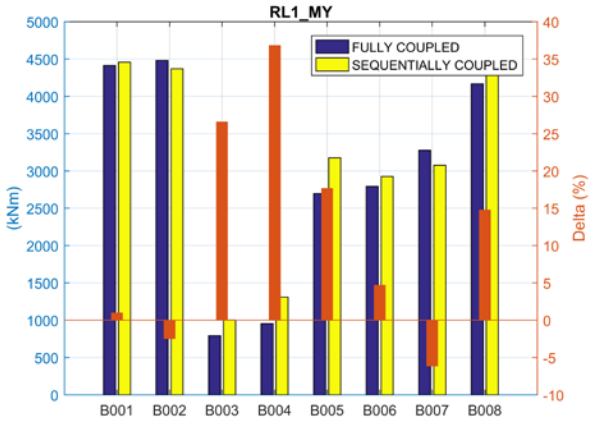
RL1_MY
FULLY COUPLED
SEQUENTIALLY COUPLED
(kNm)
Delta (%)
B001
B002
B003
B004
B005
B006
B007
B008

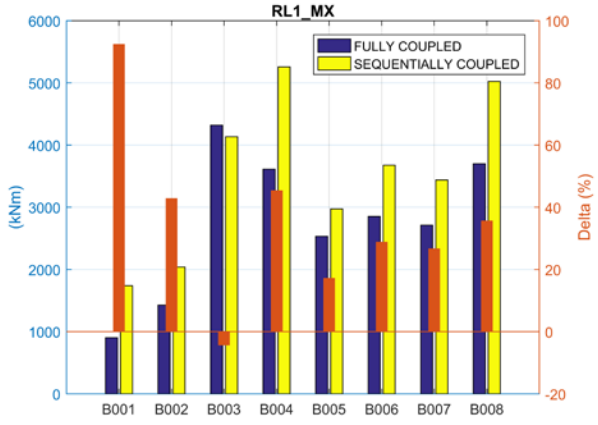
RL1_MX
FULLY COUPLED
SEQUENTIALLY COUPLED
(kNm)
Delta (%)
B001
B002
B003
B004
B005
B006
B007
B008

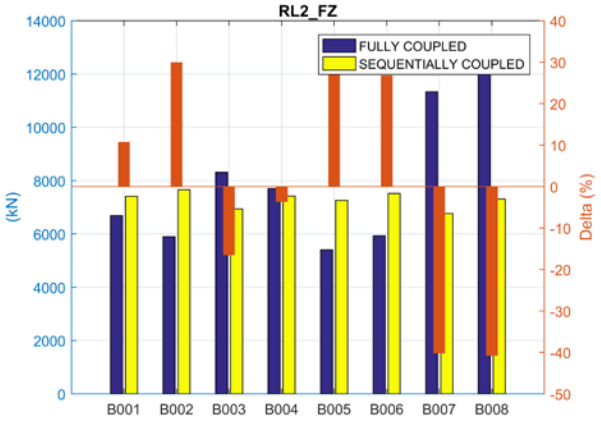
RL2_FZ
FULLY COUPLED
SEQUENTIALLY COUPLED
(kN)
Delta (%)
B001
B002
B003
B004
B005
B006
B007
B008

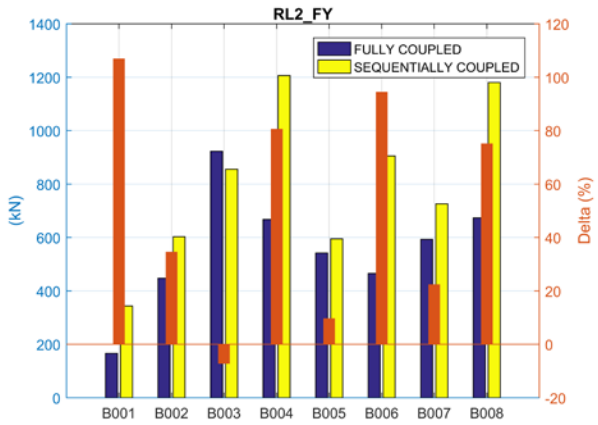
RL2_FY
FULLY COUPLED
SEQUENTIALLY COUPLED
(kN)
Delta (%)
B001
B002
B003
B004
B005
B006
B007
B008

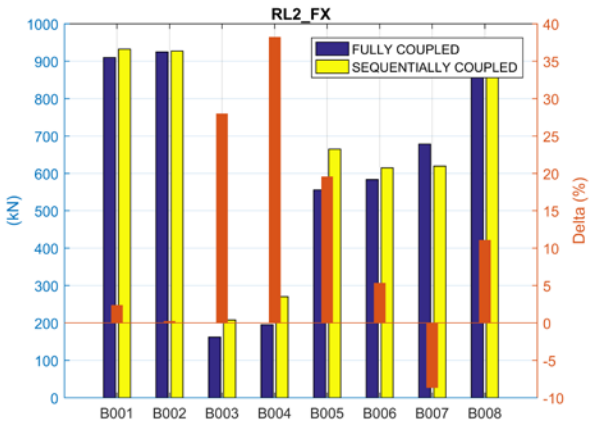
RL2_FX
FULLY COUPLED
SEQUENTIALLY COUPLED
(kN)
Delta (%)
B001
B002
B003
B004
B005
B006
B007
B008

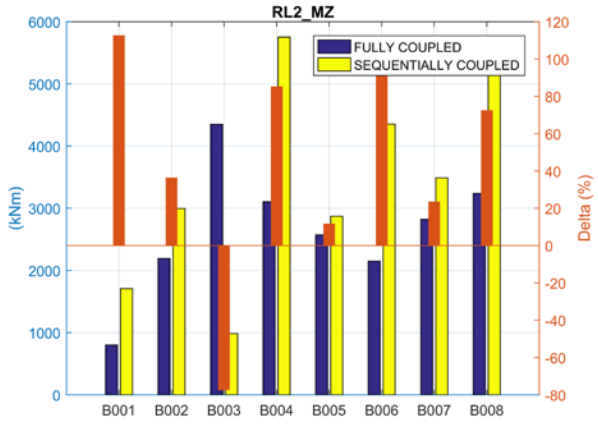
RL2_MZ
FULLY COUPLED
SEQUENTIALLY COUPLED
(kNm)
Delta (%)
B001
B002
B003
B004
B005
B006
B007
B008

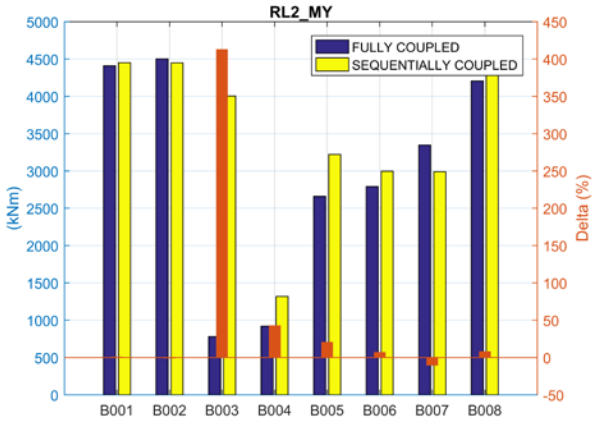
RL2_MY
FULLY COUPLED
SEQUENTIALLY COUPLED
(kNm)
Delta (%)
B001
B002
B003
B004
B005
B006
B007
B008

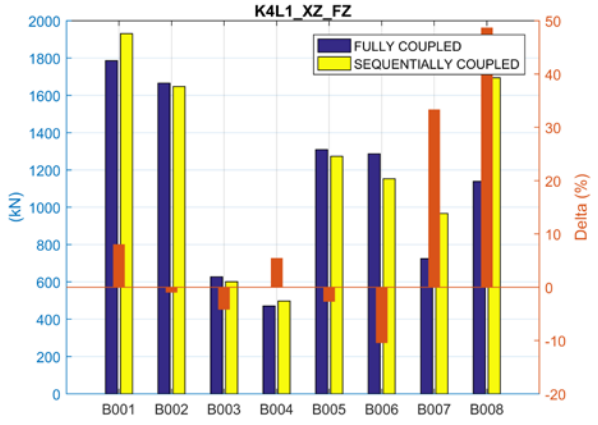
K4L1_XZ_FZ
FULLY COUPLED
SEQUENTIALLY COUPLED
(kN)
Delta (%)
B001
B002
B003
B004
B005
B006
B007
B008

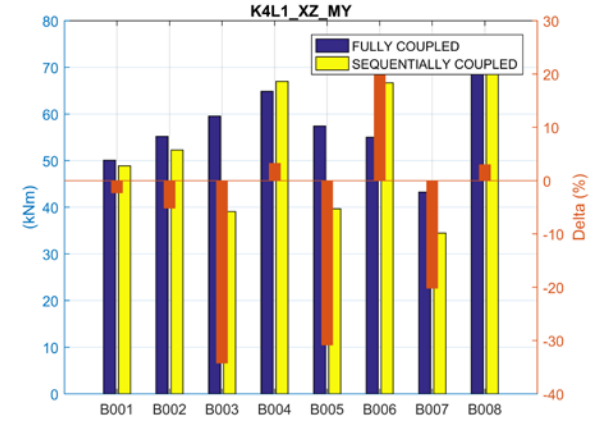
K4L1_XZ_MY
FULLY COUPLED
SEQUENTIALLY COUPLED
(kNm)
Delta (%)
B001
B002
B003
B004
B005
B006
B007
B008

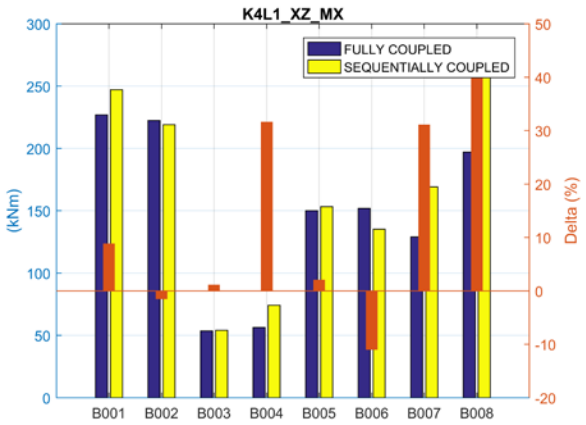
K4L1_XZ_MX
FULLY COUPLED
SEQUENTIALLY COUPLED
(kNm)
Delta (%)
B001 B002 B003 B004 B005 B006 B007 B008

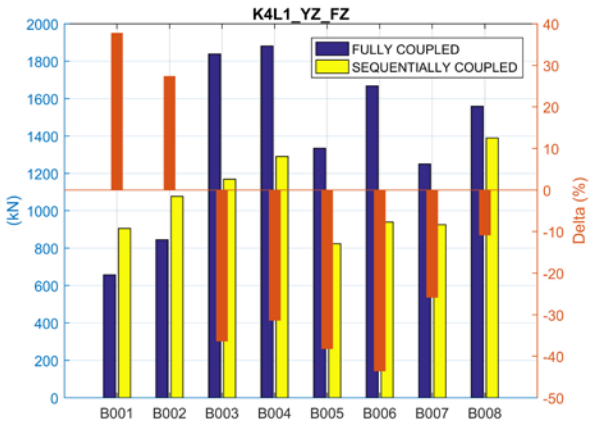
K4L1_YZ_FZ
FULLY COUPLED
SEQUENTIALLY COUPLED
(kN)
Delta (%)
B001 B002 B003 B004 B005 B006 B007 B008

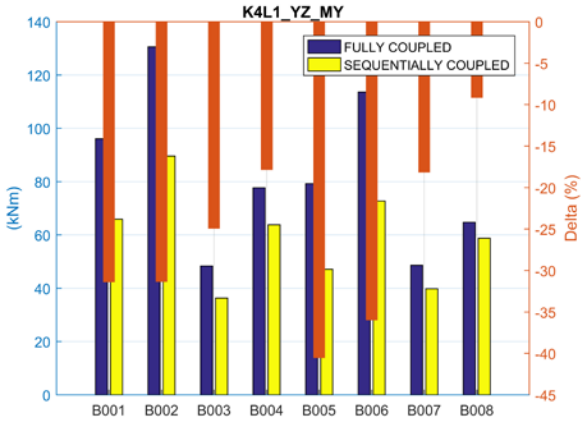
K4L1_YZ_MY
FULLY COUPLED
SEQUENTIALLY COUPLED
(kNm)
Delta (%)
B001 B002 B003 B004 B005 B006 B007 B008

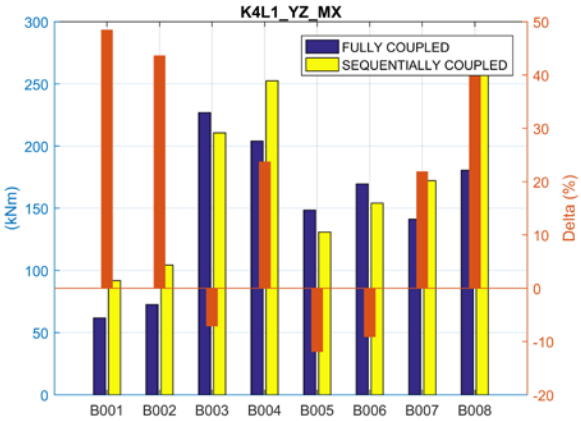
K4L1_YZ_MX
FULLY COUPLED
SEQUENTIALLY COUPLED
(kNm)
Delta (%)
B001 B002 B003 B004 B005 B006 B007 B008

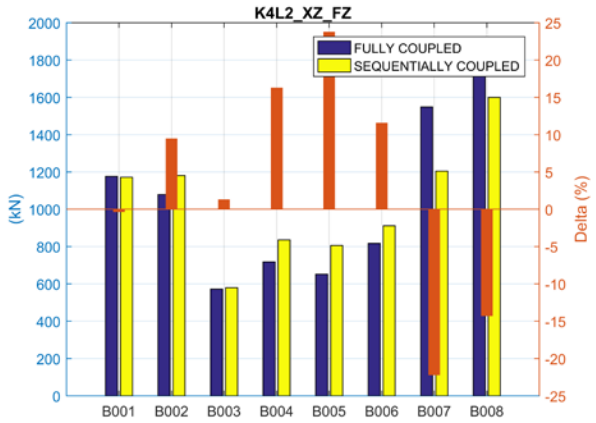
K4L2_XZ_FZ
FULLY COUPLED
SEQUENTIALLY COUPLED
(kN)
Delta (%)
B001 B002 B003 B004 B005 B006 B007 B008

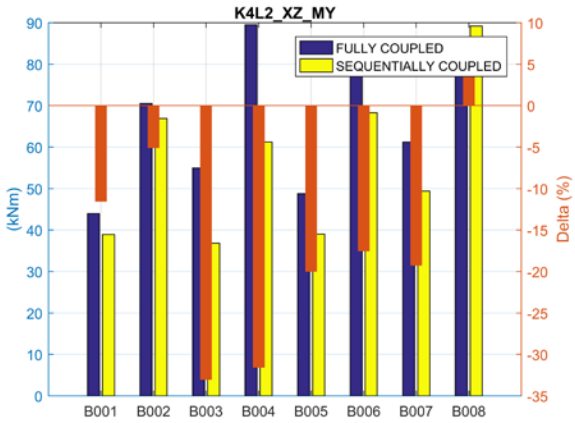
K4L2_XZ_MY
FULLY COUPLED
SEQUENTIALLY COUPLED
(kNm)
Delta (%)
B001 B002 B003 B004 B005 B006 B007 B008

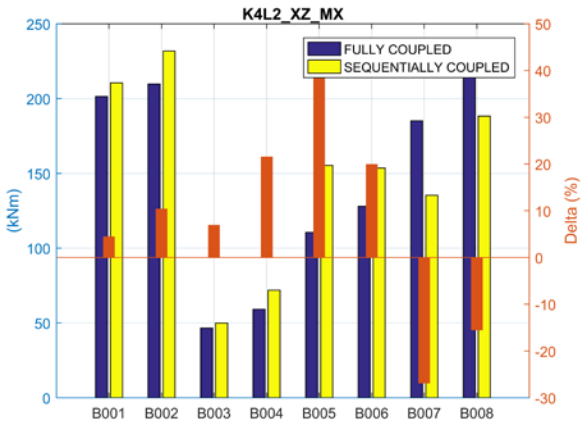
K4L2_XZ_MX
FULLY COUPLED
SEQUENTIALLY COUPLED
(kNm)
Delta (%)
B001
B002
B003
B004
B005
B006
B007
B008

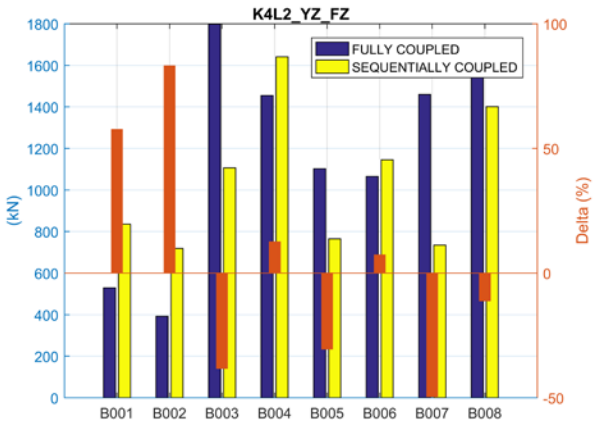
K4L2_YZ_FZ
FULLY COUPLED
SEQUENTIALLY COUPLED
(kN)
Delta (%)
B001
B002
B003
B004
B005
B006
B007
B008

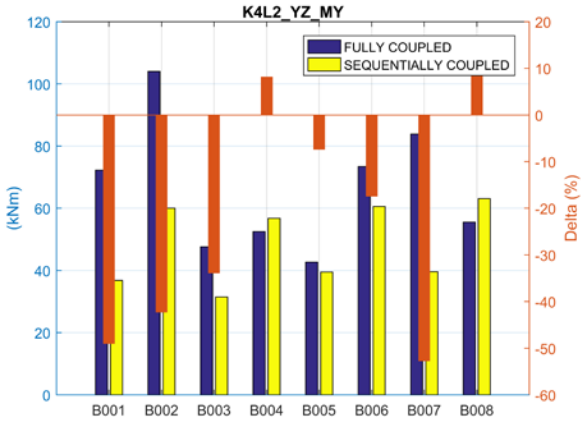
K4L2_YZ_MY
FULLY COUPLED
SEQUENTIALLY COUPLED
(kNm)
Delta (%)
B001
B002
B003
B004
B005
B006
B007
B008

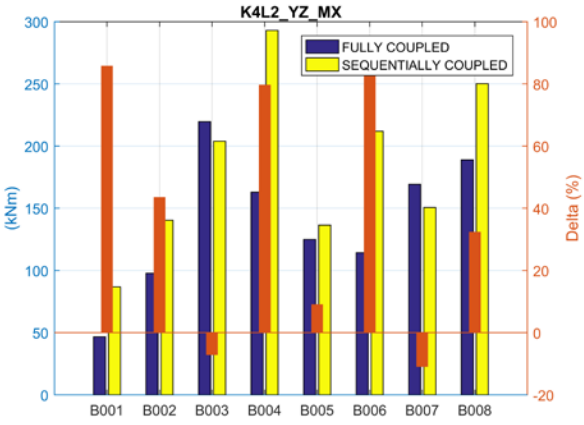
K4L2_YZ_MX
FULLY COUPLED
SEQUENTIALLY COUPLED
(kNm)
Delta (%)
B001
B002
B003
B004
B005
B006
B007
B008